

This is my second review of the manuscript OS-2018-15. I acknowledge that the authors have responded and incorporated all my previous comments in the revised version, and I therefore think the manuscript can be published after a very few corrections are considered by the authors.

All remarks detailed below by the referee were considered.

In the new revised manuscript, the previous corrections (previous revised manuscript) remain in red and the new ones are in blue.

P2 Line 25: "and is in charge of the global high resolution ocean analyses and forecasts" is a repetition of Line 19-20.

The sentence has been changed.

P4L3 Suggest rephrasing: "was run ... to catch-up the real-time analysis and forecast system by ingesting "reprocessed" input data (atmospheric forcing, observations, etc.)"

I think the word "databases" is too vague in this context.

The sentence has been rephrased.

P5L23

"current NEMO 3.6 stable version that is now the standard version of the code."

I think it is better to say "the latest official release of NEMO" instead of "stable", "current" or "standard".

We changed it.

P9L7: It is clearer now, however it would be better to state explicitly that the inter-annual signal of the background errors is present only in the hindcast (reprocessed system) and not in the real time system, if I understand correctly. Suggest indeed writing clearly the differences between these two systems.

We clarified the time period over which the anomalies were calculated and we added this sentence in the text: "Currently, the anomalies used in real time come from the set of anomalies computed over the 2007-2015 period with no real time extension of this set. We therefore make the hypothesis that the set of anomalies computed over a period prior to real time is able to represent correctly the background error covariance over the real time period."

Is the QC1 (Equation 1) able to retain observations with large innovations but far from climatology? (in case of regimes far from climatology). If so, suggest stating it clearly.

Yes, the QC1 is able to retain observations with large innovations but far from climatology. It was already stated in the previous corrected manuscript (see section 2.3.1, page 12, lines 22-26).

P15L21: "whose motions".

We changed it.

Section 3.4.1

I think the title itself is not clear, what is anomaly in this context? Innovations or analysis increments? It is important to make clear if the filtering is applied to the assimilation inputs (innovations) or outputs (analysis increments).

We added in the first paragraph of section 3.4.1 the following sentence: "Another way to remove the very short scales would be to filter the analysis increments before injecting them into the model. This choice would have led to a less optimal analysis and to a loss of balance between the different components of the increment."

Moreover, we have clarified at the end of the section 2.2 that the anomalies were inputs of the analysis.

Section 3.4.1

If there is a reference about effective resolution of DUACS, would be good to insert it.

This was already inserted in the previous corrected manuscript (see section 3.4.2, page 21 - line 33).

Change the occurrences of "doesn't/don't" to "does not/do not"

We changed it.

Recent updates on the Copernicus Marine Service global ocean monitoring and forecasting real-time 1/12° high resolution system

Jean-Michel Lellouche¹, Eric Greiner², Olivier Le Galloudec¹, Gilles Garric¹, Charly Regnier¹, Marie Drevillon¹, Mounir Benkiran¹, Charles-Emmanuel Testut¹, Romain Bourdalle-Badie¹, Florent Gasparin¹, Olga Hernandez¹, Bruno Levier¹, Yann Drillet¹, Elisabeth Remy¹, Pierre-Yves Le Traon^{1,3}

¹ Mercator Ocean, Ramonville Saint Agne, France

² Collecte Localisation Satellites, Ramonville Saint Agne, France

³ IFREMER, 29280, Plouzané, France

Correspondence to: Jean-Michel Lellouche (jlellouche@mercator-ocean.fr)

Abstract

Since October 19, 2016, and in the framework of Copernicus Marine Environment Monitoring Service (CMEMS), Mercator Ocean delivers in real-time daily services (weekly analyses and daily 10-day forecasts) with a new global 1/12° high resolution (eddy-resolving) monitoring and forecasting system. The model component is the NEMO platform driven at the surface by the IFS ECMWF atmospheric analyses and forecasts. Observations are assimilated by means of a reduced-order Kalman filter with a [three-dimensional 3D](#) multivariate modal decomposition of the [backgroundforecast](#) error. Along track altimeter data, satellite sea surface temperature, sea ice concentration and in situ temperature and salinity vertical profiles are jointly assimilated to estimate the initial conditions for numerical ocean forecasting. A 3D-VAR scheme provides a correction for the slowly-evolving large-scale biases in temperature and salinity.

This paper describes the recent updates applied to the system and discusses the importance of fine tuning of an ocean monitoring and forecasting system. It details more particularly the impact of the initialization, the correction of precipitation, the assimilation of climatological temperature and salinity in the deep ocean, the construction of the [backgroundforecast](#) error

1 covariance and the adaptive tuning of observations error on increasing the realism of the
2 analysis and forecasts.

3 The scientific assessment of the ocean estimations are illustrated with diagnostics over some
4 particular years, assorted with time series over the time period 2007-2016. The overall impact
5 of the integration of all updates on the products quality is also discussed, highlighting a gain
6 in performance and reliability of the current global monitoring and forecasting system
7 compared to its previous version.

8

9 **1 Introduction**

10 Mercator Ocean monitoring and forecasting systems have been routinely operated in real-time
11 since early 2001. ~~They and~~ have been regularly upgraded by increasing complexity,
12 expanding the geographical coverage from regional to global and improving models and
13 assimilation schemes (Brasseur et al., 2006; Lellouche et al., 2013).

14 ~~After having successfully coordinated the European MyOcean and MyOcean2 projects~~
15 ~~(<http://www.myocean.eu>), Mercator Ocean was officially entrusted by the European~~
16 ~~Commission on November, 11, 2014 to implement and operate the Copernicus Marine~~
17 ~~Environment Monitoring Service (CMEMS), as part of the European Earth observation~~
18 ~~program Copernicus (<http://marine.copernicus.eu>). Since January 2009, Mercator Ocean,~~
19 which had primary responsibility for the global ocean forecasts of the MyOcean and
20 MyOcean2 projects since January 2009, developed several versions of its monitoring and
21 forecasting systems for the various milestones (from V0 to V4) of the MyOcean project, and
22 more recently, for milestones V1, V2 and V3 of the Copernicus Marine Environment
23 Monitoring Service (CMEMS), as part of the European Earth observation program
24 Copernicus (<http://marine.copernicus.eu>) (see Fig. 1). ~~Mercator Ocean opened the CMEMS in~~
25 ~~May 2015 and is in charge of the global high resolution ocean analyses and forecasts. Since~~
26 ~~May 2015, in the context of CMEMS, Research and Development activities have been~~
27 ~~conducted these last years to improve the real-time 1/12° high resolution (eddy-resolving)~~
28 ~~global analysis and forecasting system. Since October 19, 2016, Mercator Ocean has~~
29 ~~delivered real-time daily services (weekly analyses and daily 10-day forecasts) with a new~~
30 ~~global 1/12° system PSY4V3R1 (hereafter PSY4V3, see Fig. 1). Note that PSY4V3 will be~~
31 ~~the system for the CMEMS V4 milestone.~~ —The main differences and links between the
32 various versions of the Mercator Ocean systems in the framework of past MyOcean project

1 | and current CMEMS are summarized in Table 1 and Table 2 for Intermediate Resolution $1/4^\circ$
2 | Global configurations (hereafter IRG) and High Resolution $1/12^\circ$ Global configurations
3 | (hereafter HRG) systems respectively.

4 | These systems are intensively used in four main areas of application: (i) maritime safety, (ii)
5 | marine resources management, (iii) coastal and marine environment, and (iv) weather, climate
6 | and seasonal forecasting (<http://marine.copernicus.eu/markets/use-cases>). As described in
7 | Lellouche et al. (2013), the evaluation of such systems includes routine verification against
8 | assimilated and independent in situ and satellite observations, as well as a careful check of
9 | many physical processes (e.g. mixed layer depth evaluation as shown in Drillet et al. (2014)).
10 | Scientific studies brought precious additional evaluation feedbacks (Juza et al., 2015; Smith et
11 | al., 2016; Estournel et al., 2016). Finally, several studies showed the added value of surface
12 | currents analyses provided by these systems for drift applications (Scott et al., 2012;
13 | Drevillon et al., 2013).

14 | ~~Since May 2015, Mercator Ocean opened the CMEMS and has been in charge of the global~~
15 | ~~high resolution ocean analyses and forecasts. In this context, R&D activities have been~~
16 | ~~conducted these last years to improve the real-time $1/12^\circ$ high resolution (eddy-resolving)~~
17 | ~~global analysis and forecasting system. Since October 19, 2016, Mercator Ocean delivers in~~
18 | ~~real-time daily services (weekly analyses and daily 10-day forecasts) with a new global $1/12^\circ$~~
19 | ~~system PSY4V3R1 (hereafter PSY4V3, and corresponding to HRG_V2V3 in Fig. 1). Note~~
20 | ~~that PSY4V3 will be the system for the CMEMS V4 milestone.~~ In this system PSY4V3, the
21 | ocean/sea ice model and the assimilation scheme benefit of from the following main updates:
22 | atmospheric forcing fields are corrected at large-scale with satellite data; freshwater runoff
23 | from ice sheets melting is added to river runoffs; a time varying global average steric effect is
24 | added to the model sea level; the last version of GOCE geoid observations are taken into
25 | account in the Mean Dynamic Topography used for Sea Level Anomalies assimilation;
26 | adaptive tuning is used on some of the observational errors; a dynamic height criteria is added
27 | to the Quality Control of the assimilated temperature and salinity vertical profiles; satellite sea
28 | ice concentrations are assimilated; and climatological temperature and salinity in the deep
29 | ocean are assimilated below 2000 m to prevent drifts in those very sparsely observed depths.

30 | The impact of all these updates can be evaluated separately, thanks to an incremental
31 | implementation, taking advantage of Mercator Ocean's specific hierarchy of system
32 | configurations running with identical set up. To this aim, short simulations (from one year to

1 a few years) were performed by adding from one simulation to another one upgrade at a time,
2 using the IRG configuration or some high resolution ~~1/12°~~ regional configuration.

3 The system PSY4V3 was run over the October 2006 - October 2016 period to catch-up the
4 real-time, assimilating the “reprocessed” observationsdatabases (along track altimeter,
5 satellite sea surface temperature, sea ice concentration and in situ temperature and salinity
6 vertical profiles) available at that time, and the so-called "near real-time"
7 observationsdatabases otherwise. Moreover, in the development phase of ~~an~~ the operational
8 system PSY4V3, it was decided to systematically perform ~~two other~~ three twin numerical
9 simulations over ~~a given~~ the same time period, maintaining the same ocean model tunings but
10 varying the complexity and the level of data assimilation. -The first one is a free simulation
11 (without any data assimilation) and the second one only benefits from temperature and
12 salinity large-scale biases correction using in situ observed temperature and salinity vertical
13 profiles. Inter-comparisons between the three simulations were then conducted in order to
14 better analyze and to try to quantify the impact of some component of the assimilation system.
15 These three versions of system have ~~also~~ been used to quantify the impact of some updates.

16 In a previous paper (Lellouche et al., 2013), the main results of the scientific evaluation of
17 MyOcean global monitoring and forecasting systems at Mercator Ocean showed how
18 refinements or adjustments to the system impacted the quality of ocean analyses and
19 forecasts. The primary objective of this paper is to describe the recent updates applied to the
20 system PSY4V3 and ~~.-The updates-~~ showing the highest impact on the products quality.
21 Updates resulting from routine system improvements are not separately illustrated and
22 discussed (bathymetry, runoffs, assimilated databases, Mean Dynamic Topography, etc.). -are
23 separately illustrated and discussedSo, , -with- a particular focus was given to ~~on~~ the
24 initialization, the correction of precipitation, the assimilation of climatological temperature
25 and salinity in the deep ocean, the construction of the ~~background~~ forecast error covariance
26 and the adaptive tuning of observations error. Another objective of this paper is to present a
27 first level evaluation of the system. The purpose here is not to perform an exhaustive
28 validation but only to check the global behavior of the system compared to assimilated
29 quantities or independent observations. Thus, an assessment of the hindcasts (2007-2016)
30 quality is conducted and improvements with respect to the previous system are highlighted in
31 order to show the level of performance and the reliability of the system PSY4V3. A
32 complementary study aimed at demonstrating the scientific value of PSY4V3 for resolving
33 oceanic variability at regional and global scale (Gasparin et al., 2018 – In revision in Journal

1 of Marine Systems). Lastly, several scientific studies have investigated local ocean processes
2 by comparing the PSY4V3 system with independent observations campaigns (Koenig et al.,
3 2017; Artana et al., 2018). This reinforces the system PSY4V3 evaluation effort.

4 This paper is organized as follows. The main characteristics of the system PSY4V3 and
5 details concerning the updates are described in Sect. 2. The impact of ~~the most~~some sensitive
6 upgrades is shown in Sect. 3. Results of the scientific evaluation, including some comparisons
7 with independent observations, are given in Sect. 4. Section 5 contains a summary of the
8 scientific assessment, as well as a discussion of the future improvements for the next version
9 of the global high resolution system.

12 **2 Description of the current global high resolution monitoring and** 13 **forecasting system PSY4V3**

14 This section contains the main characteristics of the CMEMS system PSY4V3 and details the
15 last updates to the system compared to the previous system PSY4V2R2 (hereafter PSY4V2,
16 see Fig. 1 and Table 2). A detailed description of ~~the main~~some sensitive updates is provided
17 in Sect. 3.

18 **2.1 Physical model and latest updates**

19 The system PSY4V3 uses version 3.1 of the NEMO ocean model (Madec et al., 2008). This
20 NEMO version is available since a few years and has been already used in the previous
21 system PSY4V2. ~~This was the available stable version of the code when we started the~~
22 ~~development of the system PSY4V3 a few years ago. Note that, using this version of the code,~~
23 ~~we do not access better algorithms and more sophisticated parameterizations present in the~~
24 ~~version 3.6 that is the latest official release~~current of NEMO 3.6 stable version that is now the
25 ~~standard version of the code. However, all the schemes and the parameterizations used in this~~
26 ~~version are still available in the current NEMO 3.6 stable version that is now the standard~~
27 ~~version of the code.~~The physical configuration is based on the tripolar ORCA12 grid type
28 (Madec and Imbard, 1996) with a horizontal resolution of 9 km at the equator, 7 km at Cape
29 Hatteras (mid-latitudes) and 2 km toward the Ross and Weddell seas. Z-coordinates are used
30 on the vertical and tThe 50-level vertical discretization retained for this system has a
31 decreasing resolution from 1m at the surface to 450 m at the bottom, and 22 levels within the

1 upper 100 m. A “partial cells” parameterization (Adcroft et al., 1997) is chosen for a better
2 representation of the topographic floor (Barnier et al., 2006) and the momentum advection
3 term is computed with the energy and enstrophy conserving scheme proposed by Arakawa
4 and Lamb (1981). The advection of the tracers (temperature and salinity) is computed with a
5 total variance diminishing (TVD) advection scheme (Levy et al., 2001; Cravatte et al., 2007).
6 We use a free surface formulation. External gravity waves are filtered out using the Roullet
7 and Madec (2000) approach. A laplacian lateral isopycnal diffusion on tracers ($100 \text{ m}^2 \text{ s}^{-1}$) and
8 a horizontal biharmonic viscosity for momentum ($-2e10 \text{ m}^4 \text{ s}^{-1}$) are used. In addition, the
9 vertical mixing is parameterized according to a turbulent closure model (order 1.5) adapted by
10 Blanke and Delecluse (1993), the lateral friction condition is a partial-slip condition with a
11 regionalization of a no-slip condition (over the Mediterranean Sea) and the Elastic-Viscous-
12 Plastic rheology formulation for the LIM2 ice model (Fichefet and Maqueda, 1997) has been
13 activated (Hunke and Dukowicz, 1997). Instead of being constant, the depth of light
14 extinction is separated in Red-Green-Blue bands depending on the chlorophyll data
15 distribution from mean monthly SeaWIFS climatology (Lengaigne et al., 2007). The
16 bathymetry used in the system is a combination of interpolated ETOPO1 (Amante and Eakins,
17 2009) and GEBCO8 (Becker et al., 2009) databases. ETOPO1 datasets are used in regions
18 deeper than 300 m and GEBCO8 is used in regions shallower than 200 m with a linear
19 interpolation in the 200 - 300 m layer. Internal-tide driven mixing is parameterized following
20 Koch-Larrouy et al. (2008) for tidal mixing in the Indonesian Seas, as the system does not
21 represent explicitly the tides. The atmospheric fields forcing the ocean model are taken from
22 the ECMWF (European Centre for Medium-Range Weather Forecasts) IFS (Integrated
23 Forecast System). A 3 h sampling is used to reproduce the diurnal cycle. Momentum and heat
24 turbulent surface fluxes are computed from the Large and Yeager (2009) bulk formulae using
25 the following set of atmospheric variables: surface air temperature and surface humidity at a
26 height of 2 m, mean sea level pressure and wind at a height of 10 m. Downward longwave
27 and shortwave radiative fluxes and rainfall (solid + liquid) fluxes are also used in the surface
28 heat and freshwater budgets. Compared to the previous HRG system PSY4V2, the following
29 updates were done on the model part (see Table 2):

- 30 - The bathymetry used in the system benefited from a specific correction in the Indonesian
31 Sea inherited from the INDESO system (Tranchant et al., 2016).
- 32 - In order to solve numerical problems induced by the use of z-coordinates on the vertical
33 (Willebrand et al., 2001), a relaxation toward the World Ocean Atlas 2013 (version 2)
34 2005-2012 time period (hereafter WOA13v2,

1 https://data.nodc.noaa.gov/woa/WOA13/DOC/woa13v2_changes.pdf) temperature
2 (Locarnini et al., 2013) and salinity (Zweng et al., 2013) climatology has been added at
3 Gibraltar and Bab-el-Mandeb straits. Indeed, z-coordinates, compared to sigma, isopycnal
4 or hybrid coordinates, induce excessive numerical mixing over overflow sills (Winton et
5 al., 1998). For instance, Mediterranean overflow, without any relaxation, would settle at
6 an equilibrium depth of 800 m or so otherwise instead of 1100 m observed. Sigma
7 coordinates could indeed improve the representation of overflow processes but are likely
8 to induce other problems elsewhere due to sigma gradient pressure error over steep
9 topography or excessive diapycnal mixing in the interior (Marchesiello et al., 2009). For
10 Gibraltar (respectively Bab-el-Mandeb), the relaxation area is centered at 8° W, 35° N
11 (respectively 46° E, 12° N). At the center the relaxation time is 10 days (respectively 50
12 days). This time is increased up to infinity 4° (respectively 5°) away from the center. The
13 relaxation is not constant over the vertical. It is only applied below 500 m and it is
14 increased linearly between 500 to 700 m. Between 700 m and the bottom of the ocean the
15 coefficient value is unchanged.

- 16 - Surface wind stress computation should in principle consider wind speed relative to the
17 surface ocean currents (Bidlot, 2012; Renault et al., 2016). However, this statement
18 applies to a fully coupled ocean/atmosphere system, which is not the case for the present
19 system PSY4V3. Based on sensitivity experiments and following the results obtained by
20 Bidlot (2002), we pragmatically consider only 50 % of the surface model currents in the
21 wind stress computation.
- 22 - The monthly runoff climatology is built with data on coastal runoffs and 100 major rivers
23 from the Dai et al. (2009) database (instead of Dai and Trenberth (2002) for the system
24 PSY4V2). This database uses new data, mostly from recent years, streamflow simulated
25 by the Community Land Model version 3 (CLM3) to fill the gaps, in all lands areas except
26 Antarctica and Greenland. In addition, we built mean seasonal freshwater fluxes
27 representing Greenland and Antarctica ice sheets and glaciers runoff melting. For this
28 purpose we have distributed the following mean values: 545 Gt yr⁻¹ for Greenland and
29 2400 Gt yr⁻¹ for Antarctic (corresponding to freshwater fluxes of 1.51 mm yr⁻¹ and 6.65
30 mm yr⁻¹ respectively). These values are in the range of estimations given by the IPCC-
31 AR13 (Church et al., 2013). They have been applied along Greenland and Antarctica
32 coastlines, and over an open ocean ~~mean values, 1.51 mm yr⁻¹ for Greenland and 6.65~~
33 ~~mm yr⁻¹ for Antarctica, onto a~~ domain varying seasonally and defined by the
34 climatological presence of icebergs observed by the Altiberg icebergs database project

1 (Tournadre et al., 2013). Domain covered by giant icebergs from Silva et al. (2006)
2 comple~~ment~~tes southern most areas not covered by Altiberg data. One third of these
3 quantities is applied off shore and two third along Greenland and Antarctic coastlines. We
4 also used ~~negative variations of water masses estimated from GRACE negative gridded~~
5 ~~GRACE anomalies~~ (Bruinsma et al., 2010) to distribute spatially these runoffs along
6 coastlines.

- 7 - As the Boussinesq approximation is applied to the model equations, conserving the ocean
8 volume and varying its mass, the simulations do not properly directly represent the global
9 mean steric effect on the sea level (Greatbatch, 1994). For improved consistency with
10 assimilated satellite observations of sea level anomalies, which are unfiltered from the
11 global mean steric component, a time-evolving global average steric effect is added to the
12 sea level in the simulation. This global average steric effect has been computed as the
13 difference between two successive daily global mean dynamic heights (vertical
14 integration, from the surface to the bottom, of the specific volume anomaly).
- 15 - Due to large known biases in precipitations (Stephens et al., 2010; Kidd et al., 2013), a
16 satellite-based large-scale correction of precipitations has been performed, except at high
17 latitudes (poleward of 65° N and 60° S). This is detailed in Sect. 3.
- 18 - In order to avoid mean sea-surface-height drift due to the large uncertainties in the water
19 budget closure, the following two treatments were applied:
 - 20 o The surface freshwater global budget ~~has been is~~-set to an imposed seasonal cycle
21 (Chen et al., 2005). Only spatial departures from the mean global budget are kept
22 from the forcing.
 - 23 o A trend of 2.2 mm yr⁻¹ has been added to the surface mass budget in order to
24 somewhat represent the recent estimate of the global mass addition to the ocean
25 (from glaciers, land water storage changes, Greenland and Antarctica ice sheets
26 mass loss) (Chambers et al., 2017). This term is implemented as a surface
27 freshwater flux in the open ocean domain infested by observed icebergs.

28 2.2 Data assimilation and latest updates

29 The data are assimilated by means of a reduced-order Kalman filter derived from a SEEK
30 filter (Brasseur and Verron, 2006), with a ~~three-dimensional 3D~~ multivariate modal
31 decomposition of the ~~backgroundforecast~~ error and a 7-day assimilation cycle. It includes an
32 adaptive-error estimate and a localization algorithm. This data assimilation system is called

1 SAM (Système d'Assimilation Mercator). The ~~backgroundforecast~~ error covariance is based
2 on the statistics of a collection of ~~three-dimensional~~^{3D} ocean state anomalies, ~~typically a~~
3 ~~few hundreds (250 anomalies for PSY4V3)~~. The anomalies are computed from a long
4 numerical experiment (~~2007-2015~~ 9-year period for PSY4V3) with respect to a running
5 mean in order to estimate the 7-day scale error on the ocean state at a given period of the year.
6 A Hanning low-pass filter is used to create the running mean with a cut-off frequency equal to
7 $1/24 \text{ days}^{-1}$. The background error covariances in SAM rely on a fixed basis, seasonally-
8 variable ensemble of anomalies. They also contain the inter-annual signal from the 9-year
9 simulation. This choice implies that, at each analysis step, a sub-set of anomalies (250
10 anomalies) is used to improve the dynamic dependency. A significant number of anomalies
11 are kept from one analysis to the other, thus ensuring error covariance continuity. Currently,
12 the anomalies used in real time come from the set of anomalies computed over the 2007-2015
13 period with no real time extension of this set. We therefore make the hypothesis that the set of
14 anomalies computed over a period prior to real time is able to represent correctly the
15 background error covariance over the real time period. Altimeter data, in situ temperature and
16 salinity vertical profiles, and satellite sea surface temperature and sea ice concentration are
17 jointly assimilated to estimate the initial conditions for numerical ocean forecasting. In
18 addition, a 3D-VAR scheme provides a correction for the slowly-evolving large-scale biases
19 in temperature and salinity (Lellouche et al., 2013).

20 Compared to the previous HRG system PSY4V2, the following updates were done on the data
21 assimilation part (see Table 2):

- 22 - CMEMS satellite ~~near real-time~~ sea ice concentration OSI SAF
23 ([http://marine.copernicus.eu/documents/QUID/CMEMS-OSI-QUID-011-001to007-](http://marine.copernicus.eu/documents/QUID/CMEMS-OSI-QUID-011-001to007-009to012.pdf)
24 [009to012.pdf](http://marine.copernicus.eu/documents/QUID/CMEMS-OSI-QUID-011-009to012.pdf)) is a new observation assimilated in the system PSY4V3. For this, a separate
25 monovariate/monodata analysis is carried out for the ice variables, in parallel to that for
26 the ocean. The two analyses are completely independent.
- 27 - CMEMS OSTIA SST (delayed time (reprocessed) until the end of 2006:
28 <http://marine.copernicus.eu/documents/QUID/CMEMS-OSI-QUID-010-011.pdf>, then
29 near real-time: [http://marine.copernicus.eu/documents/QUID/CMEMS-OSI-QUID-010-](http://marine.copernicus.eu/documents/QUID/CMEMS-OSI-QUID-010-001.pdf)
30 [001.pdf](http://marine.copernicus.eu/documents/QUID/CMEMS-OSI-QUID-010-001.pdf)) is assimilated in the system PSY4V3, instead of near real-time AVHRR SST
31 from NOAA in PSY4V2. A particular attention has been devoted to the computation of
32 the model equivalent. As OSTIA provides the foundation SST (considered nominally at
33 10 m depth), the SST model equivalent is performed by calculating the night-time average
34 of the first level of the model temperature. Moreover, only one SST map is assimilated on

1 [the fifth day of the 7-day cycle. Cloudy regions are filled by the analysis performed in](#)
2 [OSTIA product.](#)

- 3 - In addition to the quality control based on temperature and salinity innovation statistics
4 (detection of spikes, large biases), already present in the previous system, a second quality
5 control has been developed and is based on dynamic height innovation statistics (detection
6 of small vertically constant biases). This is detailed in Sect. 2.3.
- 7 - A new hybrid MDT, based on the “CNES-CLS13” MDT (Rio et al., 2014) with
8 adjustments made using the Mercator GLORYS2V3 (GLobal Ocean ReanalYsis and
9 Simulation – stream 2 – version 3) reanalysis and with an improved Post Glacial Rebound
10 (also called Glacial Isostatic Adjustment), has been used. This new hybrid MDT also
11 takes into account the last version of the GOCE geoid. This replaces the previous hybrid
12 MDT used in the previous system PSY4V2, which was based on the “CNES-CLS09”
13 MDT derived from observations (Rio et al., 2011). The new hybrid MDT significantly
14 reduces (not shown) sea level bias (more than 5 cm in some areas) and consequently
15 temperature and salinity in regions where the topography makes difficult the mean sea
16 surface estimation (e.g. Indonesia, Red Sea and Mediterranean Sea).
- 17 - A consistent along track SLA dataset
18 (<http://marine.copernicus.eu/documents/QUID/CMEMS-SL-QUID-008-032-051.pdf>),
19 with a 20-year altimeter reference period, is assimilated all along the simulation
20 performed with the system PSY4V3. [Reprocessed observations are assimilated until the](#)
21 [end of August 2015. Near real-time observations are assimilated afterward.](#)
- 22 - The CORA 4.1 CMEMS in situ [reprocessed](#) database (Szekely et al., 2016;
23 <http://marine.copernicus.eu/documents/QUID/CMEMS-INS-QUID-013-001b.pdf>) has
24 been assimilated for the 2006-2013 period. In addition to Argo and other in situ data sets,
25 this database includes temperature and salinity vertical profiles from sea mammal
26 (elephant seals) database (Roquet et al., 2011) to compensate for the lack of such data at
27 high latitudes. From 2014 to present, the near-real time CMEMS product
28 (<http://marine.copernicus.eu/documents/QUID/CMEMS-INS-QUID-013-030-036.pdf>) is
29 assimilated.
- 30 - As the prescription of observation errors in the assimilation systems is not sufficiently
31 accurate, adaptive tuning of observation errors for the SLA and SST has been
32 implemented. The method has been adapted from diagnostics proposed by Desroziers et
33 al. (2005) and is detailed in Sect. 3.

- 1 | - New three-dimensional~~3D~~ observation errors files for the assimilation of in situ
2 | temperature and salinity data have been re-computed from the MyOcean IRG system
3 | PSY3V3R3 (see Fig. 1 and Table 1) using an offline version of the adaptive tuning
4 | method mentioned above.
- 5 | - A weak constraint towards the WOA13v2 climatology on temperature and salinity in the
6 | deep ocean (below 2000 m) has been included in the two components (3D-VAR and
7 | SEEK filter) of the assimilation scheme to prevent drifts in temperature and salinity and as
8 | a consequence to obtain a better representation of the sea level trend at global scale in the
9 | system. The method consists in assimilating vertical climatological profiles of temperature
10 | and salinity at large scale and below 2000 m in regions drifting away from the
11 | climatological values, using a non-Gaussian error at depth. This is detailed in Sect. 3.
- 12 | - The time window for the 3D-VAR bias correction was reduced from 3 to 1 month to
13 | obtain a correction that is more in line with the current physics, which is made possible by
14 | the good spatial and temporal distribution of the Argo network from 2006.
- 15 | - In the previous system PSY4V2, the SSH increment was the sum of barotropic and
16 | baroclinic (dynamic) height increments as in Benkiran and Greiner, 2008. Dynamic height
17 | increment was calculated from the temperature and salinity increments, while the
18 | barotropic increment was an output of the analysis. Barotropic height was computed
19 | without the wind effect. In the system PSY4V3, we directly use the total SSH increment
20 | given by the analysis to take into account, among other things, the wind effect like the
21 | hydraulic control near the straits (Song, 2006; Menemenlis et al., 2007).
- 22 | - The uncertainties in the MDT estimate and the sparsity of the observation networks (both
23 | altimetry and in situ profiles) on the 7-day assimilation window do not allow to accurately
24 | estimate the observed global mean sea level. Moreover, the mean sea level time evolution
25 | is the result of an imposed trend for mass inputs (2.2 mm yr^{-1} , see Sect. 2.1) together with
26 | a diagnostic steric effect re-computed from model T and S. Therefore, the global mean
27 | increment of the total sea surface height is set to zero and the mean sea level is not
28 | controlled by data assimilation.
- 29 | - The background error covariance matrices needed for data assimilation are defined using
30 | anomalies of the different variables coming from a simulation in which only a 3D-VAR
31 | large scale bias correction of T, S has been performed (instead of using a free run- as was
32 | done in the previous system PSY4V2). This new approach is more consistent because it
33 | better mimics the final operational system, which uses also the 3D-VAR bias correction.
34 | Moreover, these anomalies, which are inputs of the analysis, -are spatially filtered in order

1 to retain only the effective model resolution and in order to avoid injecting noise in the
2 increments. This is detailed in Sect. 3.

3 **2.3 Additional Quality Controls on in situ observations**

4 To minimize the risk of erroneous observations being assimilated in the model, the system
5 PSY4V3 carries out two successive Quality Controls (QC1 and QC2) on the assimilated
6 temperature (T) and salinity (S) vertical profiles. These are done in addition to the quality
7 control procedures performed by the data producers. This observation screening is known as
8 background quality control. In both cases (QC1 and QC2), we estimate two parameters, which
9 are the mean and standard deviation of model innovations. These parameters are then used to
10 define space- and season-dependent threshold values which correspond to the mean plus N
11 times the standard deviation The N parameter is chosen empirically to reach a compromise
12 between rejecting a lot of profiles (if the criterion is too strict) and rejecting in average no
13 more than 1 % of profiles which are contained in the tails of the probability density function
14 of the innovations.

15 **2.3.1 Quality Control QC1**

16 The first quality control QC1 has been already described in Lellouche et al. (2013) and can be
17 summarized as follows. An observation is considered suspicious if the two following
18 conditions are both satisfied:

$$19 \quad \begin{cases} |innovation| > threshold \\ |observation - climatology| > 0.5 * |innovation| \end{cases} \quad (1)$$

20

21 where the spatially and seasonally varying *threshold* value comes from statistics (mean,
22 standard deviation) computed with the very large number of temperature and salinity
23 innovations collected in the Mercator GLORYS2V1 (GLobal Ocean ReanalYsis and
24 Simulation – stream 2 – version 1) reanalysis (1993-2009). The first condition of equation (1)
25 is a test on the innovation. It determines whether the innovation is abnormally large which
26 would most likely be due to an erroneous observation. The second condition avoids rejecting
27 “good” observations (i.e. an observation close to the climatology) even if the innovation is
28 high due to the model background being biased. This first quality control QC allows ~~the~~
29 detection of spikes and large biases.

1 2.3.2 Quality Control QC2

2 The second quality control QC2 is based on dynamic height innovation (vertical integration
 3 from the surface to the bottom) statistics and allows ~~detecting-detection of~~ small biases which
 4 are present ~~in~~ the whole water column, and thus can induce large errors. It basically says
 5 that the thermal or haline component of dynamic height innovation ($hdyn(innov_T)$ or
 6 $hdyn(innov_S)$) cannot exceed some threshold in height ($threshold_T$ for thermal component or
 7 $threshold_S$ for haline component). It can be summarized as follows. A vertical profile is
 8 rejected if the following condition is satisfied:

$$9 \quad \left\{ \begin{array}{l} \text{For temperature : } \frac{|c * hdyn(innov_T)|}{\sum dz_T} > threshold_T \\ \text{For salinity : } \frac{|c * hdyn(innov_S)|}{\sum dz_S} > threshold_S \end{array} \right. \quad (2)$$

10

$$11 \quad \text{where } \left\{ \begin{array}{l} c = 200 / \sum dz \quad \text{if } 0 < \sum dz \leq 200 \\ c = 500 / \sum dz \quad \text{if } 200 < \sum dz \leq 500 \\ c = \sum dz \quad \text{if } \sum dz > 500 \end{array} \right. \quad (3)$$

12

13 and dz_T is the model layer thickness corresponding to the temperature observation (same for
 14 dz_S and salinity). These last conditions (Eq. (3)) prevent the threshold from being reached too
 15 quickly in shallow areas.

16 The average and standard deviation of the thermal or haline components of dynamical height
 17 innovation have been calculated from a global simulation at $1/4^\circ$, which is a twin simulation
 18 of the PSY4V3 one. Note that the simulation at $1/4^\circ$ also assimilates the CORA 4.1 CMEMS
 19 in situ database. The temperature and salinity threshold ~~two-dimensional2D~~ fields used by
 20 QC2 are then computed as the average plus six times the standard deviation of the dynamical
 21 height innovations (Fig. 2). With these temperature and salinity thresholds, the system will
 22 reject more easily biased salinity profiles in the tropics and biased temperature profiles in
 23 strong currents.

24 It should also be noted that the QC2 quality control rejects the entire vertical profile while the
 25 QC1 quality control only rejects aberrant temperature and/or salinity values at some given
 26 depths on the vertical profile.

27 Figure 3a shows an example of a “wrong” temperature profile detected by the QC2 (and not
 28 by the QC1) at the end of July 2008. In this case, $threshold_T$ is equal to 0.3 m (Fig. 3b). The
 29 first condition of Eq. (2) is satisfied and the profile is rejected. When this profile is

1 assimilated (simulation without QC2), abnormal temperature RMS innovation values appear
2 at the temporal position (July 2008) of this profile in the Azores region (Fig. 3c). Using QC2
3 quality control allows solving the problem for this particular profile but also for some others
4 profiles (see Fig. 3c).

5 Statistics of the QC1 and QC2 quality controls are summarized in Fig. 4, where the
6 percentage of suspicious temperature and salinity profiles is given as a function of the year
7 over the 2007-2016 period. This percentage is relatively stable for both temperature and
8 salinity profiles, with little year-to-year variability, except for the years 2012 and 2013 where
9 more suspicious temperature and salinity profiles than usual were detected. Nevertheless, this
10 percentage remains relatively low (less than 0.35 % for temperature and 3.5 % for salinity),
11 knowing that the number of temperature profiles available each year ranges between 1.1
12 million and 1.7 million and the number of salinity profiles between 150,000 and 600,000.

14 **3 Impact of some sensitivemajor updates**

15 Most of the deficiencies in the systems can be related to these main recurring problems:
16 initialization, atmospheric forcing biases, abyssal circulation and efficiency of the
17 assimilation schemes. The first three problems are related to uncertainties in poorly observed
18 areas or parameters (i.e. deep ocean, ice thickness) and to intrinsic errors of the atmospheric
19 forcing. The last problem is related to linearity and stationarity hypotheses in the assimilation
20 schemes. In this section, we detail ~~the~~some solutions adopted for the system PSY4V3,
21 reducing uncertainties in the thermohaline component and allowing flow dependence in our
22 assimilation scheme. These solutions correspond to a part of the updates mentioned in section
23 2 and that do not result from routine system improvements.

25 **3.1 Initialization of oceanic simulation**

26 One way to initialize physical ocean model simulations is by using climatological values of
27 temperature and salinity from databases and assuming the velocity field is zero at the start.
28 The model physics then spins up a velocity field in balance with the density field. Another
29 common way to initialize a model is with fields from a previous run of that model, or with the
30 results from another model.

1 Given that data assimilation of the current observation network rapidly (in about ~~63~~ months)
2 adjusts the model state in the first 1000 m, the first solution has been chosen to ~~avoid~~
3 minimize potential drifts occurring after some years of simulation. Compared with the
4 previous system PSY4V2 starting in October 2012 from the WOA09 ~~three-dimensional3D~~
5 climatology (see Fig. 1), the PSY4V3 system starts in October 2006 using improved initial
6 climatological conditions. For that, we chose to use ENACT-ENSEMBLES EN4 1° global
7 product (Good et al., 2013) which consists in monthly objective analyses. The great interest of
8 these monthly fields is that a ~~three-dimensional3D~~ observation weight (between 0 and 1)
9 describes the influence of the observations for each field. This information helps to retain
10 only the observed points and not the perpetual climatology. This allows the computation of
11 validated trends for each month and of climatology for a particular date. For that, a pointwise
12 linear regression and in particular the Kendall's robust line-fit method (Hoaglin et al., 1983) is
13 used, allowing us to obtain an initial condition called "robust EN4" for any time based only
14 on real observations.

15 Two free simulations (without any data assimilation) have been performed with the system
16 PSY4V3, using either WOA09 or robust EN4 as initial condition in October 2006. Figure 5
17 shows the box-averaged innovations of temperature and salinity as a function of time and
18 depth over the October 2006 - December 2007 period. The top left panel reveals that, using
19 WOA09 as initial condition, a fresh bias appears in the first 100 meters of the innovation,
20 particularly more pronounced at the surface. It is not anymore the case when using robust
21 EN4 to initialize the model (top right panel). For temperature, the bottom left panel exhibits
22 cold biases above 100 m and below 300 m that are considerably reduced by using robust EN4
23 as initial condition (bottom right panel). The warm and salty bias between 200 m and 300 m is
24 slightly reinforced. ~~It mostly concerns the main thermocline whose motions are well~~
25 ~~correlated with the altimetry. but it concerns only the top 300 m and~~ this bias will be
26 corrected by the assimilation of altimetry and Argo profiles. Deeper biases are reduced with
27 this new initialization where Argo profiles are missing.

28 **3.2 Correction of precipitations**

29 Many studies (e.g. Janowiak et al., 1998; Janowiak et al., 2010; Kidd et al., 2013) have
30 compared reanalysis and atmospheric model precipitation fields with observation-based
31 datasets, and have shown that atmospheric model products always bring significant and
32 systematic errors, and are not able to close the global average freshwater budget. For instance,

1 Janowiak et al. (2010) found that the IFS operational model and ERA-Interim reanalysis (Dee
2 et al., 2011) from ECMWF perform well for temporal variability with respect to observational
3 datasets, but they globally overestimate the daily precipitations. Although progresses have
4 been made in the ECMWF forecast model, substantial errors still occur in the tropics (Kidd et
5 al., 2013). The correction of atmospheric forcing within ocean applications has already been
6 successfully explored by adjusting atmospheric fluxes via observational datasets in global
7 applications (Large and Yeager, 2009; Brodeau et al., 2010). Other studies only focused on
8 precipitation correction (Troccoli and Kallberg, 2004; Storto et al., 2012).

9 The proposed method in this paper consists of correcting the daily precipitation fluxes by
10 means of a monthly climatological coefficient, inferred from the comparison between the
11 Remote Sensing Systems (RSS) Passive Microwave Water Cycle (PMWC) product (Hilburn,
12 2009) and the IFS ECMWF precipitations. We use remote PMWC product because of its
13 relative high $1/4^\circ$ resolution able to represent more accurately narrow permanent features such
14 as the Intertropical Convergence Zone. The use of spatially varying monthly climatological
15 coefficient is justified by the fact that the inter-annual variability is well captured by the
16 ECMWF forecast model and allows us to apply the correction outside the special sensor
17 microwave/imager era. This latter assertion is a limitation of the method as it assumes the
18 operational ECMWF forecast model has a constant bias. In order to avoid discontinuities
19 when either PMWC or ECMWF products exhibit zero precipitation, e.g. in arid areas, we do
20 not apply any correction in monthly mean values less than 1 mm of rainfalls fluxes. Also, in
21 order to keep the more accurate small-scale signal from the high resolution forcing, the
22 correction is only applied to large-scale component obtained by a low-pass Shapiro filter.
23 Hilburn et al. (2014) provided accuracy of RSS over ocean rain retrievals validated against
24 well established long-term in situ datasets such as observations from Pacific Marine
25 Environment Laboratory rain gauges on moored buoys in the tropics. They found that on
26 monthly averages, the standard deviation between satellite and buoy is 15.5 %. The
27 differences are greatest in the Indian Ocean and Western Pacific. We then arbitrarily capped
28 the correction beyond 20 % in order to take into account these satellite-based retrievals errors.
29 Lastly, we did not apply the correction poleward 65° N and 60° S because of lack and
30 important biases of satellite-based precipitations estimate (Lagerloef et al., 2010) at high
31 latitudes.

32 Figure 6 represents the difference between the IFS precipitations coming from ECMWF and
33 the PMWC product using satellite data, before and after large scale correction. As already
34 pointed out by Stephens et al. (2010), original IFS forcings exhibit a systematic over-

1 estimation of precipitation within the inter-tropical convergence zones (up to 3 mm day⁻¹) and
2 under-estimation at mid- and high-latitudes (up to -4 mm day⁻¹). After correction, the mean
3 bias compared with PMWC is reduced from 0.47 to 0.19 mm day⁻¹.

4 To validate this correction, two global ocean hindcast simulations of several years, using only
5 the 3D-VAR large-scale biases correction in temperature and salinity, have been performed,
6 one with IFS correction and the other without. Figure 7 represents the mean surface salinity
7 innovation (difference between the assimilated observation and the model) on the year 2011.

8 At the global scale, the bias reduction is not very significant, but these maps demonstrate
9 that the IFS correction is beneficial in many local areas. The strongest benefice concerns the
10 Tropics where the IFS correction allows to ,reduc~~ing~~ing the magnitude of the near-surface
11 salinity fresh mean bias in the Tropics down to 0.5 psu. The fresh bias reduction in the
12 Tropics reaches 0.15 psu in average.

13 **3.3 Assimilation of climatological temperature and salinity climatology in the** 14 **deep ocean**

15 Due to unresolved processes (internal waves, spurious mixing in overflow regions, tidal
16 mixing) and inaccurate atmospheric forcing (bulk formulas), the model may drift at depth. The
17 model may exhibit significant drift at depth that can be related to the misrepresentation of
18 several processes for which an exhaustive list would be hard to give here. Difficulties
19 encountered by ocean model using z-coordinates in overflow regions are likely to be largely
20 responsible for this. In addition, Eulerian vertical coordinates (vs lagrangian, isopycnal
21 coordinates) may add a spurious diapycnal component in the interior where mixing is
22 essentially in the isopycnal direction. Lastly, the model lacks of an accurate interior mixing
23 scheme such as the one of De Lavergne et al. (2016) that does take into account internal tidal
24 wave mixing (tides are not explicitly resolved in PSY4V3). Interior mixing is indeed crudely
25 represented by spatially constant background diffusivity in the model.

26 -For systems which assimilate observations in a multivariate way, the problem can be more
27 critical because of the deficiencies of the background error covariances that may contain
28 spurious correlations for extrapolated and/or poorly observed variables. Unfortunately, there
29 are very few temperature and salinity profiles below 2000 m to constrain the model drift.
30 Hence, the climatology is currently the only source of information at depth to prevent the
31 model from drifting. Virtual vertical profiles of temperature and salinity below 2000 m are
32 built from the monthly WOA13v2 climatology. These virtual observations are geographically

1 positioned on the model horizontal grid with a coarse resolution ($1^\circ \times 1^\circ$) and on the model
 2 vertical levels from 2200 m to the bottom.

3 As in Greiner et al. (2006), we define empirically the standard deviations (departures from the
 4 climatology) σ_T for temperature and σ_S for salinity, as a simple linear vertical profile:

$$5 \quad \begin{cases} \sigma_T = \text{MAX} \left(\left(\frac{0.6-z/10^4}{3} \right); 0.05 \right) \\ \sigma_S = \sigma_T / 8 \end{cases} \quad (4)$$

6 where z is the depth (in meters).

7 We define then σ_{TS} the density departure from the climatology:

$$8 \quad \sigma_{TS} = \alpha \sigma_T + \beta \sigma_S \quad (5)$$

9 where α represents the thermal expansion coefficient and β the saline contraction coefficient.

10 Following Jackett and McDougall (1995), these coefficients are assumed to depend only on
 11 latitude and depth of the ocean as illustrated by Fig. 8.

12 If we note d_{TS} the density innovation, d the temperature or the salinity innovation and σ the
 13 temperature or the salinity departure from the climatology, the value of the climatological
 14 error e is prescribed as:

$$15 \quad \begin{cases} \text{If } |d_{TS}| \leq 2 \sigma_{TS} \text{ then } e = \infty \text{ (observation rejected)} \\ \text{If } |d_{TS}| > 2 \sigma_{TS} \text{ then } \begin{cases} \text{if } 2\sigma < |d| < 3\sigma \text{ then } e = \text{MIN} \left(\frac{2\sigma}{3} \left(\frac{|d|}{|d|-2\sigma} \right); 20\sigma \right) \\ \text{if } |d| \geq 3\sigma \text{ then } e = 2\sigma \\ \text{if } |d| \leq 2\sigma \text{ then } e = 20\sigma \end{cases} \end{cases} \quad (6)$$

16

17 A non-Gaussian error is used to impose a weak constraint on the model at depth (Fig. 9). That
 18 way, we correct the model drift without constraining a slow moderate variability or trend.
 19 Basically, the hypothesis is that small to medium departures from the climatology (2σ or less)
 20 has an even probability. For instance, a 0.2°C model warming at 2000 m due to a positive
 21 North Atlantic Oscillation pattern must not be corrected as zero. Indeed, a 0.2°C cooling is as
 22 likely as the warming, since the climatology is the time average of those anomalies. So, only
 23 large departures from climatology (3σ or more) should be corrected. It corresponds to highly
 24 unlikely events that are typical of model drifts. An interesting point is that model drift is often
 25 corrected locally, downstream the outflow, before it spreads out (see Fig. 10). Ideally, it gives
 26 a little regional correction instead of a large basin scale bias.

1 To validate this kind of assimilation, two global ocean simulations of several years, using
2 only the 3D-VAR large-scale biases correction in temperature and salinity, have been
3 performed. Due to the high computational cost of the system PSY4V3, the assimilation of
4 WOA13v2 below 2000 m has been tested with a global intermediate-resolution system at $\frac{1}{4}^\circ$,
5 which is, in all other aspects, very close to the high resolution system PSY4V3. All in situ
6 observations have been used as well.

7 In practice, the assimilation of WOA13v2 climatological profiles below 2000 m in the system
8 concerns mostly some regions where the steep bathymetry might be an issue for the model
9 (Kerguelen Plateau, Zapiola Ridge, and Atlantic ridge). Figure 10 shows mean temperature
10 (left) and salinity (right) innovations (WOA13v2 climatological profiles minus model) in
11 2013 at 2865 m. The assimilation of these climatological profiles occurs more or less at the
12 same locations over the time period 2007-2016. Since the conditions of the system of
13 equations (6) relate to the density innovation, we have a perfect symmetry of the temperature
14 and salinity data which are assimilated. This has the effect of not disturbing the density
15 gradients too much.

16 If we focus on latitudes between 30° S and 60° S, Fig. 11 represents temperature (top panels)
17 and salinity (low panels) annual anomalies over depth (500 - 5000 m) and time (2007-2014).
18 The simulation on the left does not assimilate climatological vertical profiles while the
19 simulation on the right assimilates some. These maps demonstrate that the assimilation of
20 WOA13v2 below 2000 m is beneficial, reducing drifts below 2000 m. In the Antarctic
21 Circumpolar Current (ACC), the assimilation of these profiles makes it possible to maintain,
22 for instance, the Antarctic Bottom Water (see Gasparin et al., 2018 – In revision in Journal of
23 Marine Systems). This also impacts the vertical repartition of the steric height, without
24 degrading the quality of the results comparing with profiles from the Argo network.

25 **3.4 Construction of the backgroundforecast error covariance**

26 The seasonally varying backgroundforecast error covariance is based on the statistics of a
27 collection of three-dimensional3D ocean state anomalies. This approach is based on the
28 concept of statistical ensembles in which an ensemble of anomalies is representative of the
29 error covariance. In this way, truncation no longer occurs and all that is needed is to generate
30 the appropriate number of anomalies. The way in which these anomalies are computed from a
31 long numerical experiment is described in Lellouche et al. (2013).

1 In this section, we detail two features of the system PSY4V3 compared to the previous system
2 PSY4V2, regarding the construction of the background error covariance. First, we evaluate
3 the impact of anomaly filtering on analysis increment. Second, we evaluate the potential
4 added value on the quality of the analysis increments of the choice of the simulation from
5 which to calculate the anomalies. -In the previous system PSY4V2, a free simulation was used
6 to calculate the anomalies. For the system PSY4V3, the anomalies are computed from a
7 simulation in which only a 3D-VAR large scale bias correction of T/S has been performed.~~In~~
8 ~~the following section, we evaluate the potential added value of this choice on the quality of~~
9 ~~the analysis increments.~~

10 **3.4.1 Anomaly filtering**

11 The signal at a few horizontal grid “ Δx ” intervals in the model outputs on the native full grid
12 is not physical but only numerical (Grasso, 2000) and should not be taken into account when
13 updating an analysis. This is why several passes of a Shapiro filter have to be applied at the
14 anomalies computation stage in order to remove the very short scales that in practice
15 correspond to numerical noise. This can also help to filter out the noise from the covariance
16 matrix due to the sampling error (Raynaud et al., 2009). Another way to remove the very
17 short scales would be to filter the analysis increments before injecting them into the model.
18 This choice would have led to a less optimal analysis and to a loss of balance between the
19 different components of the increment.

20 To illustrate the impact of the anomaly filtering, we set up some experiments with different
21 levels of filtering. Each experiment consists in the assimilation of a single altimeter track over
22 one assimilation cycle. These experiments have been performed with a Mercator Ocean
23 regional system at $1/36^\circ$ using the SAM data assimilation scheme, in order to reduce the high
24 computing cost of the global system PSY4V3 as well as the time consuming to build different
25 sets of anomalies at the global scale. Figure 12 shows SLA increments obtained with these
26 different levels of anomaly filtering. It should be noted that the anomaly filtering has a direct
27 effect on the analysis increment, since the latter is a linear combination of the anomalies.

28 Figure 12a represents SLA innovation along the single assimilated track. Figure 12b,c,d
29 represents the SLA increments obtained respectively with 10, 100 and 300 Shapiro passes as
30 the anomaly filtering mentioned above (corresponding approximately to a 3, 10 and 15
31 horizontal grid “ Δx ” intervals filter). We can see that the correction under the track remains

1 more or less the same. The strongest differences occur outside the track where the innovation
2 information is extrapolated.

3 Other experiments, closer to real-time integration set up have been performed, assimilating
4 all the altimeter tracks available on a 7-day assimilation window, instead of one single track.
5 Figure 13 shows the difference of SLA increments using 10 and 300 Shapiro passes as
6 anomaly filtering (corresponding approximatively to 20 km and 80 km). The conclusions are
7 the same as those concerning the experiments with a single assimilated track. The corrections
8 under the tracks remain almost the same for the two levels of filtering. Both analyses are close
9 to the data under the tracks. The strongest differences occur outside the tracks where the
10 innovation information is extrapolated to fill the gaps. Low filtered increments (10 Shapiro
11 passes) have small-scale structures that are statistical artifacts. Small structures can cascade in
12 the model, and stay trapped between the repetitive tracks, without correction by the
13 assimilation. This happens less when more filtering (300 Shapiro passes) is performed on the
14 anomalies beyond the effective resolution of the model.

15 **3.4.13.4.2 Choice of the simulation from which to calculate the anomalies**

16 The system PSY4V3 was run over the October 2006 – October 2016 period to catch-up the
17 real-time (“OPER” simulation), starting from ~~three-dimensional~~^{3D} temperature and salinity
18 initial conditions based on the EN4 climatology. This simulation benefited from the full data
19 assimilation system, including the 3D-VAR biases correction and the SAM filter. Two other
20 simulations over the same period have been performed. The first one is a “FREE” simulation
21 (without any data assimilation) and the second one has exactly the same model tunings but
22 only benefits from the temperature and salinity 3D-VAR large-scale biases correction
23 (“BIAS” simulation).

24 Figure 14 and Figure 15 show comparisons between this triplet of PSY4 simulations and two
25 observational products. The first product is the CMEMS/DUACS (Data Unification and
26 Altimeter Combination System) Merged-Gridded Sea Level Anomalies heights in delayed
27 time on a $\frac{1}{4}^\circ$ regular horizontal grid with a 1-day temporal resolution (Pujol et al., 2016). The
28 second one is the Roemmich-Gilson Argo monthly climatology on a 1° regular horizontal grid
29 (Roemmich and Gilson, 2009) which is commonly used in the oceanographic community.
30 Figure 14a,b,c shows the 2007-2015 SSH variability for the three simulations (subsamped in
31 a similar way to DUACS). SSH variability difference is defined as the difference of SSH
32 standard deviations from PSY4 simulations and the DUACS product (Fig. 14d,e,f).

1 Comparing to the variability of the DUACS product, the fronts in high mesoscale variability
2 regions such as the Gulf Stream, the Kuroshio, the Agulhas current or the Zapiola eddy are
3 misplaced in the FREE simulation. In the BIAS simulation, these fronts are better positioned
4 due to the large-scale correction of temperature and salinity. However, this simulation
5 presents more energy compared to DUACS, apart of the main fronts. This corresponds to a
6 leakage of vorticity from the fronts due to the mean advection. Note that the gridded DUACS
7 product also underestimates the variability as wavelengths smaller than 200 km are barely
8 resolved in the gridded fields. The effective resolution of DUACS product ranges from almost
9 500 km at the Equator to 150 km at high latitude. For OPER simulation, the effective
10 resolution is relatively similar or slightly larger in the inter-tropical band and almost 100 km
11 at high latitude. The mesoscale features are well constrained in the OPER simulation with the
12 information coming from satellite data.

13 Time-averaged density differences along the equatorial Pacific between two ENSO events
14 (“Oct-Dec 2008 minus Oct-Dec 2009”), computed from the PSY4 simulations and from the
15 Roemmich-Gilson Argo monthly Climatology, are shown in Fig. 15. The SCRIPPS Argo
16 product presents a higher density difference in the eastern part of the equatorial Pacific. It
17 corresponds to the change from moderate La Niña conditions early 2008 to moderate El Niño
18 conditions in 2009. The FREE simulation is not dense enough in the east compared to
19 observations particularly at the pycnocline depth (1025 kg/m^3 isopycn). The BIAS simulation
20 intensifies the density difference. The OPER simulation gets even closer to the SCRIPPS
21 Argo product. There is also an upward tilt of the density difference maximum in agreement
22 with the observations.

23 In summary, the BIAS simulation better represents the density fronts on the horizontal (Gulf
24 Stream) and on the vertical (Pacific pycnocline). The covariance matrix deduced from this
25 simulation has information on the density gradients that is well placed. This is valuable off the
26 equator through geostrophy, and at the equator to control the zonal pressure gradient. The
27 variance in sea level is stronger than the DUACS one (see Fig. 14e) but the most important
28 point for the construction of the anomalies is to have well-placed density gradients. In the
29 OPER simulation and as mentioned in Lellouche et al. (2013) in the description of the data
30 assimilation system SAM, an adaptive scheme will correct the variance and will give an
31 optimal background model error variance based on a statistical test formulated by Talagrand
32 (1998).

1 3.5 Adaptive tuning of observation errors

2 In order to refine the prescription of observation errors (instrumental and
3 representativenessity errors), adaptive tuning of ~~observation~~ errors for the SLA and SST has
4 been implemented in PSY4V3. We let “Talagrand method” (Talagrand, 1998) to adjust the
5 background error.– Instrumental error does no²t change with time. On the contrary, the
6 representativeness error is really flow-dependent. Taking into account the representativeness
7 error is particularly important for assimilated OSTIA SST because the sky is clear only 30%
8 of the time in average. The method has not been used for temperature and salinity vertical
9 profiles because of the reduced number of in situ data compared with satellite data. Then,
10 hree-dimensional~~3D~~ fixed observation errors are then used for the assimilation of in situ
11 temperature and salinity vertical profiles.

12 The method consists in the computation of a ratio, which is a function of observation errors,
13 innovations and residuals (Desroziers et al., 2005). It helps correcting inconsistencies on the
14 specified observation errors. This ratio can be expressed as:

$$15 \quad \mathit{ratio} = \frac{\mathit{residual}(\mathit{innovation})^T}{\mathit{observation\ error}} \quad (7)$$

16
17 Ideally, *ratio* is equal to ~~one~~one. When the ratio is less (respectively larger) than ~~one~~one, it means
18 that the observation error is overestimated (respectively underestimated). The objective of this
19 diagnostic is to improve the error specification by tuning an adaptive weight coefficient acting
20 on the error of each assimilated observation. As a first guess of the method, the initial
21 prescribed observation error matches the one used in the previous system (Lellouche et al.,
22 2013) where the observation error variance was increased near the coast and on the shelves
23 for the assimilation of SLA, and increased only near the coast (within 50 km of the coast) for
24 the assimilation of SST.

25 Figure 16 represents the temporal evolution of the ratio defined in Eq. (7) for Envisat satellite.
26 At the beginning of the simulation, the observation error is overestimated (ratio less than
27 ~~one~~one). The ratio tends to 1 after only a few weeks of simulation.

28 For SLA (Fig. 17), the a priori prescribed observation error is globally significantly reduced.
29 The median value of the error changed from 5 cm to 2.5 cm in a few assimilation cycles and
30 allows for better results. This method allows us to have more realistic and evolutive
31 observation error maps which can provide valuable information for the space agencies.

1 The realism of tropical oceans is crucial for seasonal forecasting applications. Tropical
2 Instability Waves (TIWs) can be diagnosed from SST (Chelton et al., 2000). These Kelvin
3 Helmholtz waves initiate at the interface between areas of warm and cold sea surface
4 temperatures near the Equator and form a regular pattern of westward-propagating waves.
5 Figure 18 gives an example of adjustment of the observation error to the model physics and
6 atmospheric variability. The SST anomalies in the equatorial Pacific clearly show the
7 propagation westwards of TIWs in the second half of the year. This is more pronounced
8 during episodes of La Niña (mid-2007 and mid-2010). The observation error anomalies
9 estimated by “Desroziers method” show that the error increases when these TIWs are more
10 marked. This can be explained two ways. First, the representativeness error increases because
11 the data is not corresponding exactly at the right time and the right position to the model
12 counterpart. In case of clouds, SST value can result from OSTIA time or space interpolation.
13 This would be detrimental with the fast propagation of TIWs. Second, large errors can result
14 of a by uncertainties in SST observations (clouds) and model shift of the TIWs structures. The
15 error decreases in the reverse case.

16 We have also performed an Empirical Orthogonal Function (EOF) analysis to assess the
17 variability of the SST observation error (Fig. 19). Mode 1 is associated to the seasonal cycle
18 and mode 2 (not shown) corresponds to the migration of the seasonal signal. Mode 3 is
19 associated to the inter-annual signal with for instance the transition La Niña / El Niño,
20 showing that the SST error is able to adapt both to the seasonal and inter-annual fluctuations.

21

22 **4 Scientific assessment**

23 This section describes the PSY4V3 system’s quality assessment with diagnostics over
24 particular years, together with time series over multiyear periods. To evaluate the quality of
25 the system, the departure from the assimilated observations (SST, SLA, T/S vertical profiles
26 and sea ice concentration) is measured. Moreover, the analyses are also compared with
27 observations that have not been assimilated by the system such as tide gauges, velocity
28 measurements from drifting buoys, NOAA SST and AMSR sea ice concentration. NOAA
29 SST and AMSR sea ice analyses are not fully independent, since the upstream observations
30 are the same than for assimilated CMEMS OSTIA SST and OSI Sea Ice concentrations, but
31 comparisons to a variety of estimates using different algorithms and protocols provides a
32 useful consistency analysis.

1 4.1 SST

2 4.1.1 Assimilated SST

3 The OSTIA product is assimilated in the system PSY4V3. Compared to the previous system
4 PSY4V2, some large scale cold biases with respect to OSTIA are reduced in the Indian,
5 Eastern South Pacific, and western North Pacific (not shown). On the other hand, warm biases
6 are not reduced, especially in regions of strong inter-annual warm events such as the Eastern
7 Tropical Pacific where strong El Niño took place in 2015/2016, but also in the ACC, the Gulf
8 Stream and the Greenland Current (Fig. 20a). Some inconsistencies can be found between
9 OSTIA SST and in situ near surface temperature, particularly in the North Pacific where the
10 system PSY4V3 presents a cold bias compared to in situ near surface temperature but a warm
11 bias compared to OSTIA SST (Fig. 20b). Figure 20c shows the difference between drifting
12 buoys SST and the system PSY4V3 over the year 2015. The drifting buoys SST data are
13 present in the CMEMS in situ database used by Mercator but they have not been assimilated
14 in the system because the depth of these data is a nominal value and we chose to assimilate
15 only data with a measured depth value. Although we plan to assimilate these data in the future
16 system, we use currently this data as independent information. This allows us to see that SST
17 from in situ vertical profiles and SST from drifting buoys are coherent with each other. We
18 thus find again the cold bias highlighted by the comparison with -SST from in situ vertical
19 profiles in the North Pacific. It is a lack of stratification in the model, which causes mid-
20 latitude cold surface biases during (boreal) summer and a warm bias between 50 m and 100
21 m.

22 We checked also the time series of the mean and the RMS of the misfit (innovation) between
23 the observed SSTs and the model. For OSTIA SST, which is the gridded SST assimilated in
24 PSY4V3, we obtain a mean warm bias of -0.1 °C and a RMS error of 0.45 °C (Fig. 21). Time
25 series of the differences between the model and NOAA AVHRR SST, which was assimilated
26 in the previous PSY4V2 system, are also shown on Fig. 21. This allows to compare both
27 gridded SST products. Seasonal fluctuations of the SST biases on global average can be seen
28 as a lack of stratification in the model, which causes stronger mid-latitude warm biases during
29 (boreal) summer (and a warm bias between 50 m and 100 m). For in situ SST, the bias is
30 smaller, suggesting that OSTIA and AVHRR might beare colder than in situ near surface
31 observations on global average. We can notice a drop in the RMS of in situ surface data in

1 | January 2014, which is due to the use of near real-time observations, where most of the
2 | surface observations do not have sufficient quality flag.

3 | **4.1.2 Comparison with an ~~independent~~ high resolution SST external product**

4 | CLS (Collecte Localisation satellites) operates since 2002 a near real-time oceanography data
5 | service named CATSAT, for scientific, institutional or private users (support to fishery
6 | management or to the offshore oil and gas industry). These data include satellite observations
7 | such as chlorophyll-a, SST and altimetry. Maps of SST are computed from Aqua/MODIS, S-
8 | NPP/VIIRS and Metop/AVHRR infra-red sensors at 2 km resolution, using nighttime data
9 | only to avoid diurnal warming effects. We can then evaluate the system ability to produce the
10 | mesoscale by comparing with the CATSAT daily SST product. On Fig. 22, the CATSAT
11 | daily snapshot can be considered as an independent dataset since the OSTIA SST assimilated
12 | in the system has mostly seen microwave measurements during two weeks, as it was very
13 | cloudy in the Gulf of Mexico. 31st of March 2016 is the first clear day showing well, from
14 | infrared measurements, the Loop Current and other structures in the western part of the Gulf
15 | of Mexico. The Loop Current is almost forming a closed meander. This is reproduced by the
16 | system PSY4V3, as well as secondary structures like the filament in the North (Fig. 22).
17 | Visible limitations of this 1/12° system concern the fine sub-mesoscale that can not be
18 | resolved, and the lack of tidal mixing along Yucatan coasts (Kjerfve, 1981).

19 | **4.2 Temperature and salinity vertical profiles**

20 | For the T/S vertical profiles, we checked time series of the RMS of the difference between the
21 | model analysis and the observations, for temperature on the left and for salinity on the right
22 | (Fig. 23) in the whole water column. We compare observation and – climatology (red line),
23 | the previous system PSY4V2 (blue line), and the new system PSY4V3 (black line).

24 | On global average, and compared to the previous system PSY4V2, the system PSY4V3
25 | slightly degrades the temperature statistics (-0.03 °C) but it significantly greatly improves the
26 | salinity statistics by decreasing the 0-5000 m RMS salinity by 0.1 psu. This allows-enables us
27 | to get a more accurate description of the water masses. This better balance arises from the
28 | new in situ errors that give more weight to the salinity data (not shown). We can also notice
29 | that the systems are always better than the climatology. The comparison to climatology is a
30 | minimum performance indicator that the system must achieve. The differences with the
31 | climatology are worse from the beginning of the year 2013. It can be explained by the fact

1 that six different decades of WOA13v2 monthly climatology can be found on the NODC
2 website from 1955 to 2012. We chose the available 2005-2012 “truncated decade” (near of
3 our time period simulation) even if it is biased to cold, given the strong La Niña event on
4 2010-2011. Previous decades (before 2005) are even colder and can no longer be used for
5 recent dates. Moreover, 2005-2012 “truncated decade” does no^t contain the period of
6 transition towards El Niño events and in particular the strong one occurring in 2015. So, in
7 situ temperature and salinity vertical profiles we assimilated in the system and which see this
8 transition are coherent with this WOA13v2 product until the end of year 2012 and this is no
9 longer the case afterward.

10 Moreover, the system PSY4V3 experiences a slight warm bias (negative observation minus
11 forecast difference) in subsurface (25 - 500 m) on global average (not shown). For the year
12 2015, part of this signal comes from the strong inter-annual ENSO signals in the Tropical
13 Pacific where the near surface bias is also warm, as well as in the ACC and the Gulf Stream.
14 Seasonal cold surface biases appear in the mid latitudes, linked with a lack of stratification
15 during summer. Summer warming is injected too deep ~~and-which~~ results in subsurface
16 spurious warming and ~~a too-shallow~~ mixed layer that is too shallow. However, these biases
17 remain small on global average.

18 4.3 Sea Level

19 4.3.1 Assimilated SLA

20 The system PSY4V3 is closer to altimetric observations than the previous one with a global
21 forecast RMS difference of around 6 cm instead of 7 cm for the system PSY4V2 (not shown).
22 This RMS difference is consistent with the prescribed a priori observations errors (about 2 cm
23 for altimeters instrumental error and 4 cm for MDT error in average). The statistics come
24 from the data assimilation innovations computed from the forecast used as the background
25 model trajectory, and give an estimate of the skill of the optimal model forecast. These scores
26 are averaged over all seven days of the data assimilation window, which means the results are
27 indicative of the average performance over the seven days, with a lead time equal to 3.5 days.

28 More precisely, on the year 2015, the SLA mean and RMS errors are considerably reduced in
29 the new system PSY4V3 compared to the previous one (Fig. 24). The mean bias is reduced by
30 0.3 cm (from -0.8 cm to 0.5 cm) and the RMS is reduced by 2.4 cm (from 7.9 cm to 5.5 cm).
31 This is mainly due to the use of the “Desroziers” method to adapt the observations errors

1 | online, which yields to more information from the observations being used (see Sect. 3.5).
2 | These improvements occur in nearly all regions of the ocean but are more pronounced in
3 | some regions (e.g. North Atlantic, Hudson Bay, Labrador Sea). In some others regions (e.g.
4 | Indonesian or west tropical Pacific), ~~it remains~~ some errors in sea level remain and are linked
5 | to the uncertainty in the MDT or missing parametrisations in the model (interaction wave-
6 | current, tides).

7 | **4.3.2 Comparison to tide gauge data**

8 | The system PSY4V3 produces hourly outputs at the surface that can be compared with tide
9 | gauge measurements. For that, we used the BADOMAR product ([Lefevre et al., 2005](#)) which
10 | is a specific processed tide gauges database developed and maintained at CLS and consists of
11 | filtered tide gauge data from the GLOSS/CLIVAR ([Global sea Level Observing](#)
12 | [System/Climate Variability and Predictability](#)) “fast” sea level data tide gauge network
13 | ([GLOSS Implementation Plan, 2012](#)). These tide gauge data are corrected from inverse
14 | barometer effect and tides. High frequency model SSH compares well with tide gauges in
15 | many places, with a slight improvement in PSY4V3 with respect to PSY4V2 (not shown).
16 | The best agreement between the system PSY4V3 and tide gauges is found in the tropical
17 | band, as can be seen in Fig. 25, while shelf regions and closed seas are less accurate. This
18 | confirms the latitude dependence of the correlation between tide gauges and satellite altimetry
19 | or modelled SSH discussed in Vinogradov and Ponte (2011) or Williams and Hugues (2013).

20 | The improvements related to water masses and SLA lead to a correct Global Mean Sea Level
21 | (GMSL) trend. We checked the system GMSL by comparing the results with recent estimated
22 | trend from the paper of Chambers et al. (2017). We found for the model a trend of 3.2 mm yr⁻¹
23 | over the PSY4V3 simulation time period which is coherent with DUACS value (3.17 ± 0.67
24 | mm yr⁻¹). Moreover, the temporal evolution of the global mean model SSH is coherent and
25 | phased with the observations.

26 | **4.4 Sea ice concentration**

27 | **4.4.1 Assimilated sea ice concentration**

28 | The system PSY4V3 assimilates OSI SAF sea ice concentration in both hemispheres with a
29 | monovariate/monodata scheme. As expected, PSY4V3 is closer to the observations than the
30 | previous system PSY4V2 (not shown), in which no sea ice observations had been assimilated.
31 | As illustrated by Fig. 26, the system PSY4V3 has a slight overestimation of ice during the

1 melting season in summer (up to 3 % on average in both hemispheres). Conversely, the mean
2 error is stronger on average during winter (10 to 20 % underestimation, depending on the
3 year). RMS errors are also larger during summer (up to 20 % in the Arctic and 30 % in the
4 Antarctic with respect to OSI SAF observations), and they drop to less than 10 % in winter.
5 These RMS errors quantify the capacity of the system to capture weekly time changes in the
6 ice cover.

7 We have also checked the evolution of the sea ice volume diagnosed by the system PSY4V3
8 ~~which assimilates observations of sea ice concentration with a monovariate/monodata~~
9 ~~scheme~~. The data assimilation scheme SAM produces increment of sea ice concentration
10 which is the unique sea ice correction applied in the model using the Incremental Analysis
11 Update (IAU) method described in Lellouche et al. (2013). The sea ice volume then adjusts to
12 this correction considering a constant sea ice thickness. No sea ice thickness observations are
13 assimilated in the system. The risk is therefore to obtain unrealistic drifts or trends of the
14 unconstrained sea ice volume. Presently, sea ice volume retrievals from satellites are
15 associated with large uncertainties (Zygmuntowska et al., 2014). Consequently, modelled sea
16 ice volume is difficult to validate and one of the solutions is to compare modelled sea ice
17 volume from several systems.

18 Figure 27 shows the 2007-2016 evolution of sea ice volume for the system PSY4V3, the
19 PIOMAS modelled product (Schweiger et al., 2011) and the CMEMS GREP (Global
20 Reanalysis Ensemble Product, [http://marine.copernicus.eu/documents/QUID/CMEMS-GLO-](http://marine.copernicus.eu/documents/QUID/CMEMS-GLO-QUID-001-026.pdf)
21 [QUID-001-026.pdf](http://marine.copernicus.eu/documents/QUID/CMEMS-GLO-QUID-001-026.pdf)) composed by four global $\frac{1}{4}^\circ$ reanalyses and the ensemble mean with the
22 associated spread from the four members. All the modelled sea ice volumes present the same
23 2007-2016 inter-annual variability. PSY4V3 and PIOMAS are included in the spread whose
24 range ~~is reduced/decreases~~ over time from 4,000 km³ in 2007 to 3,000 km³ ~~from the year in~~
25 ~~2012 and remains almost constant afterward~~. The GLORYS2V4 reanalysis is known to have a
26 large sea ice volume compared to other reanalyses (Chevallier et al., 2017). Although we use
27 the same method for the assimilation of sea ice concentration in GLORYS2V4 and PSY4V3,
28 the sea ice volume diagnosed by PSY4V3 lies in values ranging between 13,000 and 15,800
29 km³, in a better accordance with GREP and PIOMAS products.

30 **4.4.2 Contingency table analysis**

31 The contingency table analysis approach described in Smith et al. (2016) has been applied to
32 evaluate sea ice extent as compared to observation. Satellite ice concentration coming from

1 AMSR2 (L1B brightness with a NASA team 2 algorithm to compute sea ice concentration)
2 has been used as independent observation to provide a general assessment in the detection of
3 false alarms if ice coverage. Although this type of evaluation is usually done on forecasts, we
4 used hindcasts. For the computation of the statistics we have used a stereo-polar grid at a 20
5 km resolution. In each cell of that grid we have then computed binary values corresponding to
6 ice/open water conditions for the model and the sea ice observations by using a 40 %
7 concentration threshold. We have also restricted our study to the Proportion Correct Total
8 (PCT), following the conclusion of Smith et al. (2016), saying that it was more insightful to
9 refer to the PCT rather than others proportions. The PCT quantity is defined as $PCT = (\text{Hit ice} + \text{Hit water})/n$ (see Table 3), where n is the total number of observations with a sea ice
10 concentration greater than 15 %. A value of one corresponds to a perfect score.
11

12 Figure 28 shows times series of PCT for PSY4V2 and PSY4V3 systems. The lower PCT
13 values are due mostly to an excessive melt in spring and summer for both Arctic and
14 Antarctic. However, the assimilation of sea ice concentration improves significantly the total
15 hit rate during these periods.

16 4.5 Currents

17 The aim of this section is to use velocity observations which were not assimilated in the
18 system to assess the level of performance of PSY4V3 compared to the previous PSY4V2
19 system. The mean currents are checked by comparing the model to velocity observations
20 coming from Argo floats when they drift at the surface and in situ Atlantic Oceanographic
21 and Meteorological Laboratory (AOML) surface drifters. A paper by Grodsky et al. (2011)
22 revealed that an anomaly in the drogue loss detection system of the Surface Velocity Program
23 buoy had led to the presence of undetected undrogued data in the “drogued-only” dataset
24 distributed by the Surface Drifter Data Assembly Center. Rio (2012) applied a simple
25 procedure using altimeter and wind data to produce an updated dataset, including a drogue
26 presence flag as well as a wind slippage correction. ~~Therefore, We therefore we~~ used this new
27 “drogued-only” surface drifter dataset coming from CMEMS in situ TAC ([Rio and Etienne,](http://marine.eopernicus.eu/documents/QUID/CMEMS-INS-QUID-013-044.pdf)
28 [2017http://marine.eopernicus.eu/documents/QUID/CMEMS-INS-QUID-013-044.pdf](http://marine.eopernicus.eu/documents/QUID/CMEMS-INS-QUID-013-044.pdf)) to
29 check mean model currents.

30 Figure 29 represents zonal drift innovation for PSY4V2 and PSY4V3 systems. Although
31 some biases persist, mostly in the western tropical basins, significant improvements are
32 obtained almost everywhere with the new system PSY4V3, and more particularly in the

1 equatorial Pacific. The mean bias is reduced (from 0.1 m s^{-1} to 0.08 m s^{-1}), the South
2 Equatorial Current is slower and there is also less noise in PSY4V3. Improvements are also
3 obtained, to a lesser extent, for meridional drift (not shown). The velocities have been slightly
4 improved in terms of velocity values but also in terms of currents direction (angle between
5 observed and modelled velocities). The mean angle difference is reduced from 9.1 degrees to
6 7.2 degrees. These improvements can be attributed to the new MDT used and the more
7 adapted filtering of anomalies. However, large biases persist in the western tropical Pacific
8 (very strong in 2015 because of the strong El Niño event) with a spurious extension of the
9 northern branch of the South Equatorial Current. This is probably linked to the uncertainty
10 still present in the MDT and unresolved or missed parameterized physical processes.

11 More locally, a comparison of the 2007-2015 averaged drifts from the system PSY4V3 and
12 the observations over the Indonesian region has been performed (not shown). Currents in this
13 region are very difficult to resolve because of the many narrow straits and the strong tidal
14 mixing. The retroflexion of the westward South and North Equatorial Currents (along Papua
15 and near 12° N) into the eastward North Equatorial Counter Current (near 4° N) are well
16 reproduced structures in the Pacific. The system South Equatorial Current is a little too strong
17 at the edge of the warm pool but it is about the only weakness. The complex flow in the
18 Sulawesi Sea, the Makassar Strait and the South China Sea is also well reproduced by the
19 system. The correlation is 0.70 (respectively 0.64) for the zonal (respectively meridional)
20 velocity.

21 **5 Summary and ways for improvement of the future system**

22 The Mercator Ocean system PSY4V3, in an operational mode since October 19, 2016,
23 benefits of many important updates. PSY4V3 has a quite good statistical behaviour with an
24 accurate representation of the water masses, the surface fields and the mesoscale activity.
25 Most of the components of the system PSY4V3 have been improved compared to the
26 previous version: global mass balance, three-dimensional~~3D~~ water masses, sea level, sea ice
27 and currents. Major variables like sea level and surface temperature are hard to distinguish
28 from the data.

29 In this paper, the updates showing the highest impact on the products quality and that do not
30 result from routine system improvements, have been illustrated and evaluated separately. A
31 particular focus was therefore made on the initialization, the correction of precipitation, the

1 assimilation of climatological temperature and salinity in the deep ocean, the construction of
2 the ~~background~~~~forecast~~ error covariance and the adaptive tuning of observations error.

3 Initial climatological condition has been improved in order to be more consistent with the
4 vertical profiles of temperature and salinity which has been assimilated thereafter. Rather than
5 taking directly the climatological temperature and salinity of the month corresponding to the
6 start of the simulation, we performed a pointwise linear regression, allowing to obtain an
7 initial condition at the appropriate time and based only on real observations. One-year free
8 simulations have been performed and show that biases are globally reduced.

9 Uncertainties inherent to atmospheric analyses and forecasts can induce large errors in the
10 ocean surface fluxes. For instance a slight shift in the position of a storm can induce local
11 errors in salinity, temperature and currents. In the tropical band, precipitations are
12 systematically overestimated. Moreover, large scale salinity biases can appear because the
13 global average freshwater budget is not closed. For this reason, IFS ECMWF atmospheric
14 analysed and forecasted precipitations have been corrected at large scale using satellite-based
15 PMWC product. This correction is beneficial in many areas, reducing the magnitude of the
16 near-surface salinity fresh mean bias in the Tropics down to 0.5 psu. This surface fresh bias
17 reduction in the Tropics reaches 0.15 psu in average.

18 Due to ~~misun~~resolved processes ~~es and inaccurate atmospheric forcing~~, the model may also drift
19 at depth. To keep some water mass properties, the DRAKKAR group used restoring of
20 temperature and salinity toward annual climatology of Gouretski and Koltermann (2004) in
21 specific areas. This choice was driven by the Antarctic Bottom Water restoring zone where
22 this climatology is recognized as the more suitable. For Mercator systems which assimilate
23 observations in a multivariate way, the problem can be more critical because of the
24 deficiencies of the background errors for extrapolated and/or poorly observed variables. To
25 overcome these deficiencies, vertical climatological T/S profiles have been assimilated below
26 2000 m using a non-Gaussian error at depth, allowing the system to capture a potential
27 climate drift in the deep ocean. In practice, the assimilation of climatological profiles below
28 2000 m in the system PSY4V3 concerns mostly some regions where the steep bathymetry
29 might be an issue for the model (Kerguelen Plateau, Zapiola Ridge, and Atlantic ridge). This
30 kind of assimilation reduces drifts below 2000 m and impacts the vertical repartition of the
31 steric height, without degrading the quality of the results comparing with the profiles from the
32 Argo network.

1 We have also proposed solutions to reduce some problems related to linearity and stationarity
2 hypotheses in the assimilation schemes. The first one concerns the construction of the
3 ~~background~~~~forecast~~ error covariance. Rather than calculating the anomalies from a free
4 simulation, we chose to calculate them from a simulation benefiting only of the 3D-VAR
5 large-scale biases correction in temperature and salinity and representing better the density
6 fronts on the horizontal and on the vertical. Moreover, anomalies have been filtered in order
7 to remove the scales beyond the effective resolution of the model. The second one concerns
8 the tuning of the observations errors. Adaptive tuning of SLA and SST errors has been
9 successfully implemented. It allows us to have more realistic and evolutive SLA and SST
10 error maps.

11 All these scientific and technical choices have been validated and integrated in the system
12 PSY4V3 which has been evaluated for the period 2007-2016 by means of a thorough
13 procedure involving statistics of model departures from observations. The system PSY4V3 is
14 close to SLA along track observations with a forecast (range 1 to 7 days) RMS difference
15 below 6 cm. Moreover, the correlation of the system PSY4V3 with tide gauges is significant
16 at all frequencies, however many high frequency fluctuations of the SSH might not be
17 captured by the system because tides or pressure effects are not yet included. The description
18 of the ocean water masses is very accurate on average and departures from in situ
19 observations rarely exceed 0.5 °C and 0.1 psu. In the thermocline, RMS errors reach 1 °C and
20 0.2 psu. In high variability regions like the Gulf Stream, the Agulhas Current or the Eastern
21 Tropical Pacific, RMS errors reach more than 2 °C and 0.5 psu locally. A warm bias persists
22 in subsurface, with peaks in high variability regions such as the Eastern Tropical Pacific, Gulf
23 Stream or Zapiola. Most departures from observed SST products do not exceed the intrinsic
24 error of these products (around 0.6 °C).

25 A global comparison with independent velocity measurements (surface drifters) shows that
26 the location of the main currents is very well represented, as well as their variability.
27 However, surface currents of the mid latitudes are underestimated on average. The
28 underestimation ranges from 20 % in strong currents to 60 % in weak currents. Some
29 equatorial currents are overestimated, and the western tropical Pacific still suffer from biases
30 in surface currents related to MDT biases. On the contrary the orientation of the current
31 vectors is better represented.

32 Lastly, the system reproduces the sea ice seasonal cycle in a realistic manner. However,
33 ~~compared to assimilated data, the~~ sea ice concentrations ~~is slightly~~~~are~~ overestimated in ~~the~~

1 ~~Arctic mainly during winter seasons (due to atmospheric forcing errors and too much sea ice~~
2 ~~accumulation) and in the Antarctic during austral winter. They are and~~ underestimated during
3 ~~austral summer seasons (too much sea ice melt and errors caused by the rheology~~
4 ~~parameterization of the sea ice model).~~ A contingency table analysis approach has been also
5 used to evaluate sea ice extent as compared to observations. This approach shows clear
6 improvements due to the assimilation of sea ice concentration in the system PSY4V3.
7 Remarkable improvements have been achieved with the system PSY4V3 compared to the
8 previous version. However, some biases have been highlighted in the ocean surface features
9 as well as the ~~three-dimensional~~^{3D} ocean structure at basin, sub-basin and local scales. The
10 simulation biases may be due to the initial state (especially in the deep layer where historical
11 observation data are rare), the atmospheric forcing uncertainties, the river runoff
12 approximations, the efficiency of the assimilation scheme, and the model errors induced by
13 unresolved or parameterized physical processes. Numerous projects have already been set up
14 at Mercator Ocean to propose innovative solutions. The integration of the ingredients from
15 these projects into the future CMEMS global high resolution system is planned for 2019. The
16 improvement of numerical simulations could thus be carried out, based on sensitivity ~~tests~~
17 experiments on some model parameters (e.g. coastal runoffs, atmospheric forcing, high
18 frequency phenomena including tides, ~~more sophisticated~~multi-category sea ice model,
19 interaction and retroaction between ocean currents and waves, vertical mixing and advection
20 scheme). Better algorithms and more sophisticated parameterizations already available in the
21 version 3.6 of the NEMO code should help in the future to resolve issues related to important
22 ocean processes and to reduce model biases. It is also planned to assimilate new types of
23 observations in the system (drifting buoys SST, higher resolution SST (L3 products), satellite
24 sea surface salinity, velocity observations from AOML surface drifters, and deep-ocean
25 observations from Argo surface floats) to better constrain the modeled variables and to
26 overcome the deficiencies of the background errors in particular for extrapolated and/or
27 poorly observed variables. Another important issue is to use a shorter assimilation time
28 window and a 4D analysis in the assimilation scheme to better correct the fast evolving
29 processes. The next version of the global high resolution system will also include seasonal
30 errors for in situ vertical profiles already used in the CMEMS eddy-resolving 1992-2016
31 reanalysis GLORYS at 1/12° horizontal resolution, which is based on the system PSY4V3
32 and ~~will appear~~ed on CMEMS catalogue in April 2018.

Acknowledgements

This study has been conducted using E.U. Copernicus Marine Service Information. The authors thank Luc Vandembulcke and the anonymous reviewer for their careful reading and for providing very constructive comments which improved the manuscript. Special thanks to our Mercator Océan colleague Jérôme Chanut for his help to answer to the questions regarding the specifics of the NEMO code.

References

Amante, C. and Eakins, B. W.: ETOPO1 1 Arc-minute global relief model: procedures, data sources and analysis, NOAA Technical Memorandum NESDIS NGDC-24, 25 pp., 2009.

Arakawa, A. and Lamb, V. R.: A potential enstrophy and energy conserving scheme for the shallow water equations, Mon. Weather. Rev., 109, 18–36, 1981.

Artana, C., Lellouche, J-M., Park, Y-H., Garric, G., Koenig, Z., Sennéchaël, N., Ferrari, R., Piola, A.R., Saraceno, M., and Provost, C.: Fronts of the Malvinas Current System: surface and subsurface expressions revealed by satellite altimetry, Argo floats, and Mercator operational model outputs, J. Geophys. Res. Oceans, doi: 10.1029/2018JC013887, 2018.

Barnier, B., Madec, G., Penduff, T., Molines, J. M., Treguier, A. M., Le Sommer, J., Beckmann, A., Biastoch, A., Böning, C., Dengg, J., Derval, C., Durand, E., Gulev, S., Remy, E., Talandier, C., Theetten, S., Maltrud, M., McClean, J., and De Cuevas, B.: Impact of partial steps and momentum advection schemes in a global circulation model at eddy permitting resolution, Ocean Dynam., 56, 543-567, 2006.

Becker, J. J., Sandwell, D. T., Smith, W. H. F., Braud, J., Binder, B., Depner, J., Fabre, D., Factor, J., Ingalls, S., Kim, S.H., Ladner, R., Marks, K., Nelson, S., Pharaoh, A., Trimmer, R., Von Rosenberg, J., Wallace, G., and Weatherall, P.: Global Bathymetry and Elevation Data at 30 Arc Seconds Resolution: SRTM30_PLUS, Mar. Geod., 32, 355-371, doi: 10.1080/01490410903297766, 2009.

Benkiran, M. and Greiner, E.: Impact of the Incremental Analysis Updates on a Real-Time System of the North Atlantic Ocean, J. Atmos. Ocean. Tech., 25, 2055-2073, 2008.

1 Bidlot, J.-R.: Impact of ocean surface currents on the ECMWF forecasting system for
2 atmosphere circulation and ocean waves, GlobCurrent Preliminary User Consultation
3 Meeting, <http://globcurrent.ifremer.fr/component/k2/itemlist/category/118?Itemid=960>,
4 Brest, 7-9 March 2012.

5 Blanke, B. and Delecluse, P.: Variability of the tropical Atlantic-Ocean simulated by a
6 general-circulation model with 2 different mixed-layer physics, *J. Phys. Oceanogr.*, 23, 1363-
7 1388, 1993.

8 Brodeau, L., Barnier, B., Treguier, A.M., Penduff, T., and Gulev S.: An ERA40-based
9 atmospheric forcing for global ocean circulation models, *Ocean Modelling*, 31, issues 3-4, 88-
10 104, doi: 10.1016/j.ocemod.2009.10.005, 2010.

11 Bruinsma, S., Lemoine, J.-M., Biancale, R., and Vales, N.: CNES/GRGS 10-day gravity field
12 models (release 02) and their evaluation, *Adv. Space Res.*, 45, 4, 587-601, doi:
13 10.1016/j.asr.2009.10.012, 2010.

14 Chambers, D. P., Cazenave, A., Champollion, N., Dieng, H., Llovel, W., Forsberg, R., von
15 Schuckmann, K., and Wada, Y.: Evaluation of the global mean sea level budget between 1993
16 and 2014, *Surv. Geophys.*, 38, no. 1, 309-327, doi:10.1007/s10712-016-9381-3, 2017.

17 Chelton, D. B., Wentz, F. J., Gentemann, C. L., De Szoeki, R. A., and Schlax, M. G.:
18 Satellite microwave SST observations of transequatorial tropical instability waves, *Geophys.*
19 *Res. Lett.*, 27, 1239-1242, 2000.

20 Chen, J. L., Wilson, C. R., Tapley, B. D., Famiglietti, J. S., and Rodell, M.: Seasonal global
21 mean sea level change from satellite altimeter, GRACE, and geophysical models, *J. Geodesy*,
22 79, 532-539, doi:10.1007/s00190-005-0005-9, 2005.

23 Chevallier, M., G.C. Smith, J.-F. Lemieux, F. Dupont, G. Forget, Y. Fujii, F. Hernandez, R.
24 Msadek, K. A. Peterson, A. Storto, T. Toyoda, M. Valdivieso, G. Vernieres, H. Zuo, M.
25 Balmaseda, Y.-S. Chang, N. Ferry, G. Garric, K. Haines, S. Keeley, R. M. Kovach, T.
26 Kuragano, S. Masina, Y. Tang, H. Tsujino, X. Wang: Intercomparison of the Arctic sea ice
27 cover in global ocean-sea ice reanalyses from the ORA-IP project, *Clim. Dyn.*, 49: 1107,
28 <https://doi.org/10.1007/s00382-016-2985-y>, 2017.

29 Church, J. A., Clark, P. U., Cazenave, A., Gregory, J.-M., Jevrejeva, S., Levermann, A.,
30 Merrifield, M. A., Milne, G. A., Nerem, R. S., Nunn, P. D., Payne, A. J., Pfeffer, W. T.,
31 Stammer, D., and Unnikrishnan, A. S.: Sea Level Change. In: *Climate Change 2013: The*

1 Physical Science Basis. Contribution of Working Group I to the Fifth Assessment Report of
2 the Intergovernmental Panel on Climate Change [Stocker, T.F., D. Qin, G.-K. Plattner, M.
3 Tignor, S.K. Allen, J. Boschung, A. Nauels, Y. Xia, V. Bex and P.M. Midgley (eds.)].
4 Cambridge University Press, Cambridge, United Kingdom and New York, NY, USA, 2013.

5 Cravatte, S., Madec, G., Izumo, T., Menkes, C., and Bozec, A.: Progress in the 3D circulation
6 of the eastern equatorial Pacific in a climate, *Ocean Model.*, 17, 28-48, 2007.

7 Dai, A. and Trenberth, K. E.: Estimates of freshwater discharge from continents: latitudinal
8 and seasonal variations, *J. Hydrometeorol.*, 3, 660–687, 2002.

9 Dai A., Qian, T., Trenberth, K., and Milliman, J. D.: Changes in Continental Freshwater
10 Discharge from 1948 to 2004, *J. Climate*, vol. 22, p.2773-2792, 2009.

11 Dee, D. P., and Coauthors: The ERA-interim reanalysis: Configuration and performance of
12 the data assimilation system, *Quart. J. Roy. Meteor. Soc.*, 137, 553–597,
13 doi:<https://doi.org/10.1002/qj.828>, 2011.

14 [De Lavergne C., Madec, G., Le Sommer, J., Nurser, A. G., and Naveira-Garabato, A. C.: On](#)
15 [the consumption of Antarctic Bottom Water in the abyssal ocean, *J. Phys. Oceanogr.*, 46,](#)
16 [635–651, doi:10.1175/JPO-D-14-0201.1, 2016.](#)

17 Desroziers, G., Berre, L., Chapnik, B., and Polli, P.: Diagnosis of observation, background
18 and analysis-error statistics in observation space, *Q. J. R. Meteorol. Soc.*, 131, 3385–3396,
19 doi: 10.1256/qj.05.108, 2005.

20 Drevillon, M., Greiner, E., Paradis, D., Payan, C., Lellouche, J.M., Reffray, G., Durand, E.,
21 Law-Chune, S., and Cailleau, S.: A strategy for producing refined currents in the Equatorial
22 Atlantic in the context of the search of the AF447 wreckage. *Ocean Dynamics*, 63, 63-82,
23 DOI 10.1007/s10236-012-0580-2, 2013.

24 Drillet, Y., Lellouche, J.-M., Levier, B., Drevillon, M., Le Galloudec, O., Reffray, G.,
25 Regnier, C., Greiner, E., and Clavier, M.: Forecasting the mixed layer depth in the north east
26 Atlantic: an ensemble approach, with uncertainties based on data from operational oceanic
27 systems *Ocean Sci. Discuss.*, 11, 1435-1472, [http://www.ocean-sci-](http://www.ocean-sci-discuss.net/11/1435/2014/osd-11-1435-2014.html)
28 [discuss.net/11/1435/2014/osd-11-1435-2014.html](http://www.ocean-sci-discuss.net/11/1435/2014/osd-11-1435-2014.html), 2014.

29 Estournel, C., Testor, P., Damien, P., D’ortenzio, F., Marsaleix, P., Conan, P., Kessouri, F.,
30 Durrieu de Madron, X., Coppola, L., Lellouche, J.-M., Belamari, S., Mortier, L., Ulses, C.,
31 Bouin, M.-N., and Prieur, L.: High resolution modeling of dense water formation in the north-

1 western Mediterranean during winter 2012-2013: Processes and budget, *J. Geophys. Res.*,
2 Wiley-Blackwell, 121 (7), 5367-5392, DOI:10.1002/2016JC011935, 2016.

3 Fichet, T. and Maqueda, M. A.: Sensitivity of a global sea ice model to the treatment of ice
4 thermodynamics and dynamics, *J. Geophys. Res.*, 102, 12609-12646, 1997.

5 Good, S.A., Martin, M.J., and Rayner, N.A.: EN4: quality controlled ocean temperature and
6 salinity profiles and monthly objective analyses with uncertainty estimates, *J. Geophys. Res.*,
7 118, 6704-6716, doi:10.1002/2013JC009067, 2013.

8 Grasso, L. D.: The differentiation between grid spacing and resolution and their application to
9 numerical modelling, *B. Am. Meteor. Soc.*, 81, 579-580, 2000.

10 Greiner, E., Benkiran, M., Blayo, E., and Dibarboue, G.: MERA-11 general scientific paper,
11 1992-2002 PSY1V2 reanalysis, reference MOO-MR-431-37-MER Mercator-Ocean,
12 Toulouse, France, 71 pp., 2006.

13 Grodsky, S. A., Lumpkin, R., and Carton, J. A.: Spurious trends in global surface drifter
14 currents, *Geophys. Res. Lett.*, 38, L10606, doi: 10.1029/2011GL047393, 2011.

15 Hilburn, K.: The passive microwave water cycle product, Remote Sensing Systems (REMSS)
16 Technical Report 072409, Santa Rosa (CA), 30 pp., 2009.

17 Hilburn, K., Smith D.K., and Mears C. A.: Annual Validation report: Rain, Remote Sensing
18 Systems, www.remss.com, 2014.

19 Hoaglin D., Mosteller F., and Tukey J. W.: Understanding Robust and Exploratory Data
20 Analysis, Wiley Series in probability and mathematical statistics, New-York, 1983.

21 Janowiak, J. E., Gruber, A., Kondragunta, C. R., Livezey, R.E., and Huffman G.J.: A
22 comparison of the NCEP-NCAR reanalysis precipitation and the GPCP rain gauge-satellite
23 combined dataset with observational error considerations, *J. of Climate*, vol. 11, 2960-2979,
24 1998.

25 Janowiak, J. E., Bauer, P., Wang, W., Arkin, P. A., and Gottschalck, J.: An evaluation of
26 precipitation forecasts from operational models and reanalysis including precipitations
27 variations associated with MJO activity, *Monthly weather Review*, 138, p. 4542-4560, 2010.

28 Juza, M., Mourre, B., Lellouche, J.-M., Tonani, M., and Tintore, J.: From basin to sub-basin
29 scale assessment and intercomparison of numerical simulations in the Western Mediterranean

1 Sea, *Journal of Marine Systems*, 149, 36–49, <http://dx.doi.org/10.1016/j.jmarsys.2015.04.010>,
2 2015.

3 [Gasparin, F., Greiner, E., Lellouche, J.-M., Legalloudec, O., Garric, G., Drillet, Y., Bourdalle-](#)
4 [Badie, R., Le Traon, P.-Y., Remy, E., and Drevillon, M.: A large-scale view of oceanic](#)
5 [variability from 2007 to 2015 in the global high resolution monitoring and forecasting system](#)
6 [at Mercator-Ocean, In revision in *Journal of Marine Systems*, 2018.](#)

7 [Global Sea-Level Observing System \(GLOSS\) Implementation Plan - 2012, UNESCO/IOC](#)
8 [Technical Series No.100, 41 pp., 2012.](#)

9 Gouretski, V. V. and Koltermann, K. P.: Woce global hydrographic climatology. Technical
10 Report 35/2004, Berichte des Bundesamtes fur Seeschiffahrt und Hydrographie, 2004.

11 Jackett, D. R. and Mcdougall, T. J.: Minimal Adjustment of Hydrographic Profiles to Achieve
12 Static Stability, *J. Atmos. Oceanic Technol.*, 12, 381–389, <https://doi.org/10.1175/1520->
13 [0426\(1995\)012<0381:MAOHPT>2.0.CO;2](https://doi.org/10.1175/1520-0426(1995)012<0381:MAOHPT>2.0.CO;2), 1995.

14 Kidd, C., Dawkins, E., and Huffman, G.: Comparison of Precipitation Derived from the
15 ECMWF Operational Forecast Model and Satellite Precipitation Datasets, *Journal of*
16 *Hydrometeorology*, 14 (5), p. 1463-1482, <https://doi.org/10.1175/JHM-D-12-0182.1>, 2013.

17 Kjerfve, B.: Tides of the Caribbean Sea, *J. Geophys. Res.*, 86(C5), 4243-4247,
18 [doi:10.1029/JC086iC05p04243](https://doi.org/10.1029/JC086iC05p04243), 1981.

19 Koch-Larrouy, A., Madec, G., Blanke, B., and Molcard, R.: Water mass transformation along
20 the Indonesian throughflow in an OGCM, *Ocean Dynam.*, 58, 289-309, [doi:10.1007/s10236-](https://doi.org/10.1007/s10236-)
21 [008-0155-4](https://doi.org/10.1007/s10236-008-0155-4), 2008.

22 Koenig, Z., Provost, C., Villaceros-Robineau, N., Sennechael, N., Meyer, A., Lellouche, J.-
23 M., and Garric, G.: Atlantic waters inflow north of Svalbard: Insights from IAOOS
24 observations and Mercator Ocean global operational system during N-ICE2015, *J. Geophys.*
25 *Res. Oceans*, 122, 1254–1273, [doi:10.1002/2016JC012424](https://doi.org/10.1002/2016JC012424), 2017.

26 Lagerloef, G., Schmitt, R., Schanze, J., and Kao, H. Y.: The Ocean and the global water
27 cycle, *Oceanography*, 23(4), 82-93, <http://dx.doi.org/10.5670/oceanog.2010.07>, 2010.

28 Large, W. G. and Yeager, S. G.: The global climatology of an interannually varying air–sea
29 flux data set, *Clim. Dynam.*, 33, 341-364, [doi:10.1007/s00382-008-0441-3](https://doi.org/10.1007/s00382-008-0441-3), 2009.

1 [Lefevre, F., Sénant, E., et al. : BaDoMar: a tide gauge database used for altimeter calibration,](#)
2 [Workshop on Sea Level Variations Towards an Operational European Sea Level Service,](#)
3 [page 63, 2005.](#)

4 Lellouche, J.-M., Le Galloudec, O., Drevillon, M., Regnier, C., Greiner, E., Garric, G., Ferry,
5 N., Desportes, C., Testut, C.-E., Bricaud, C., Bourdalle-Badie, R., Tranchant, B., Benkiran,
6 M., Drillet, Y., Daudin, A., and De Nicola, C.: Evaluation of global monitoring and
7 forecasting systems at Mercator Ocean, *Ocean Sci.*, 9, 57-81, doi:10.5194/os-9-57-2013,
8 2013.

9 Lengaigne, M., Menkes, C., Aumont, O., Gorgues, T., Bopp, L., Andre, J.M., and Madec, G.:
10 Influence of the oceanic biology on the tropical Pacific climate in a coupled general
11 circulation model, *Clim. Dyn.*, 28, 503-507, DOI:10.1007/s00382-006-0200-2, 2007.

12 Levy, M., Estublier, A., and Madec, G.: Choice of an advection scheme for biogeochemical
13 models, *Geophys. Res. Lett.*, 28, 3725–3728, doi:10.1029/2001GL012947, 2001.

14 Locarnini, R. A., Mishonov, A. V., Antonov, J. I., Boyer, T. P., Garcia, H. E., Baranova, O.
15 K., Zweng, M. M., Paver, C. R., Reagan, J. R., Johnson, D. R., Hamilton, M., and Seidov,
16 D.: *World Ocean Atlas 2013, Volume 1: Temperature*. S. Levitus, Ed., A. Mishonov
17 Technical Ed.; NOAA Atlas NESDIS 73, 40 pp., 2013.

18 Madec, G. and Imbard M.: A global ocean mesh to overcome the North Pole singularity,
19 *Clim. Dynam.*, 12, 381-388, 1996.

20 Madec, G., and the NEMO team: NEMO ocean engine. Note du Pôle de modélisation, Institut
21 Pierre-Simon Laplace (IPSL), France, No. 27 ISSN, 1288-1619, 2008.

22 [Marchesiello, P., Debreu, L., and Coulevar, X.: Spurious diapycnal mixing in terrain-](#)
23 [following coordinate models: The problem and a solution, *Ocean Modelling*, 26 \(3-4\), 156-](#)
24 [169, 2009.](#)

25

26 Menemenlis, D., Fukumori, I., and Lee, T.: Atlantic to Mediterranean Sea level difference
27 driven by winds near Gibraltar Strait, *J. Phys. Oceanogr.*, 37, 359–376, 2007.

28 Pujol, M.-I., Faugère, Y., Taburet, G., Dupuy, S., Pelloquin, C., Ablain, M., and Picot, N.:
29 DUACS DT2014: the new multi-mission altimeter data set reprocessed over 20 years,
30 *Ocean Sci.*, 12, 1067-1090, doi:10.5194/os-12-1067-2016, 2016.

1 Raynaud, L., Berre, L., and Desroziers, G.: Objective filtering of ensemble-based
2 background-error variances, *Quarterly Journal of the Royal Meteorology Society*, Vol. 135,
3 Issue 642, 1177–1199, 2009.

4 Renault, L., Molemaker, M. J., McWilliams, J. C., Shchepetkin, A. F., Lemarie, F., Chelton,
5 D., Illig, S., and Hall A.: Modulation of wind work by oceanic current interaction with the
6 atmosphere, *Journal of Physical Oceanography*, 46 (6), 1685-1704, ISSN 0022-3670, 2016.

7 Rio, M. H., Guinehut, S., and Larnicol, G.: New CNES-CLS09 global mean dynamic
8 topography computed from the combination of GRACE data, altimetry, and in situ
9 measurements, *J. Geophys. Res.*, 116, C07018, doi:10.1029/2010JC006505, 2011.

10 Rio, M.H.: Use of altimeter and wind data to detect the anomalous loss of SVP-type drifter's
11 drogue, *Journal of Atmospheric and Oceanic Technology*, DOI:10.1175/JTECH-D-12-
12 00008.1, 2012.

13 Rio, M.-H., Mulet, S., and Picot, N.: Beyond GOCE for the ocean circulation estimate:
14 Synergetic use of altimetry, gravimetry, and in situ data provides new insight into geostrophic
15 and Ekman currents, *Geophys. Res. Lett.*, 41, doi:10.1002/2014GL061773, 2014.

16 [Rio M.-H. and Etienne H.: For Global Ocean Delayed Mode in-situ Observations of Ocean](http://doi.org/10.13155/41256)
17 [Surface Currents, Copernicus Quality Information Document CMEMS-INS-QUID-013-044,](http://doi.org/10.13155/41256)
18 [http://doi.org/10.13155/41256, 2017.](http://doi.org/10.13155/41256)

19 Roemmich, D. and Gilson, J.: The 2004–2008 mean and annual cycle of temperature, salinity,
20 and steric height in the global ocean from the Argo Program, *Progress in Oceanography*,
21 Volume 82, Issue 2, 81–100, <https://doi.org/10.1016/j.pocean.2009.03.004>, 2009.

22 Roquet, F., Charrassin, J. B., Marchand, S., Boehme, L., Fedak, M., Reverdin, G., and Guinet,
23 C.: Delayed-mode calibration of hydrographic data obtained from animal-borne satellite relay
24 data loggers, *J. Atmos. Ocean. Tech.*, 28, 787–801, 2011.

25 Roullet, G. and Madec, G.: Salt conservation, free surface, and varying levels: a new
26 formulation for ocean general circulation models, *J. Geophys. Res.*, 105, 23927–23942, 2000.

27 Schweiger, A., Lindsay, R., Zhang, J., Steele, M., and Stern, H.: Uncertainty in modeled
28 arctic sea ice volume, *J. Geophys. Res.*, doi:10.1029/2011JC007084, 2011.

29 Scott, R., Ferry, N., Drevillon, M., Barron, C.N., Jourdain, N.C., Lellouche, J.-M., Metzger,
30 E. J., Rio, M. H., and Smedstad, O. M.: Estimates of surface drifter trajectories in the

1 Equatorial Atlantic: a multi-model ensemble approach. *Ocean Dynamics*, 62, 1091-1109. doi
2 10.1007/s10236-012-0548-2, 2012.

3 Silva, T. A. M., Bigg, G. R., and Nicholls, K. W.: Contribution of giant icebergs to the
4 Southern Ocean freshwater flux, *J. Geophys. Res.*, 111, C03004, doi:10.1029/2004JC002843,
5 2006.

6 Smith, G.C., Roy, F., Reszka, M., Surcel Colan, D., He, Z., Deacu, D., Belanger, J.-M.,
7 Skachko, S., Liu, Y., Dupont, F., Lemieux, J-F., Beaudoin, C., Tranchant, B., Drevillon, M.,
8 Garric, G., Testut, C.-E., Lellouche, J.-M., Pellerin, P., Ritchie, H., Lu, Y., Davidson, F.,
9 Buehner, M., Caya, A., and Lajoie, M.: Sea ice forecast verification in the Canadian Global
10 Ice Ocean Prediction System, *Quarterly Journal of the Royal Meteorology Society*, Vol.142,
11 Issue 695, Pages 659–671, 2016.

12 Song, Y. T.: Estimation of interbasin transport using ocean bottom pressure: Theory and
13 model for Asian marginal seas, *J. Geophys. Res.*, 111, C11S19, doi:10.1029/2005JC003189,
14 2006.

15 [Stephens, G. L., L'Ecuyer, T., Forbes, R., Gettleman, A., Golaz, J.C., Bodas-Salcedo, A.,](#)
16 [Suzuki, K., Gabriel, P., and J. Haynes, J.: Dreary state of precipitation in global models, *J.*](#)
17 [Geophys. Res.](#), 115, D24211, doi:10.1029/2010JD014532, 2010.

18

19 Storto, A., Russo, I., and Masina, S.: Interannual response of global ocean hindcasts to a
20 satellite-based correction of precipitation fluxes, *Ocean Sci. Discuss.*,
21 <https://doi.org/10.5194/osd-9-611-2012>, 2012.

22 Szekely, T., Gourrion, J., Pouliquen, S., and Reverdin, G.: CORA, Coriolis Ocean Dataset for
23 Reanalysis. SEANOE doi:<http://doi.org/10.17882/46219>, 2016.

24 Talagrand, O.: A posteriori evaluation and verification of analysis and assimilation
25 algorithms, *Proc. of ECMWF Workshop on Diagnosis of Data Assimilation System*
26 (Reading), 17–28, 1998.

27 Tranchant, B., Reffray, G., Greiner, E., Nugroho, D., Koch-Larrouy, A., and Gaspar, P.:
28 Evaluation of an operational ocean model configuration at 1/12° spatial resolution for the
29 Indonesian seas (NEMO2.3/INDO12) – Part 1: Ocean physics, *Geosci. Model Dev.*, 9, 1037-
30 1064, 2016.

1 Troccoli, A. and P. Kallberg, P.: Precipitation correction in the ERA-40 reanalysis, ERA-40
2 Project Report Series N°13, 1-10, 2004.

3 Vinogradov, S.V. and Ponte R.M.: Low frequency variability in coastal sea level from tide
4 gauges and altimetry, *J. Geophys. Res.*, 116, C07006, doi:10/1029/2011JC007034, 2011.

5 Willebrand, J. , Barnier, B. , Böning, C. , Dieterich, C. , Killworth, P. D. , Le Provost, C. , Jia,
6 Y., Molines, J. M., and New, A. L.: Circulation characteristics in three eddy-permitting
7 models of the North Atlantic, *Progress in Oceanography*, 48(2), 123-161, 2001.

8 Williams, J. and Hughes, C.W.: The coherence of small island sea level with the wider ocean:
9 a model study, *Ocean Sci.*, 9, 111-119, 2013.

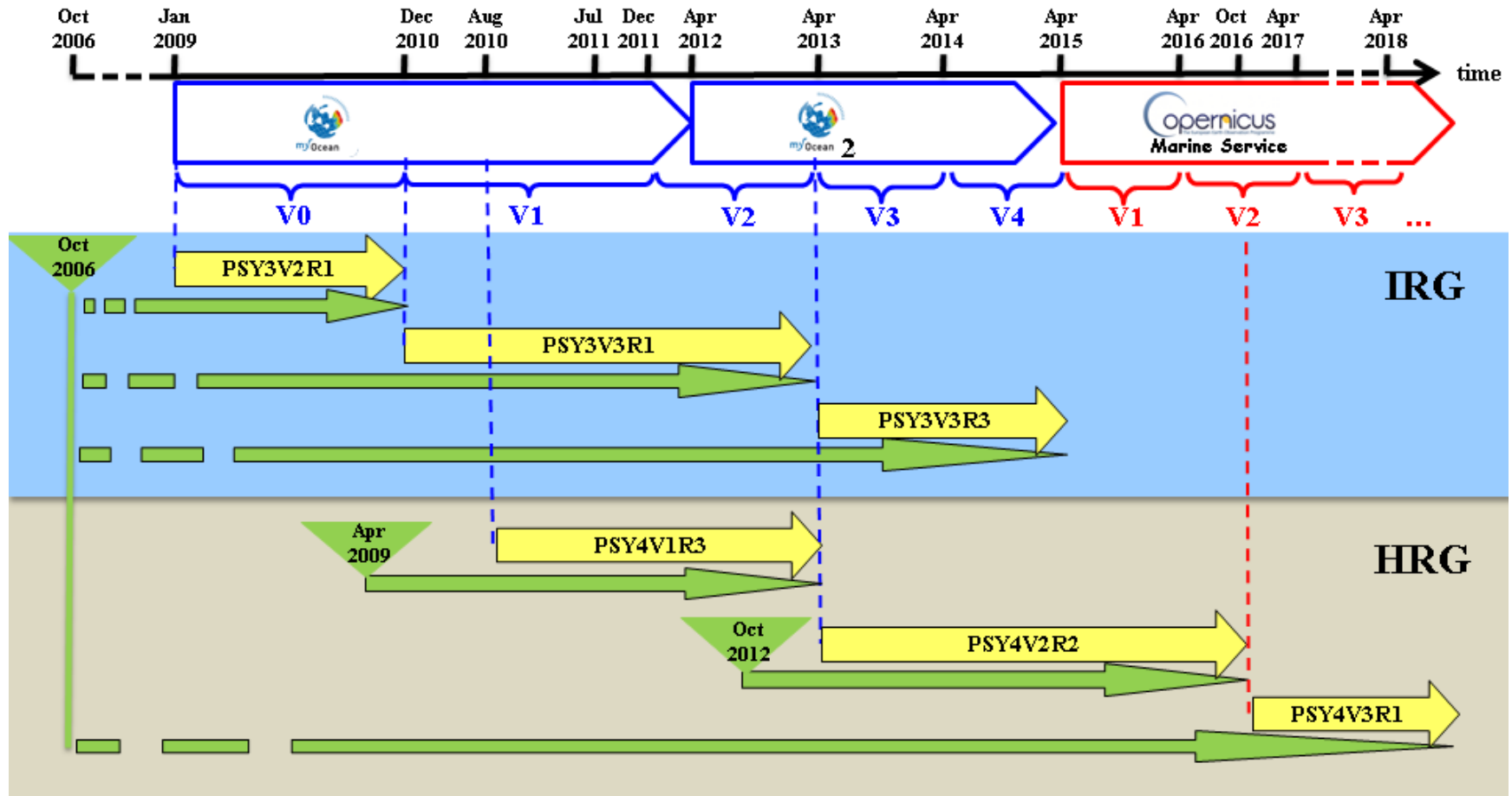
10 [Winton, M., Hallberg, R. and A. Gnanadesikan, A.: Simulation of Density-Driven Frictional](#)
11 [Downslope Flow in Z-Coordinate Ocean Models, *J. Phys. Oceanogr.*, 28, 2163-2174, 1998.](#)
12

13 Zweng, M. M., Reagan, J. R., Antonov, J. I., Locarnini, R. A., Mishonov, A., Boyer, T. P.,
14 Garcia, H. E., Baranova, O. K., Paver, C. R., Johnson, D. R., Seidov, D., and Biddle, M.:
15 World Ocean Atlas 2013, Volume 2: Salinity. S. Levitus, Ed., A. Mishonov, Technical
16 Ed.; NOAA Atlas NESDIS 74, 40 pp., 2013.

17 Zygmuntowska, M., Rampal, P., Ivanova, N., and Smedsrud, L. H.: Uncertainties in Arctic sea
18 ice thickness and volume: new estimates and implications for trends, *The Cryosphere*, 8, 705-
19 720, <https://doi.org/10.5194/tc-8-705-2014>, 2014.

20

1



2

3

4

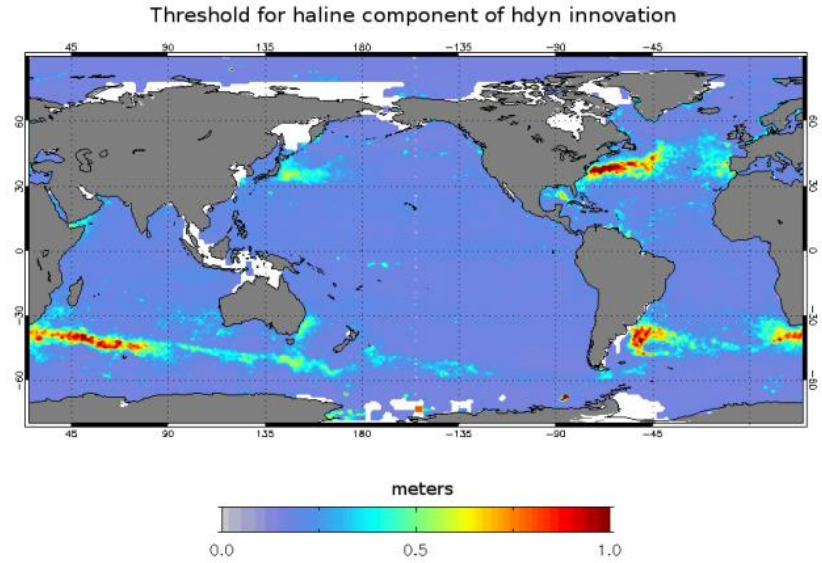
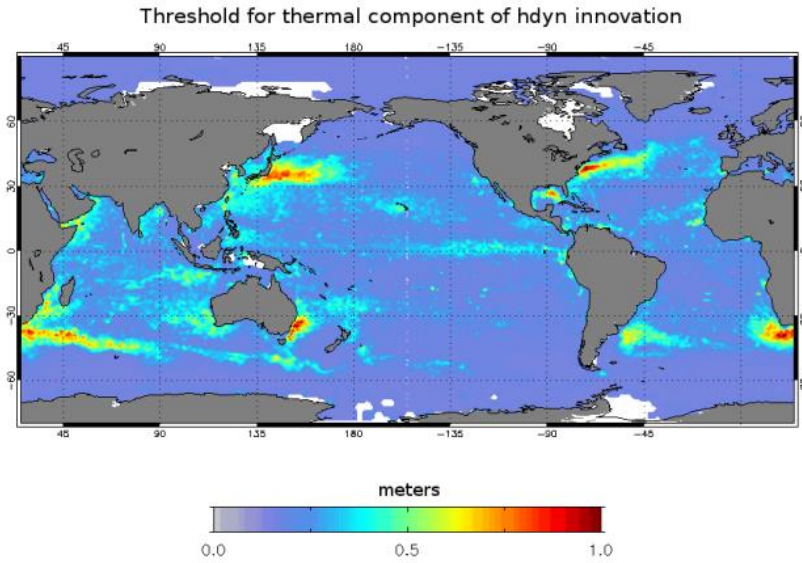
5

6

7

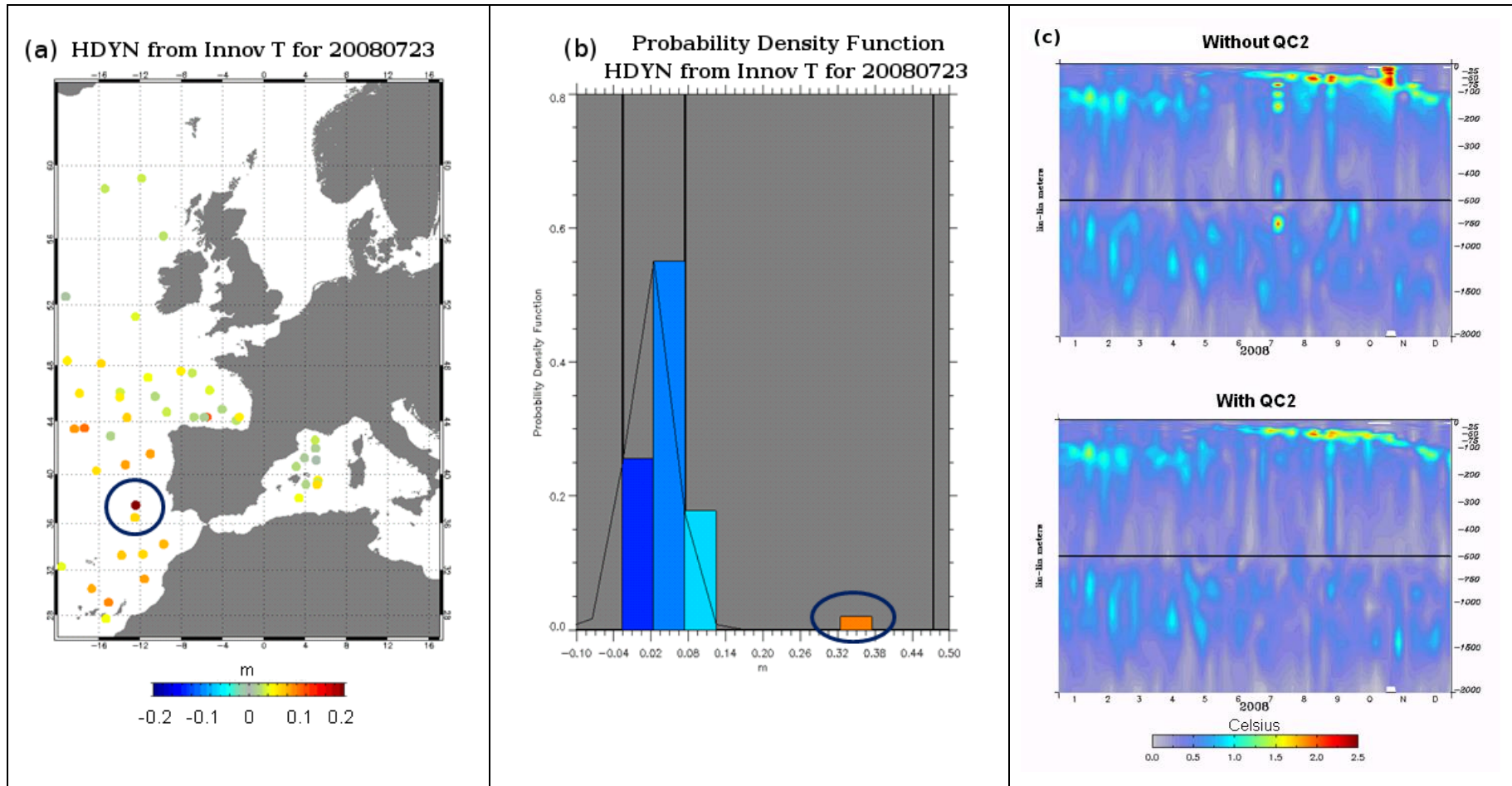
8

Figure 1: Timeline of the Mercator Ocean global analysis and forecasting systems for the various milestones (from V0 to V4) of past MyOcean project and for milestones V1, V2, V3 of the current CMEMS. Real-time productions are in yellow with the reference of the Mercator Ocean system. Available Mercator Ocean simulations are in green including the catch-up to real-time. Global Intermediate Resolution (respectively High Resolution) systems at 1/4° (respectively 1/12°) are referred to as IRG (respectively HRG). Milestones are written in blue for MyOcean project and in red for CMEMS.



1
2
3
4

Figure 2: Thresholds used for QC2 for thermal component of dynamical height innovation (left panel: $threshold_T$) and for haline component of dynamical height innovation (right panel: $threshold_S$). Units are meters.



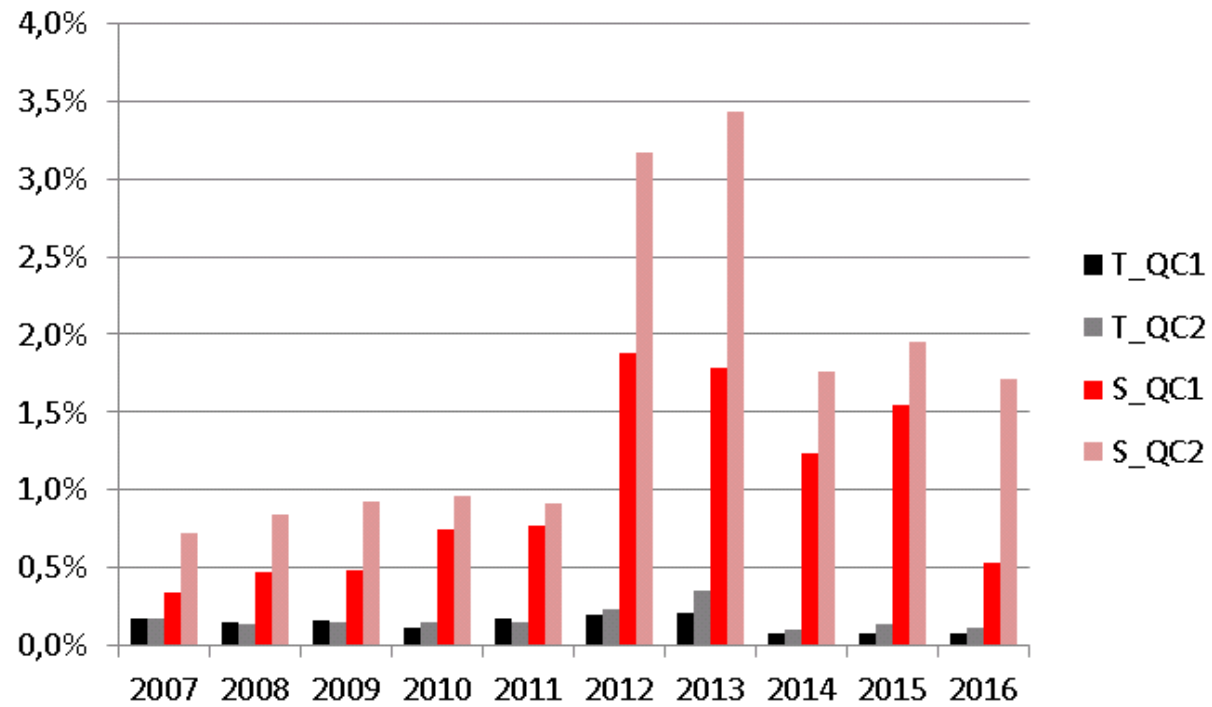
1

2

3

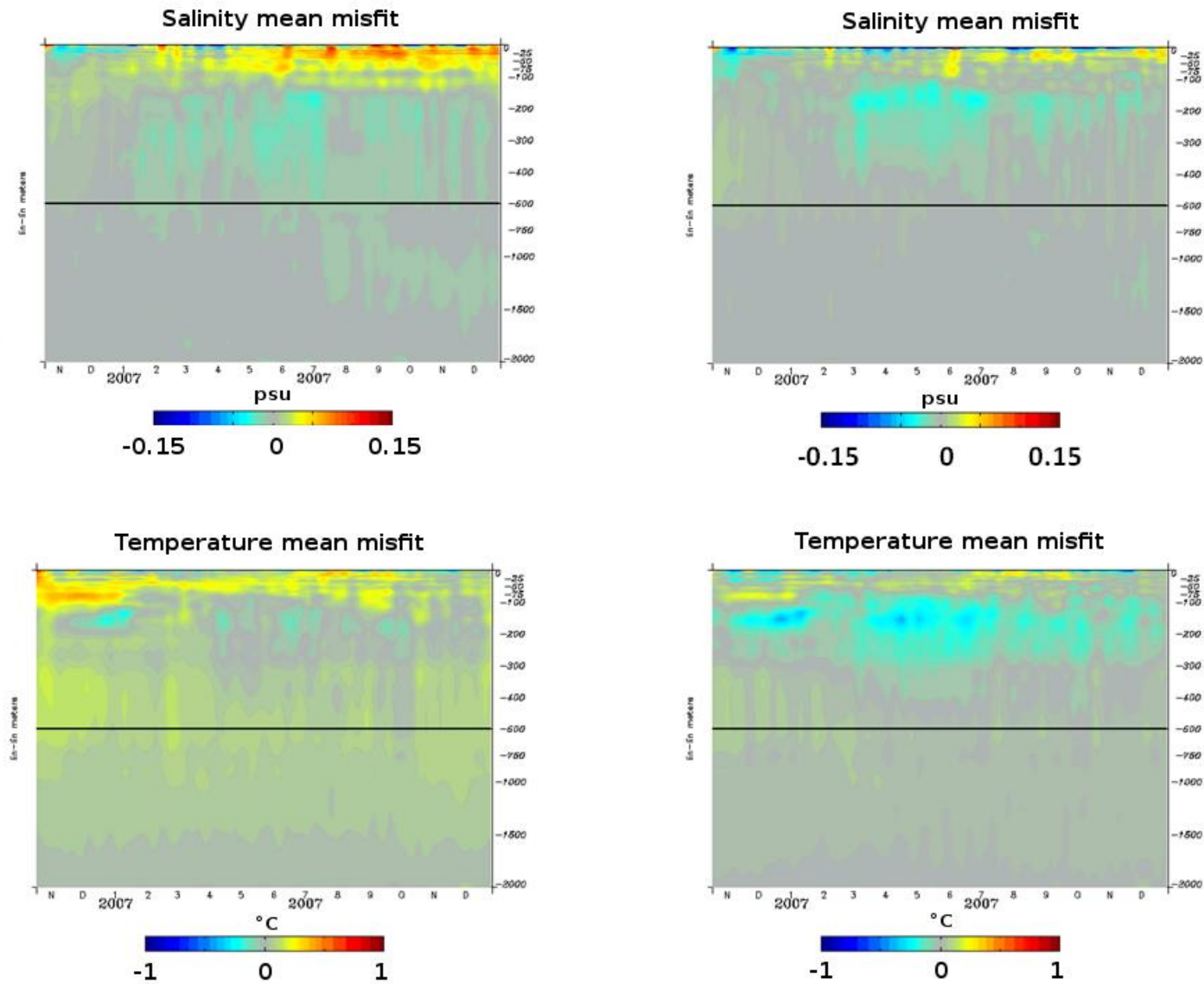
4

Figure 3: Statistics in the Azores region: a) absolute value of dynamical height innovations (in meters) from temperature innovations for the 7-day assimilation cycle from 16 July 2008 to 23 July 2008, b) PDF of these dynamical height innovations (the value 0.3 m appears in the tail of the PDF), c) RMS innovation with respect to the vertical temperature profiles over the year 2008 for two “twins” simulations (without and with QC2). These last scores are averaged over all seven days of the data assimilation window, with a lead time equal to 3.5 days. Units are °C.



1

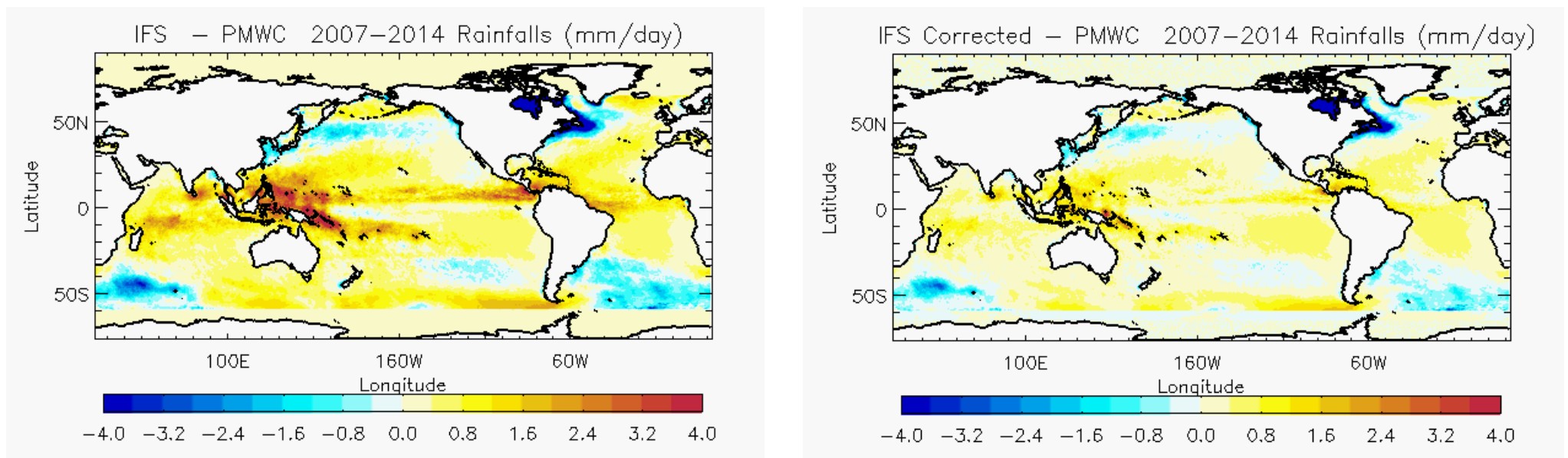
2 **Figure 4:** Statistics of suspicious temperature (T) and salinity (S) detected by QC1 (T_QC1 and S_QC1) and by QC2 (T_QC2 and S_QC2) quality controls as a function of year in the
 3 PSY4V3 2007-2016 simulation time period.



1
2
3
4

Figure 5: Diagnostics (time series) with respect to the vertical temperature and salinity profiles over the October 2006 - December 2007 period. Mean misfit between observations and model for salinity (top panels, units in psu) and for temperature (low panels, units in °C), starting from WOA9 climatology (left panels) and robust EN4 (right panels).

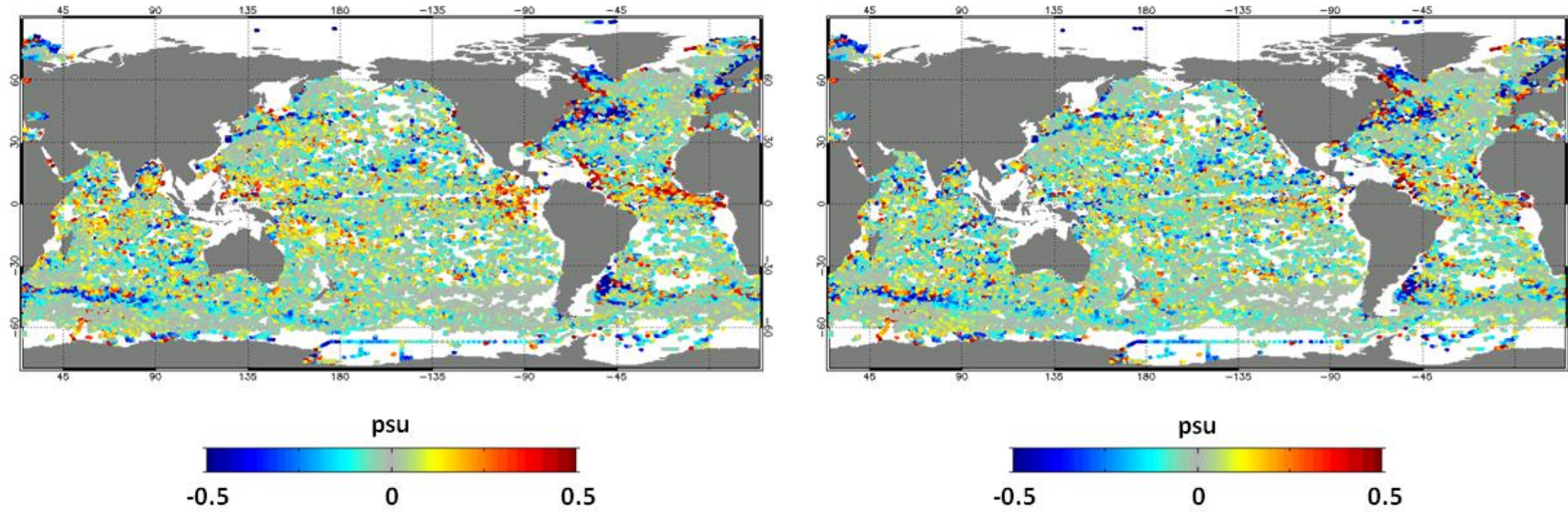
1



2

3 **Figure 6:** Mean 2007-2014 IFS ECMWF atmospheric precipitation bias (units in mm day^{-1}) with respect to PMWC product without (left map) and with (right map) correction.

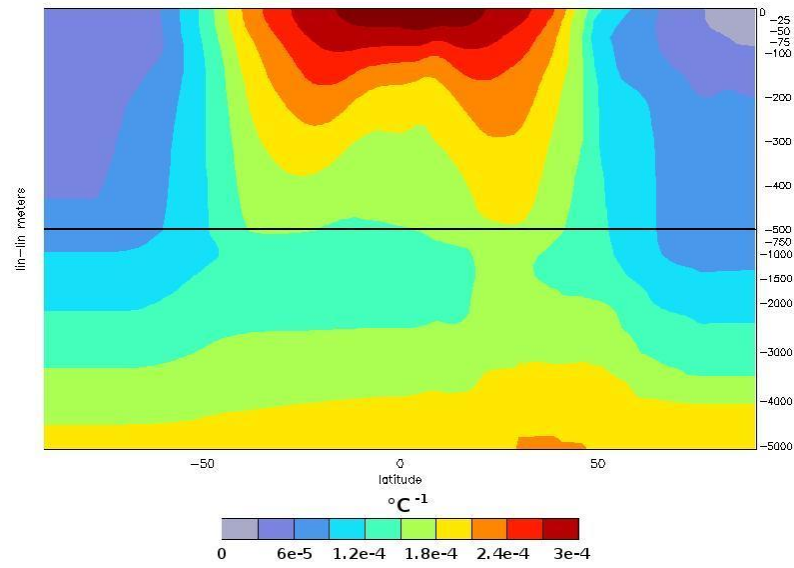
Mean surface salinity innovation (2011)



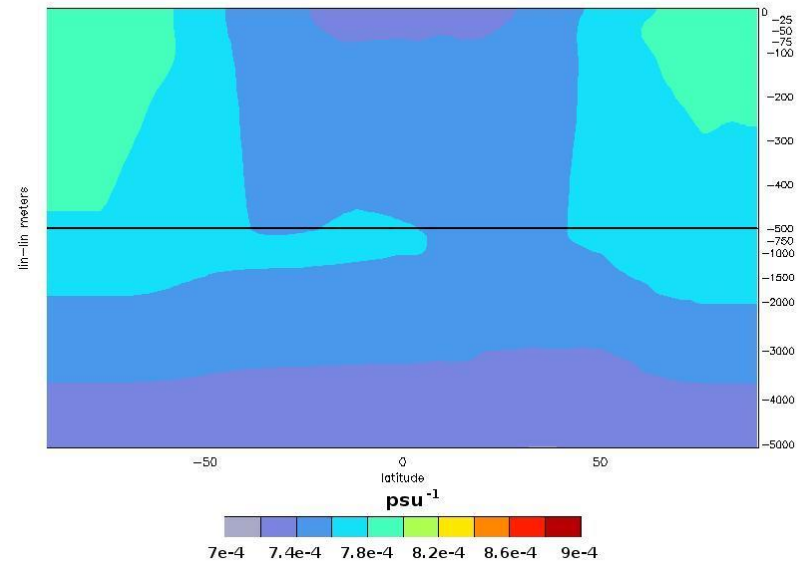
1
2
3
4

Figure 7: Mean surface salinity innovation (difference between the assimilated observation and the model, units in psu) on the year 2011. On the left, the innovation resulting from the use of the original IFS field, and on the right, the innovation resulting from the use of the corrected IFS field.

climatological thermal expansion



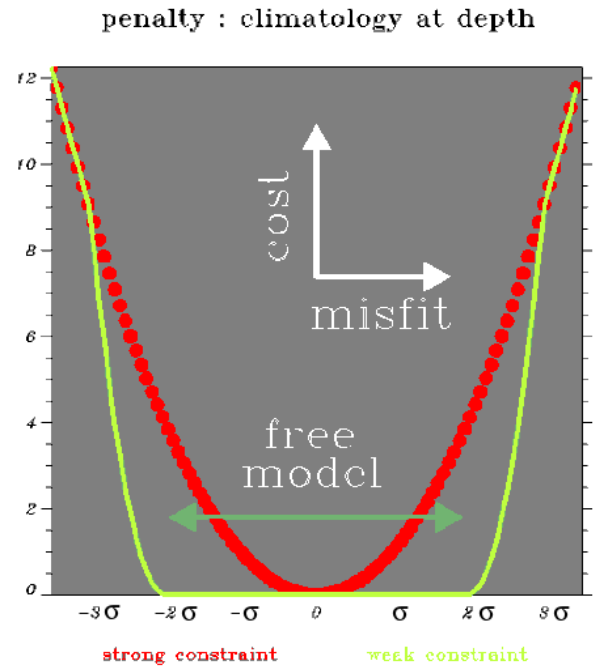
climatological saline contraction



1

2

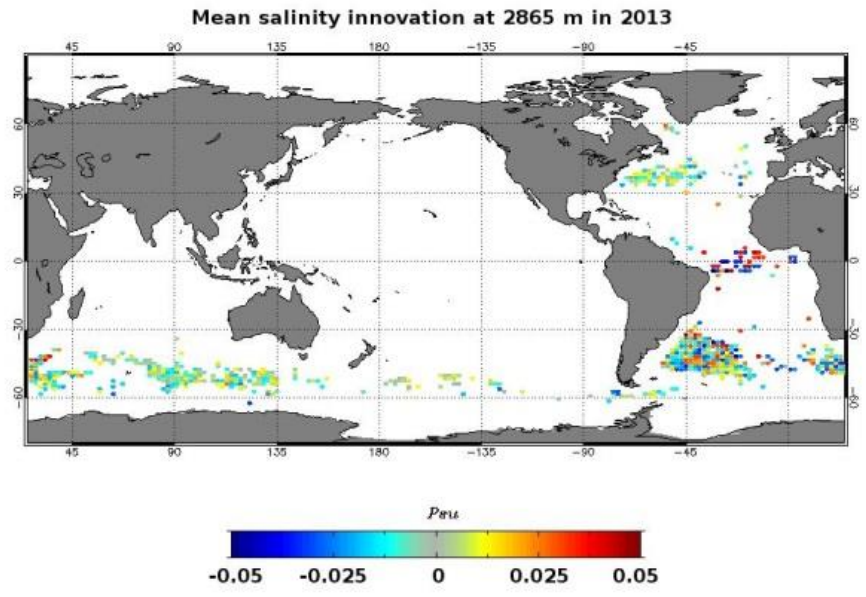
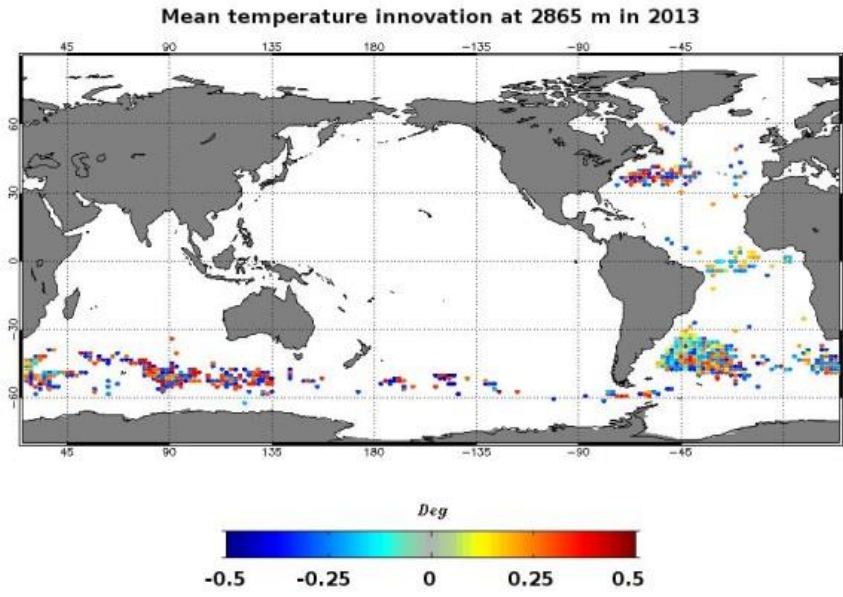
Figure 8: Climatological thermal expansion ($^{\circ}\text{C}^{-1}$) and saline contraction (psu^{-1}) as a function of the latitude and the depth.



1

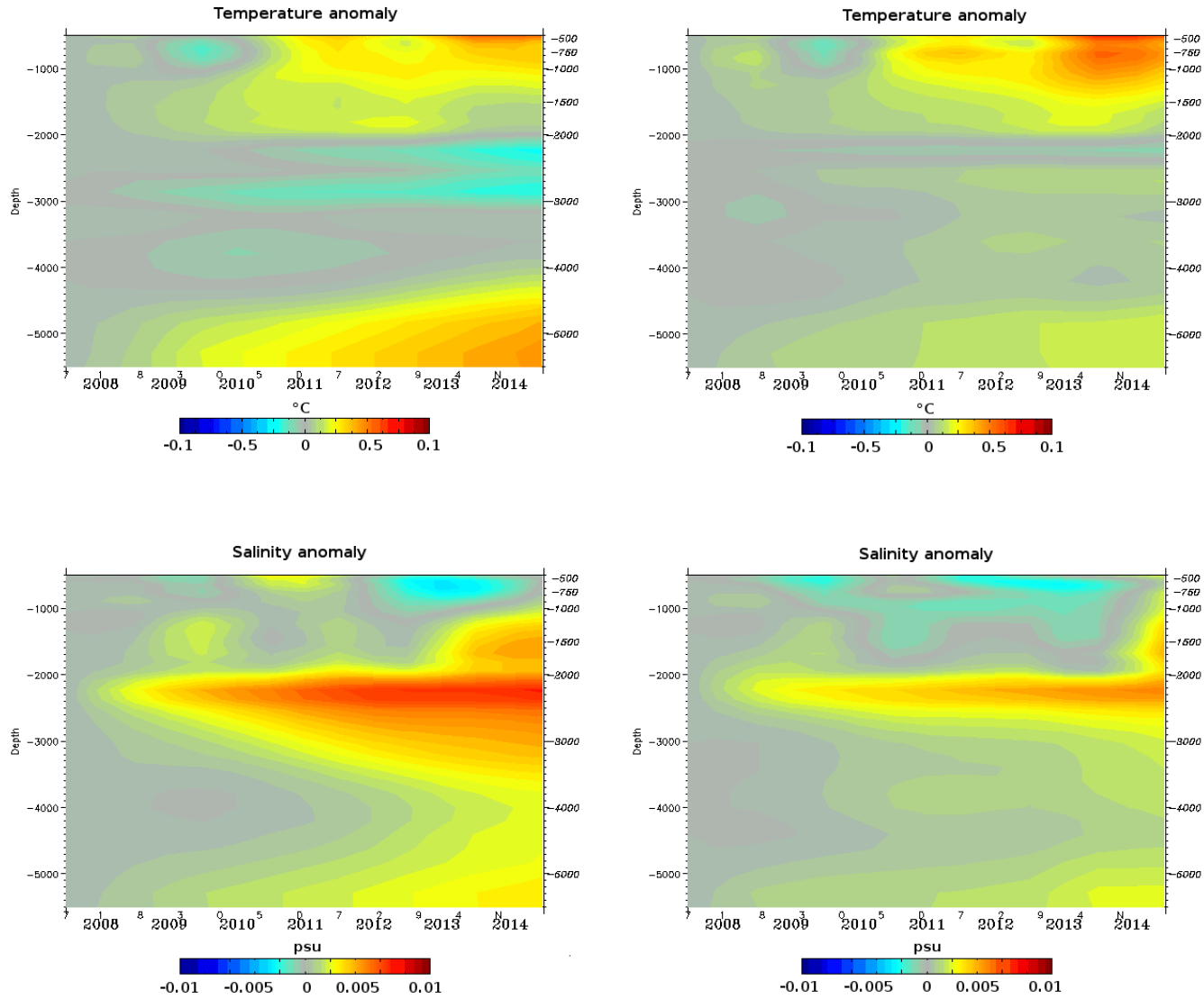
2

3 **Figure 9:** Non-Gaussian error for climatology (corresponding to a weak constrain of the system in green). A cost equal to zero corresponds to an infinite observation error, namely a system
 4 operation in a free mode (without assimilation of climatology).

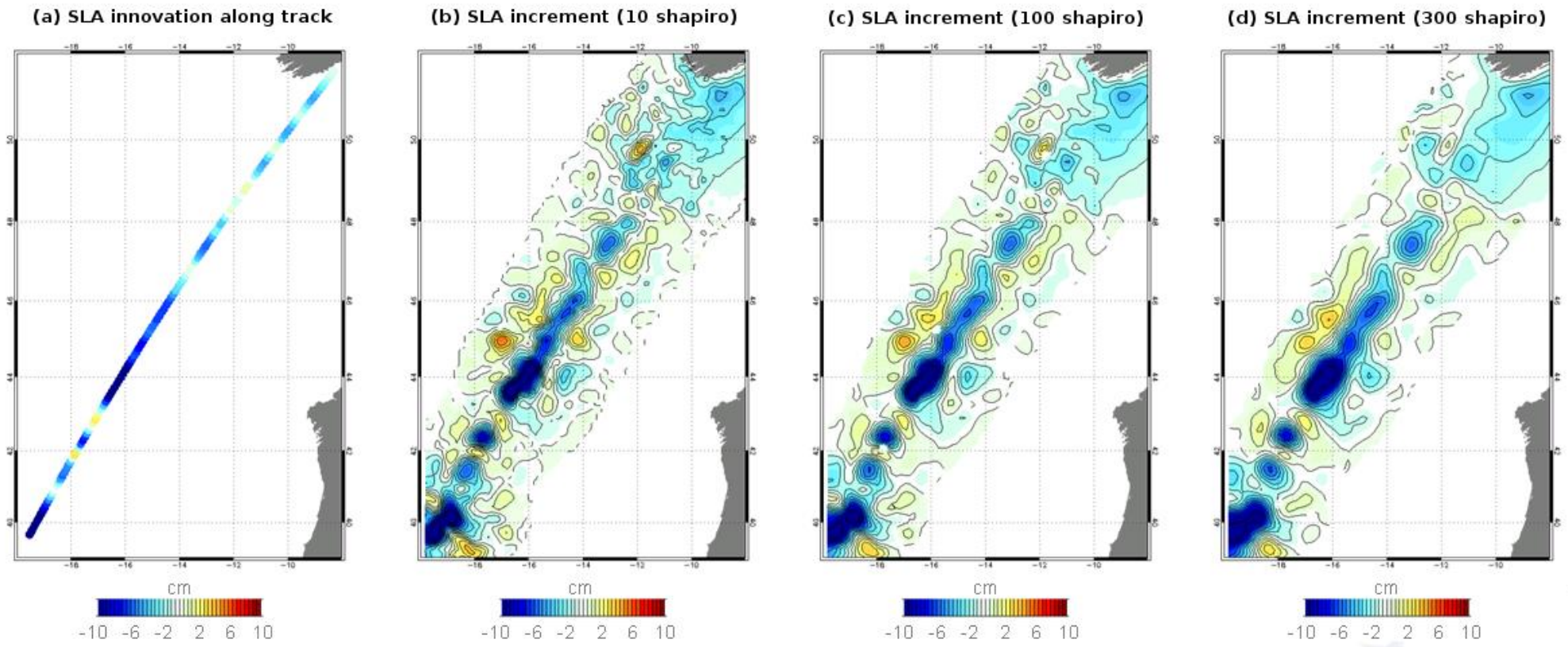


1

2 **Figure 10:** Mean temperature (on the left, units in °C) and salinity (on the right, units in psu) innovations in 2013 at 2865 m for the system PSY4V3.

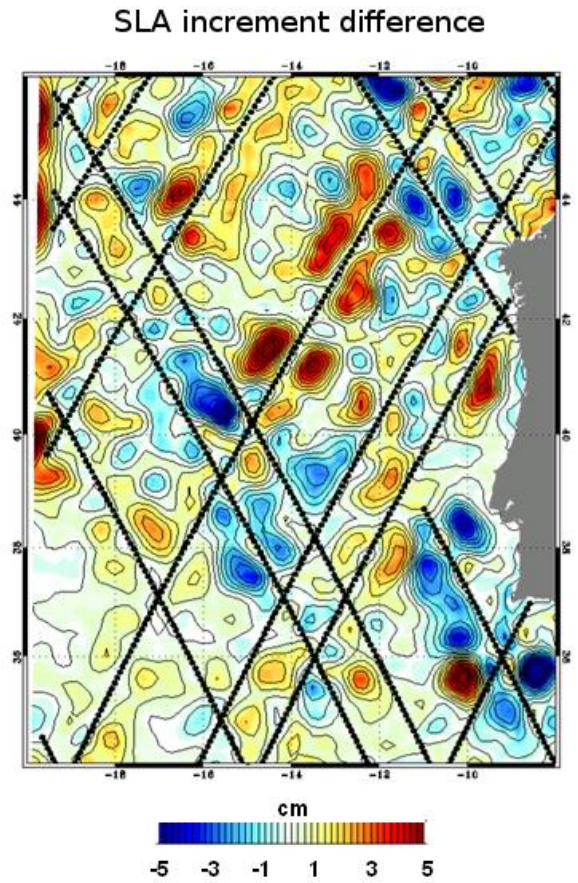


1 **Figure 11** : Temperature (top panels, units in °C) and salinity (low panels, units in psu) annual anomalies over depth (500-5000m) and time (2007-2014) for latitudes between 30° S and 60° S.
 2 The simulation on the left does not assimilate climatological vertical profiles while the simulation on the right assimilates them. Annual anomaly for a specific year is computed as the
 3 difference between the annual mean of this year and the annual mean of the year 2007.



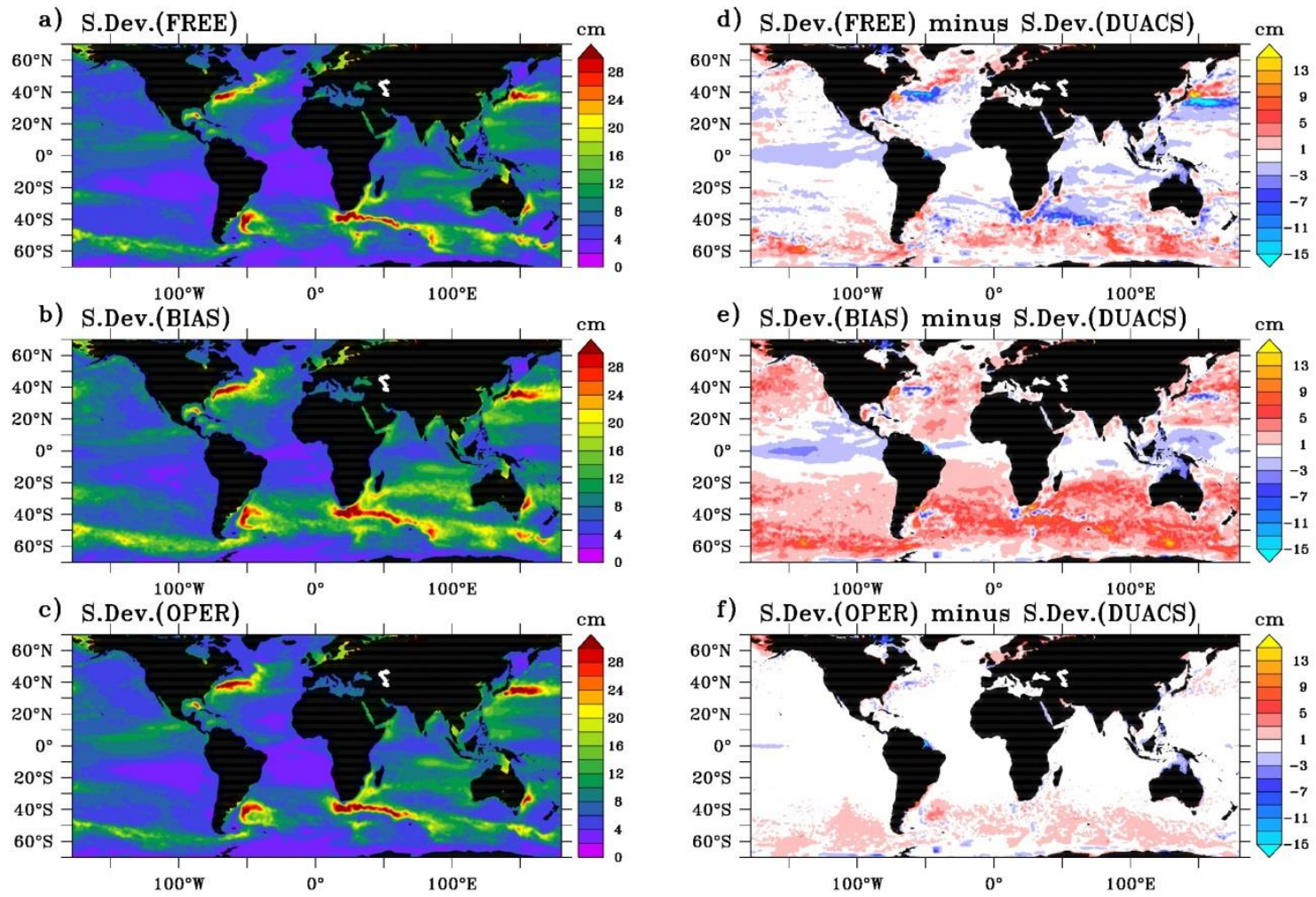
1
2
3
4

Figure 12: SLA innovation along a single assimilated track altimeter (a). SLA increments respectively with 10 (b), 100 (c) and 300 (d) Shapiro passes as anomaly filtering. These experiments have been performed with a regional system at $1/36^\circ$. Unit is cm.



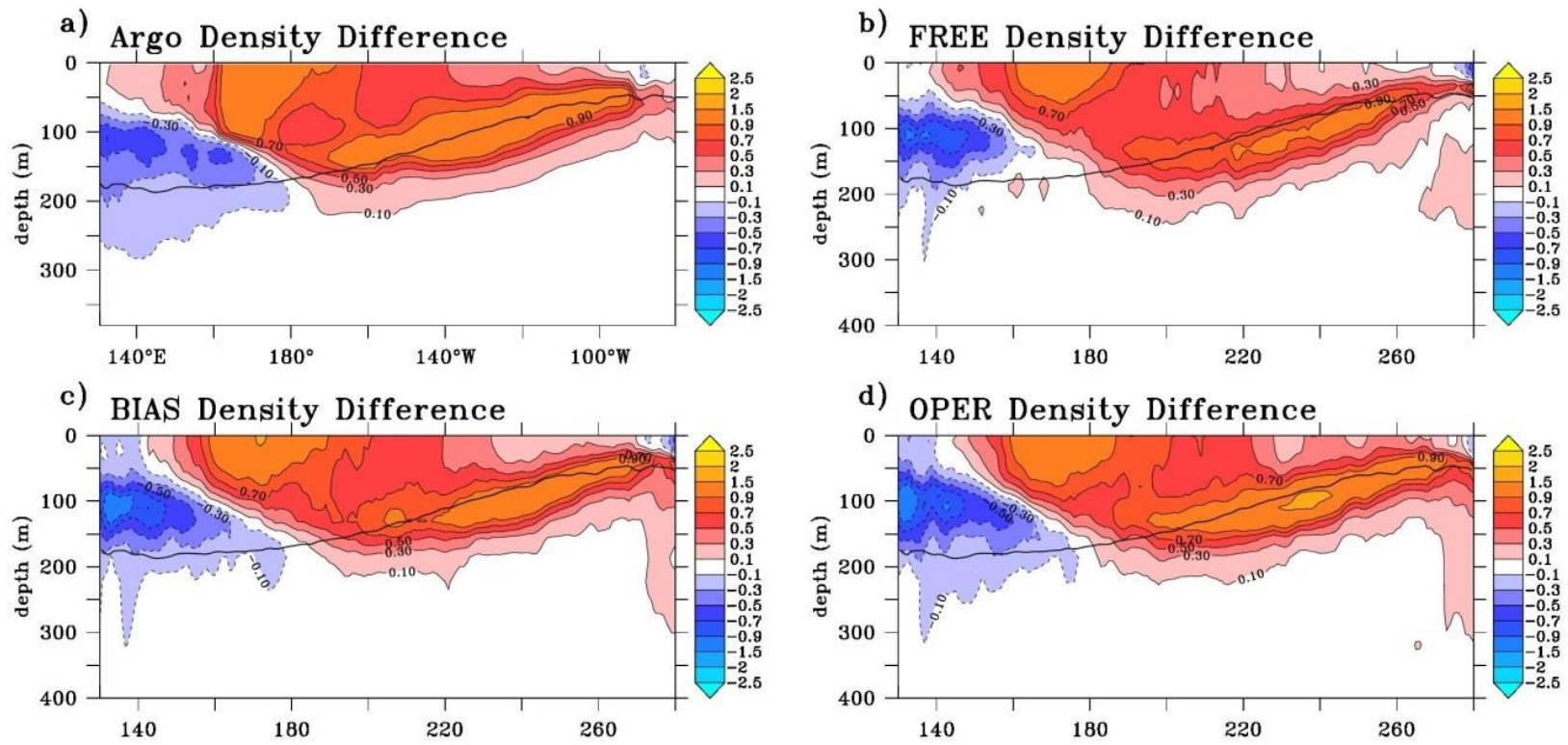
1
2
3
4

Figure 13: SLA increment difference using 10 and 300 Shapiro passes as anomaly filtering in a regional system at $1/36^\circ$. The black lines represent the position of the assimilated altimeter tracks. Unit is cm.



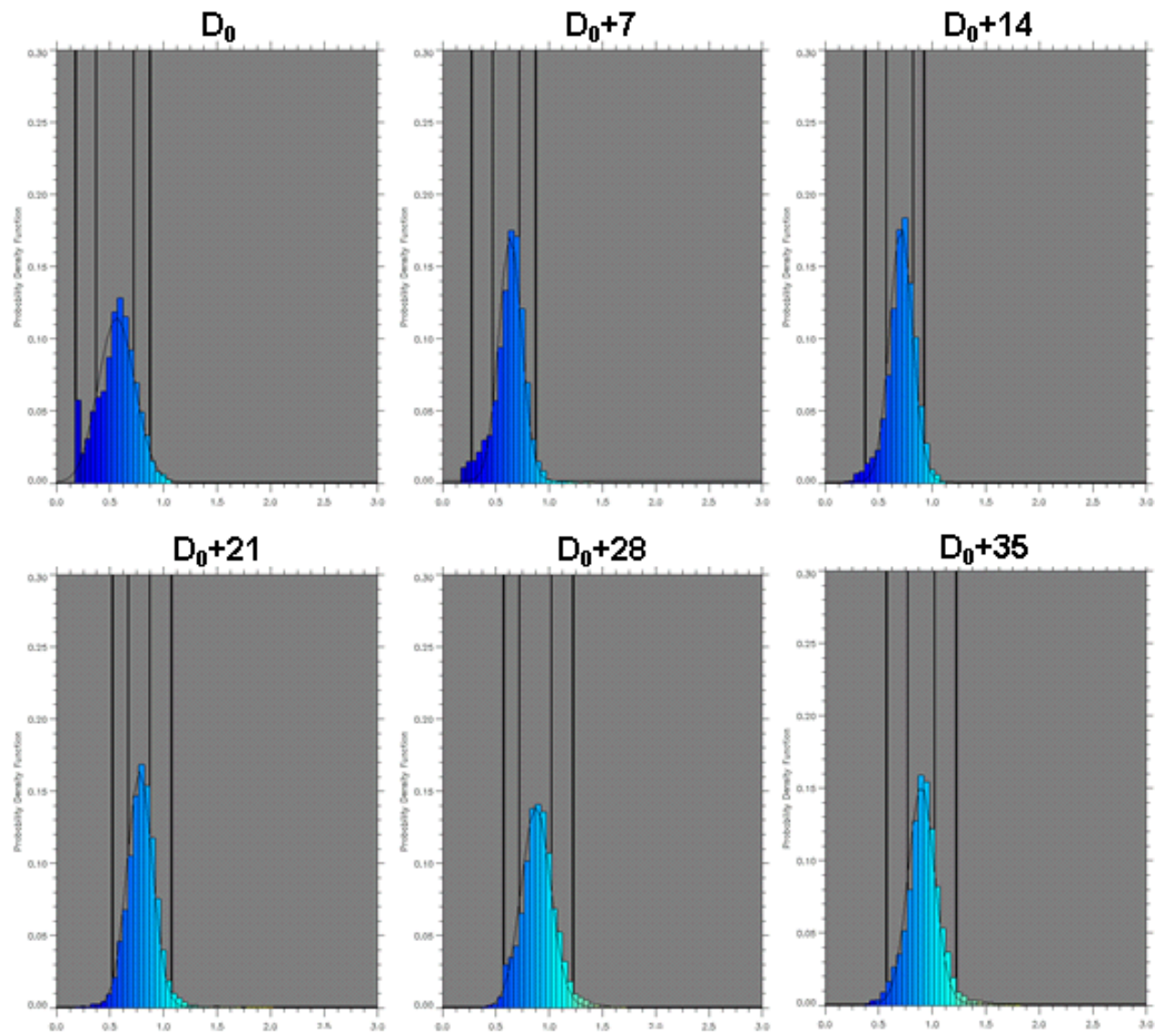
1
2
3

Figure 14: 2007-2015 SSH standard deviation (diagnostics made with 1 point every 3 horizontally and 1 day every 5) of the 1/12° PSY4 simulations (a,b,c) and difference of SSH model standard deviation with the one of DUACS gridded product (d,e,f). Units are cm.



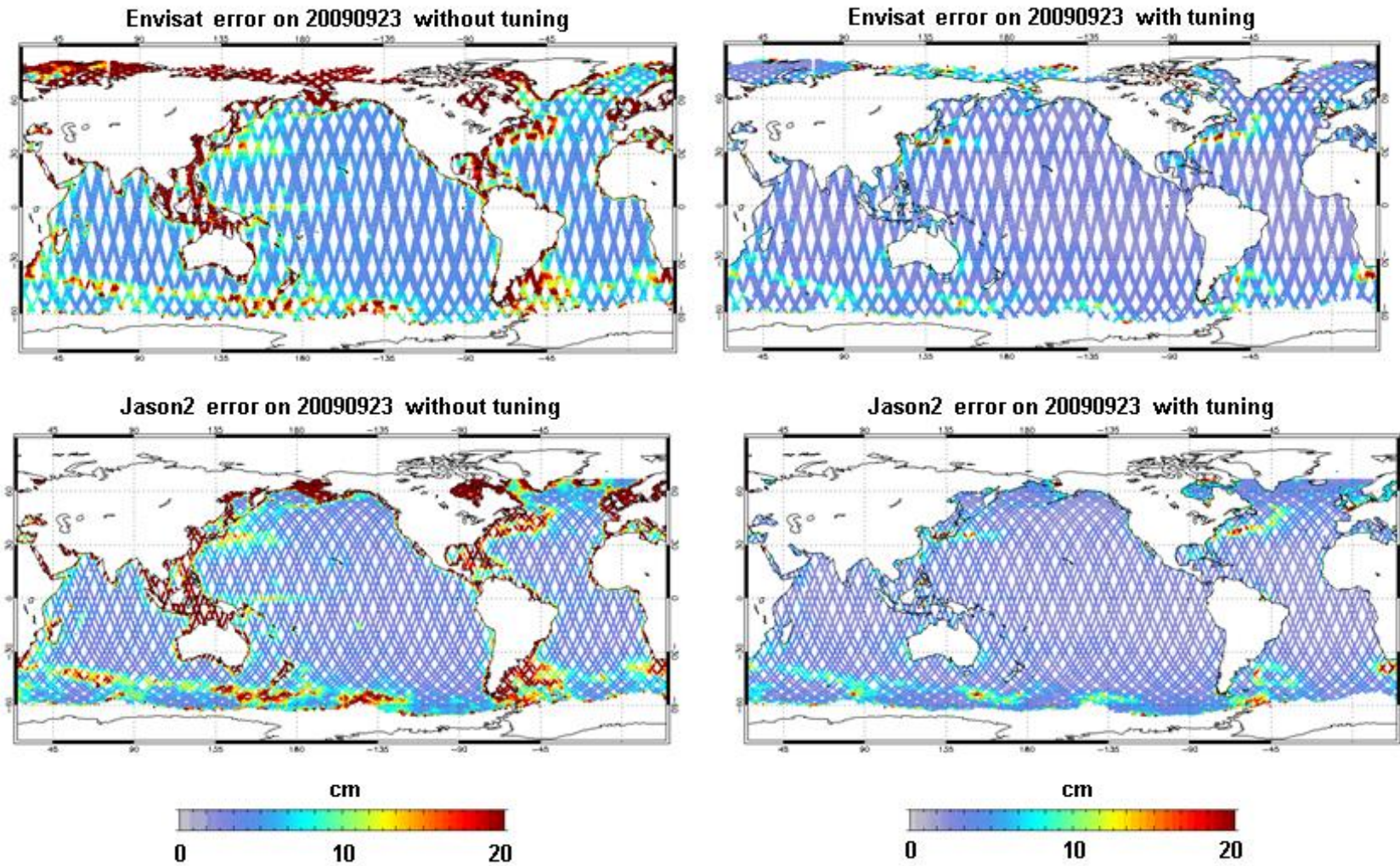
1

2 **Figure 15:** Density difference “OCT-DEC 2008 minus OCT-DEC 2009” in the equatorial Pacific (2° S-2° N) above 400 m depth (a-d) from the SCRIPPS Argo product (a), and the three 1/12°
 3 PSY4 FREE, BIAS and OPER simulations (b-d). The black line indicates the 2007-2015 Argo mean position of the pycnocline depth (isopycn 1025 kg m⁻³).



1
2
3

Figure 16: Evolution of the PDF of the ratio for Envisat satellite from D_0 to D_0+35 days. D_0 corresponds to the first day where Envisat is assimilated by the system.



1
2
3
4

Figure 17: Envisat (top panels) and Jason2 (low panels) satellite observation errors used on the 7-day assimilation cycle ending September, 23, 2009 without tuning (left panels) and with tuning (right panels) method. Unit is cm.

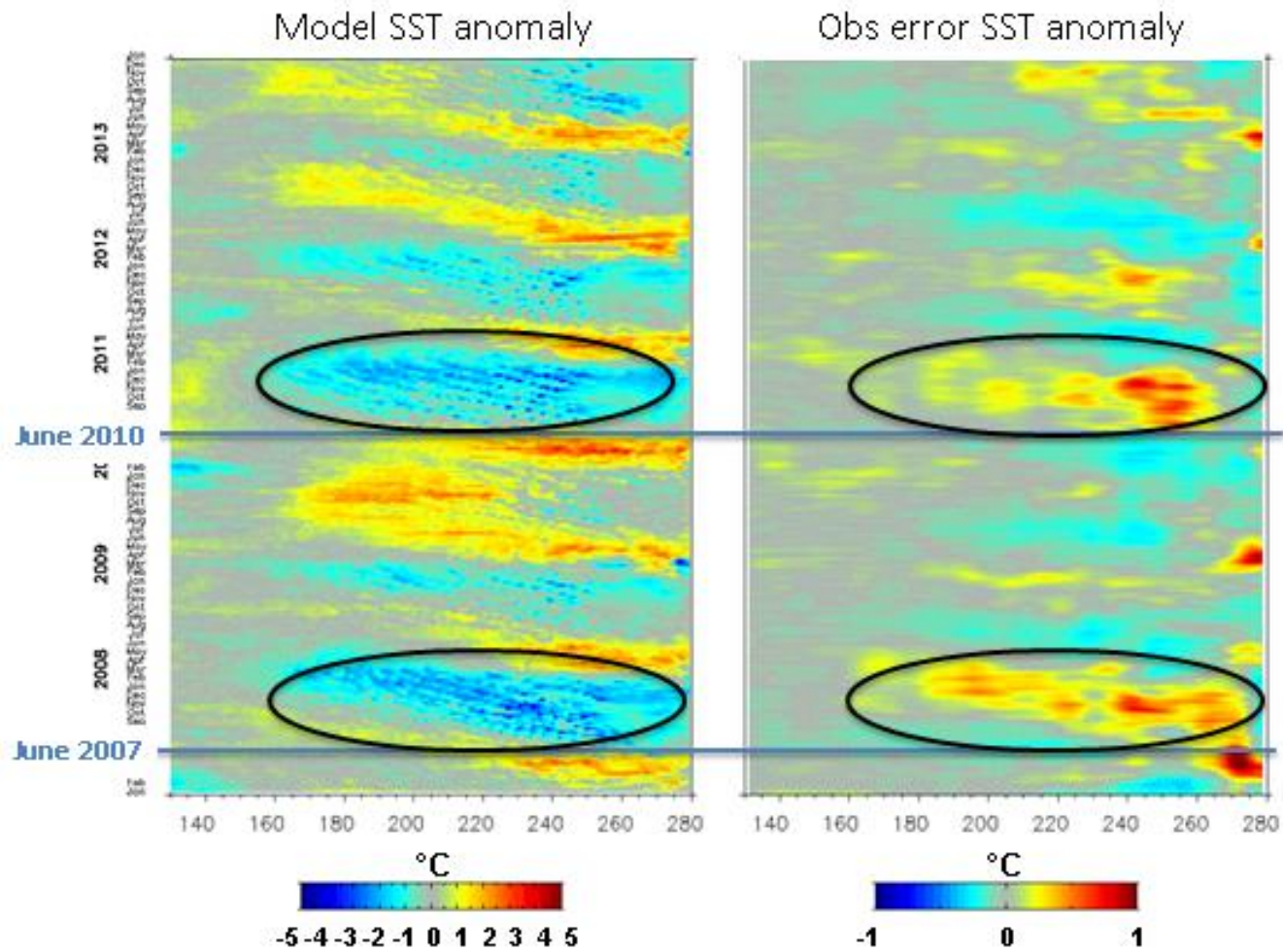
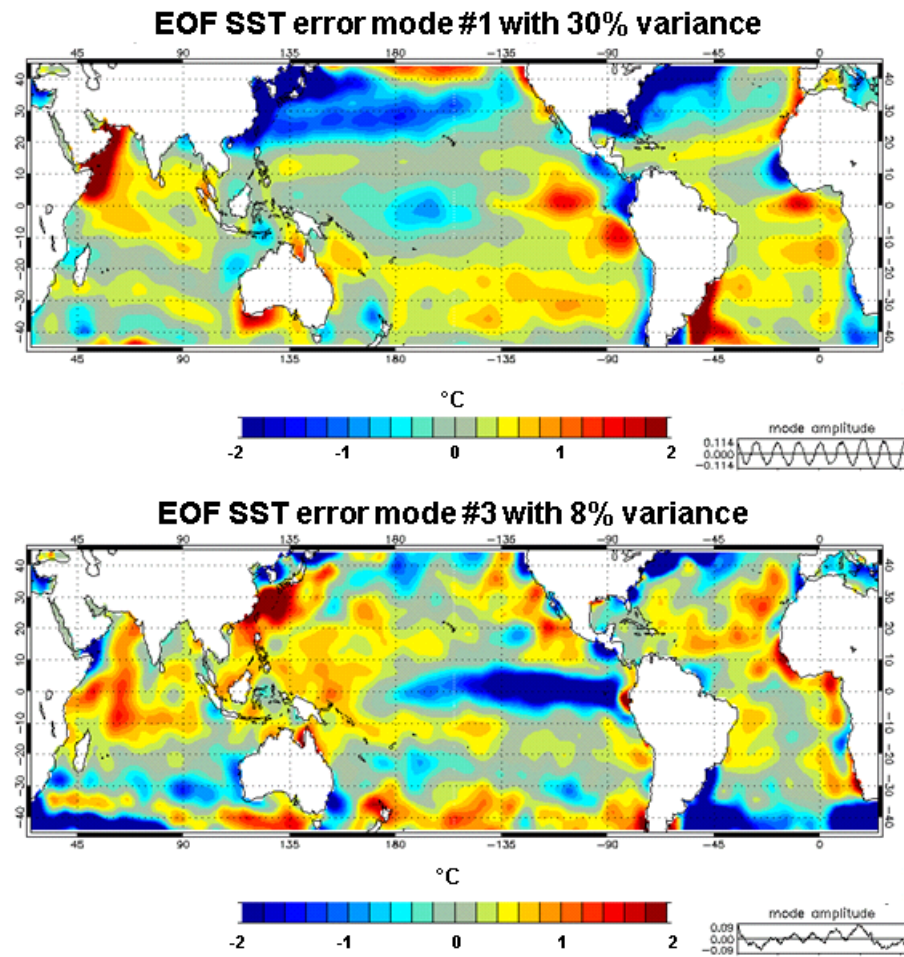
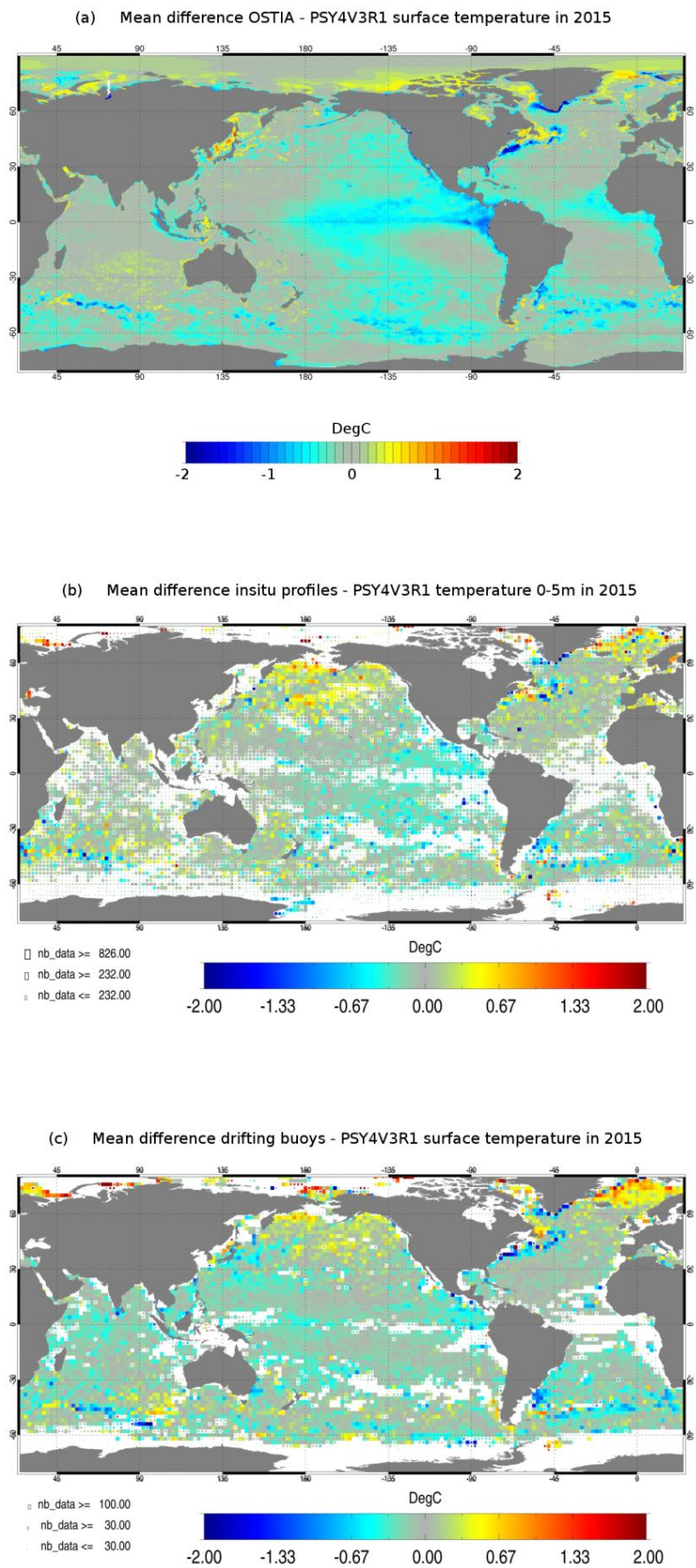


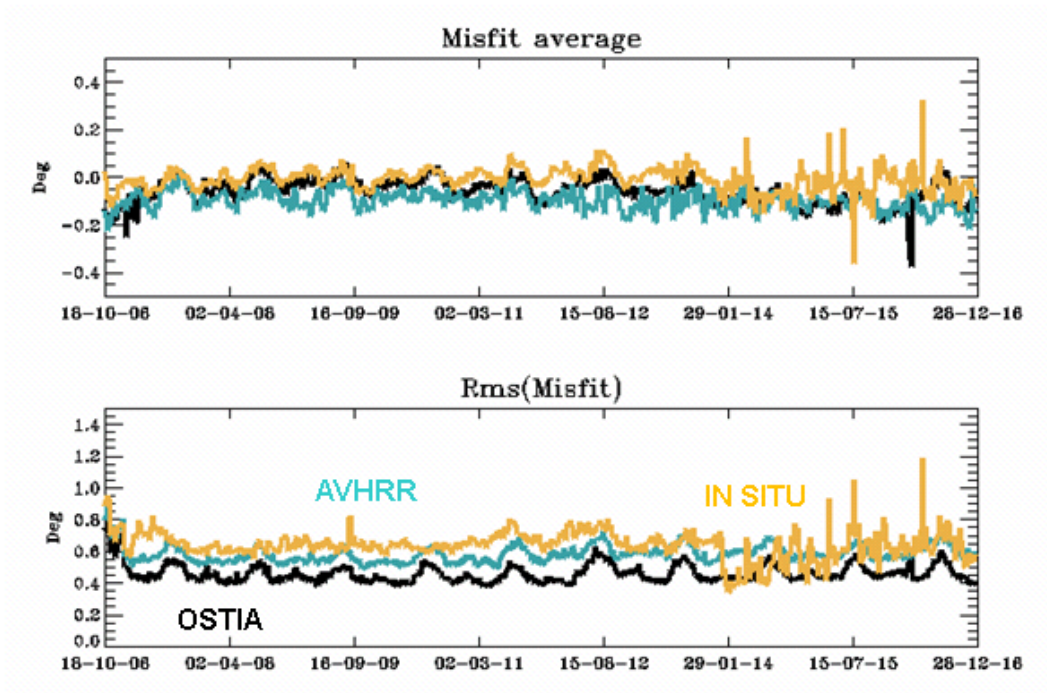
Figure 18: Evolution in time of model SST anomaly (on the left) and SST observation error anomaly tuned by “Desroziers” method (on the right) for a section at 3° N. The blue lines represent the beginning of La Niña episodes (mid-2007 and mid-2010). The black ellipses highlight periods when TIWs are more marked. Units are °C.



1
2
3 **Figure 19:** 1st EOF (top panel) and 3th EOF (bottom panel) of sea surface temperature observation error (°C) over the 2007-2015 time period. The time series at the bottom of each panel
4 correspond to the mode amplitude.
5

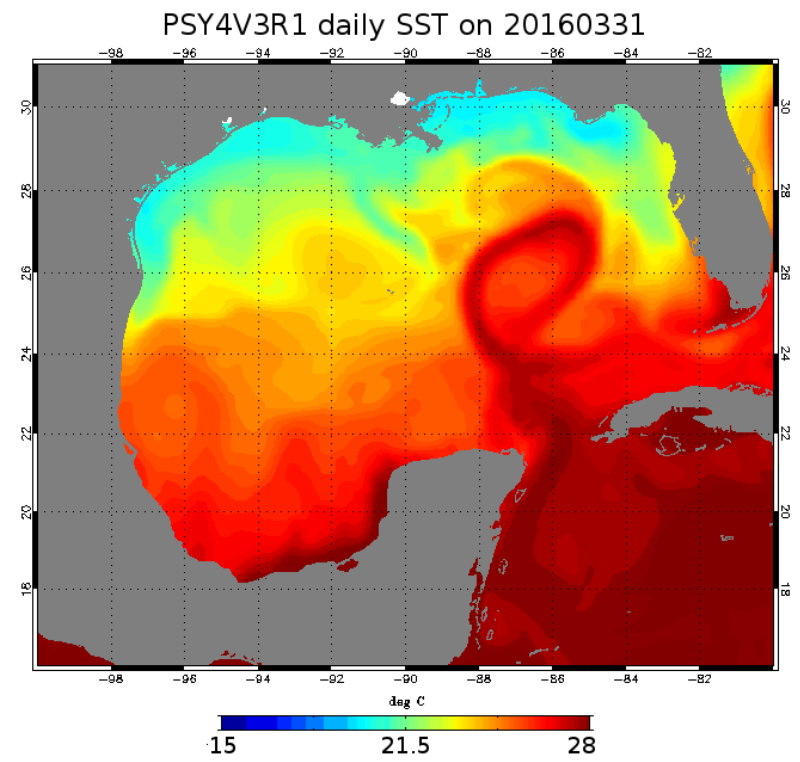
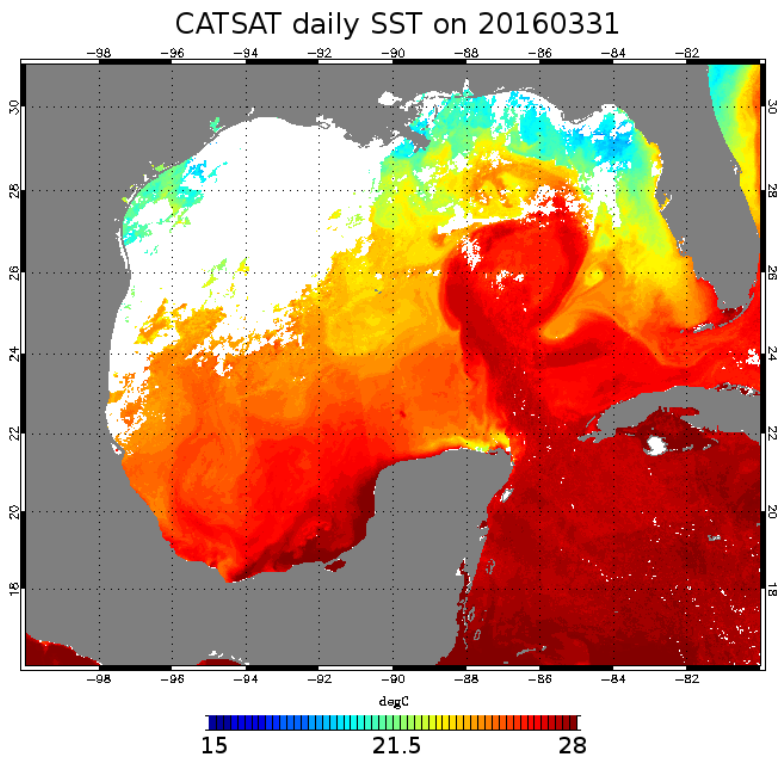


2 **Figure 20:** Mean SST residuals (units in °C) over the year 2015: OSTIA SST minus PSY4V3 (a), in situ SST minus PSY4V3 (b)
3 and drifting buoys SST minus PSY4V3 (c).



1
2
3
4
5

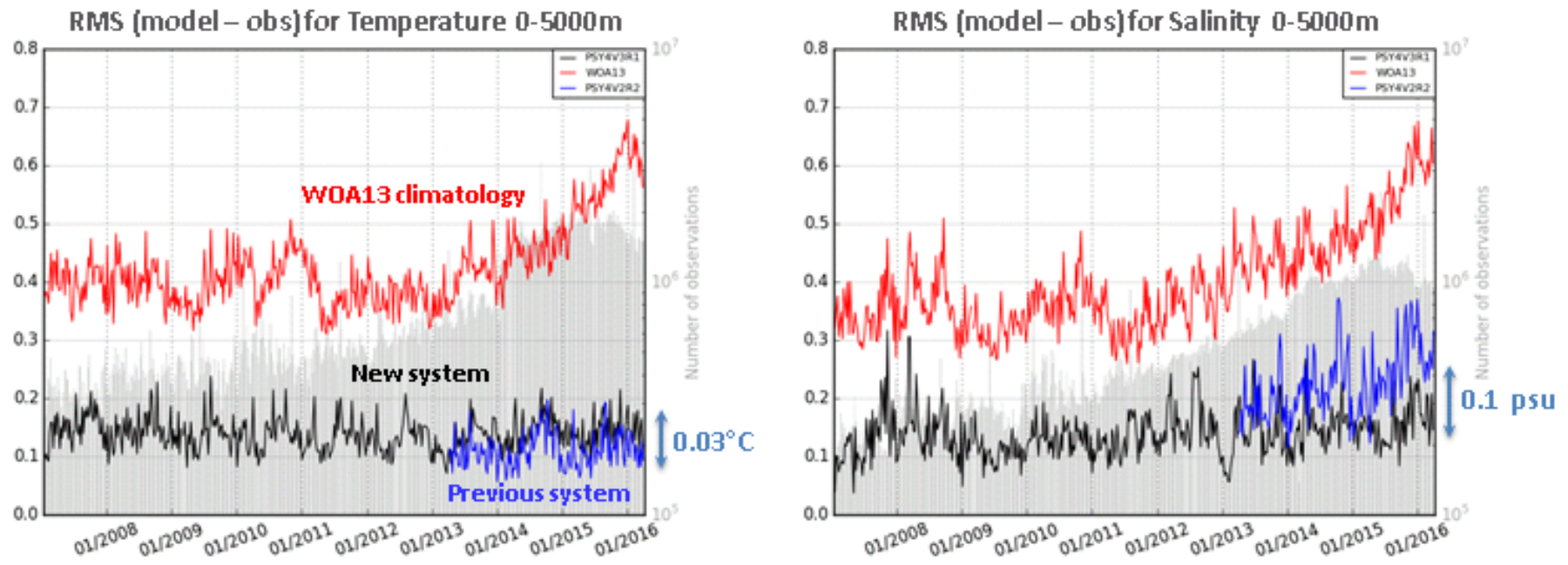
Figure 21: Time series of SST (units in °C) global misfit average (top) and RMS (bottom) for OSTIA observations (black line, assimilated), NOAA AVHRR observations (blue line, not assimilated), and in situ observations (orange line, assimilated), from October 2006 to December 2016.



1

2

Figure 22: High resolution CATSAT SST from CLS (on the left) and PSY4V3 SST (on the right) on March 31, 2016. Unit is °C.

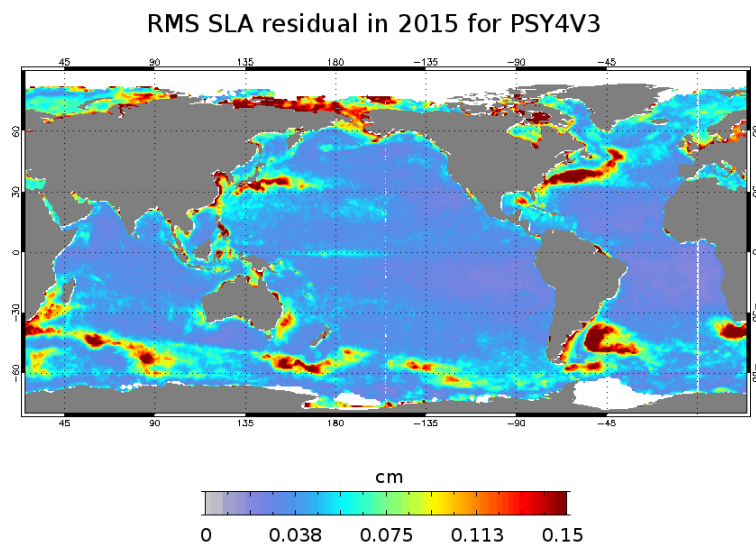
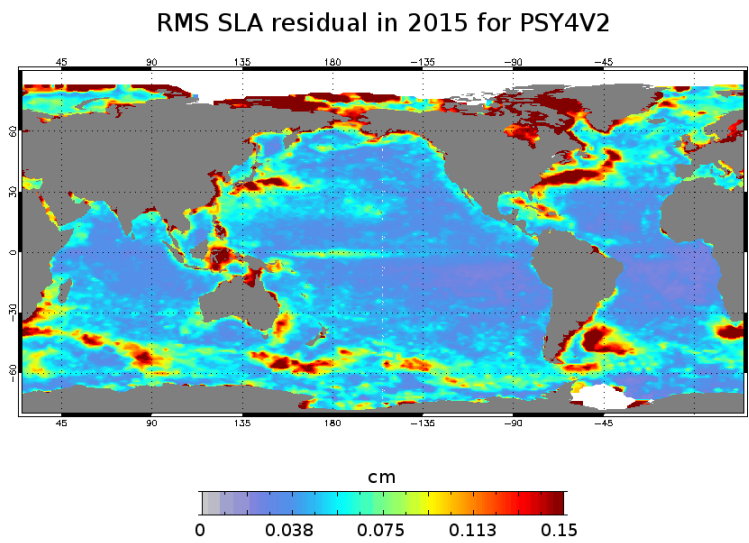
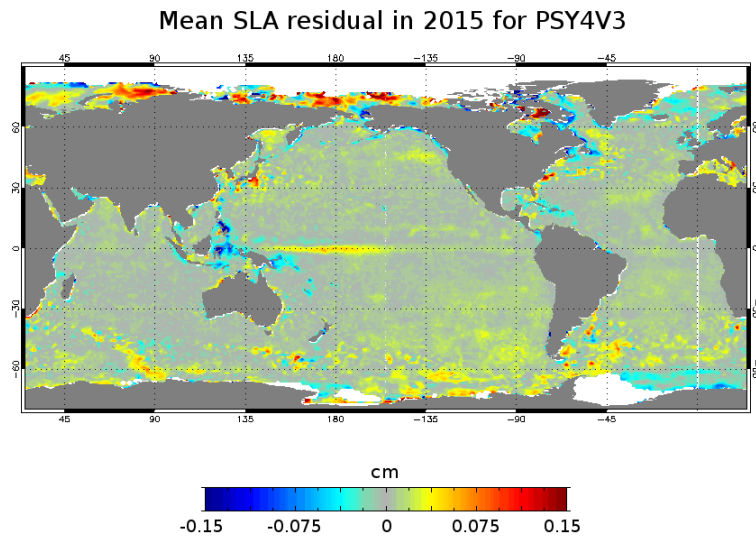
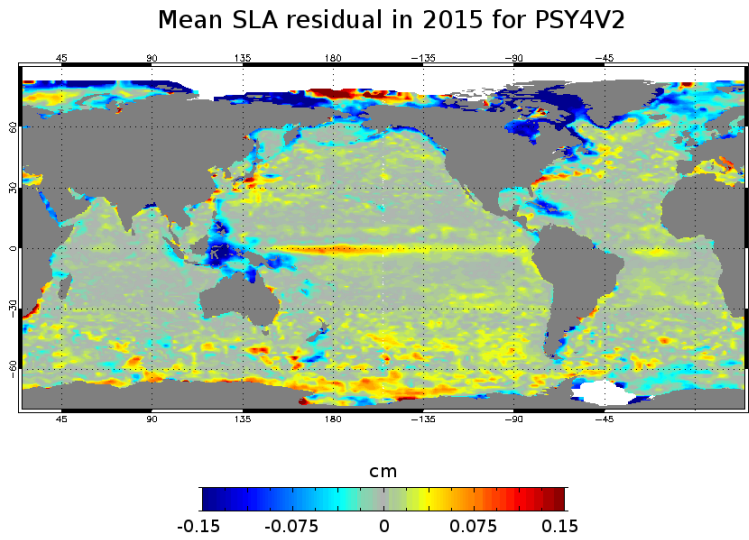


1

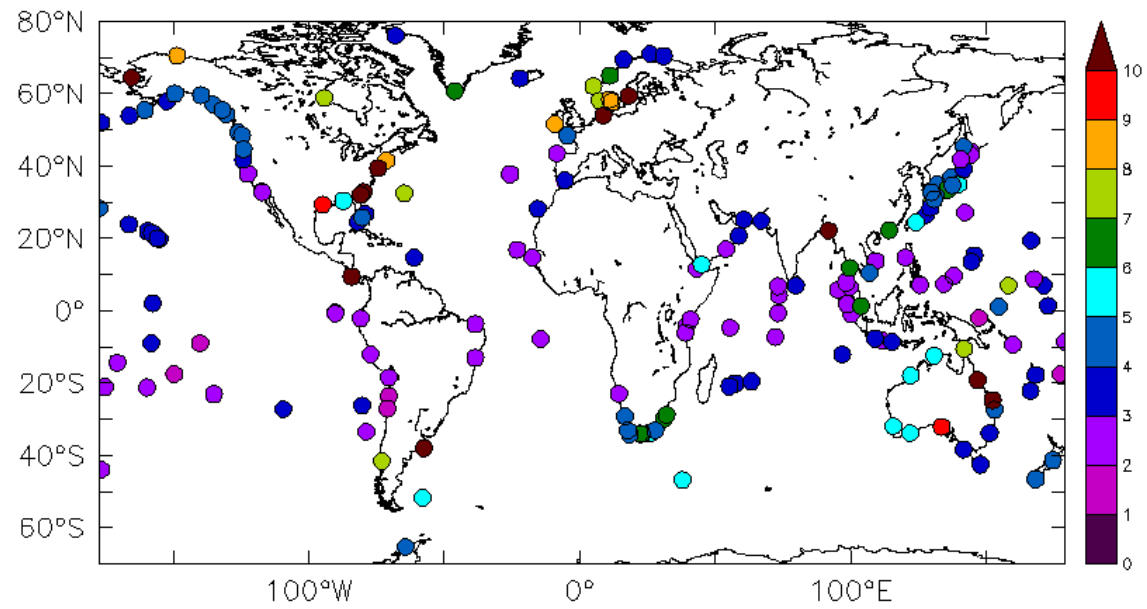
2

3

Figure 23: Time series of the 0-5000m RMS difference between the model analysis and the in situ observations for previous system PSY4V2 (in blue), new system PSY4V3 (in black) and the WOA13v2 climatology (in red). Left panel: temperature (unit in °C), right panel: salinity (unit in psu). Time series of the number of available observations appear in grey.

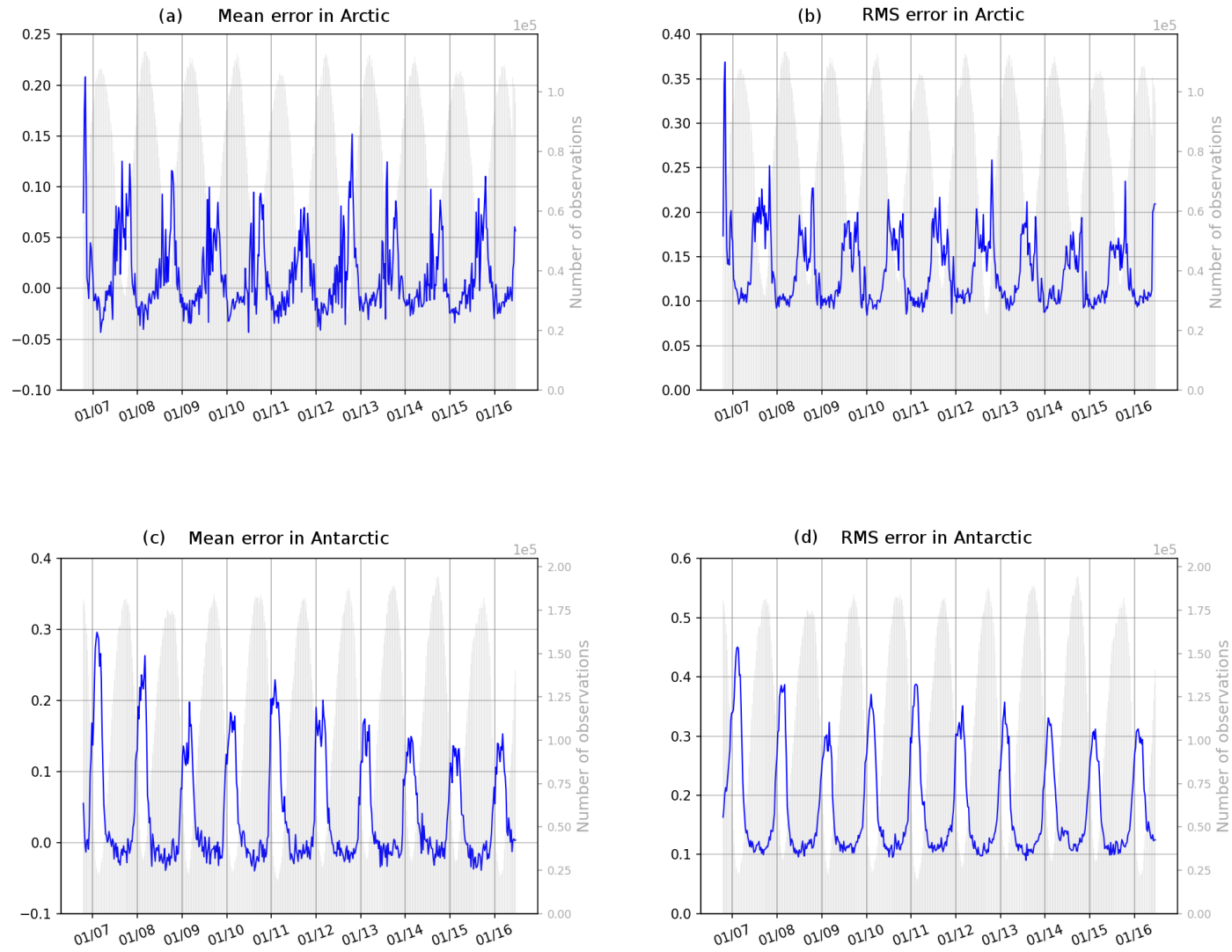


1 **Figure 24:** Mean residual errors (top panels) and RMS residual errors (low panels) of SLA in 2015, for the previous system PSY4V2 (on the left) and the new system PSY4V3 (on the right).
 2 Unit is cm.



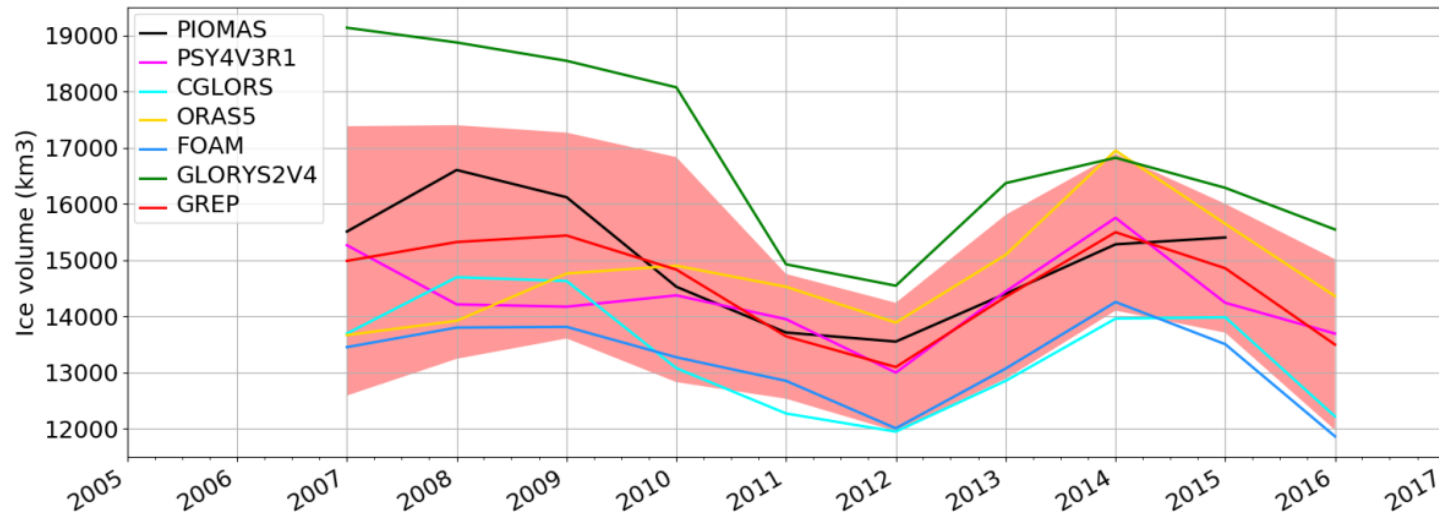
1
2
3

Figure 25: Sea surface height RMS difference between tide gauges observations and the system PSY4V3 for the year 2015. Unit is cm.



1

2 **Figure 26:** Time series of (observation-forecast) mean (a and c) and RMS (b and d) differences of sea ice concentration (0 means no ice, 1 means 100 % ice cover) in the Arctic Ocean (a and
 3 b) and Antarctic Ocean (c and d). The assimilated observations are the sea ice concentrations from OSI TAC. Time series of the number of available observations appear in grey.

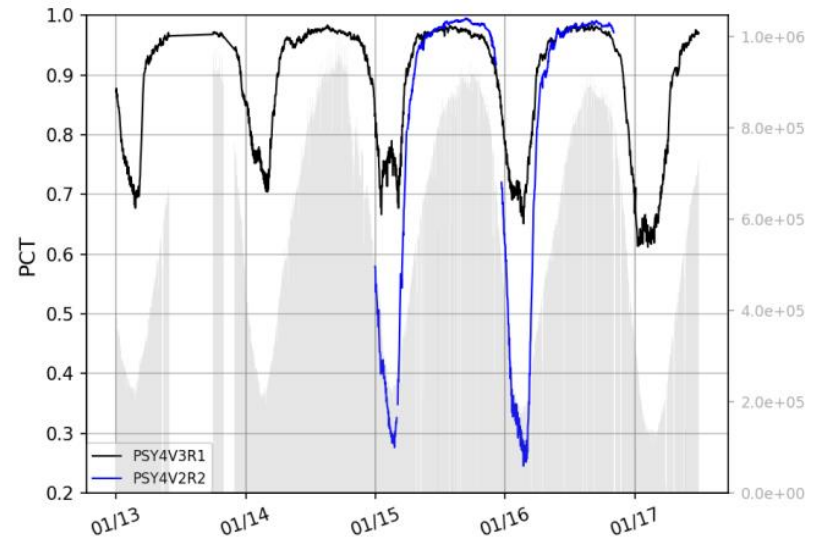
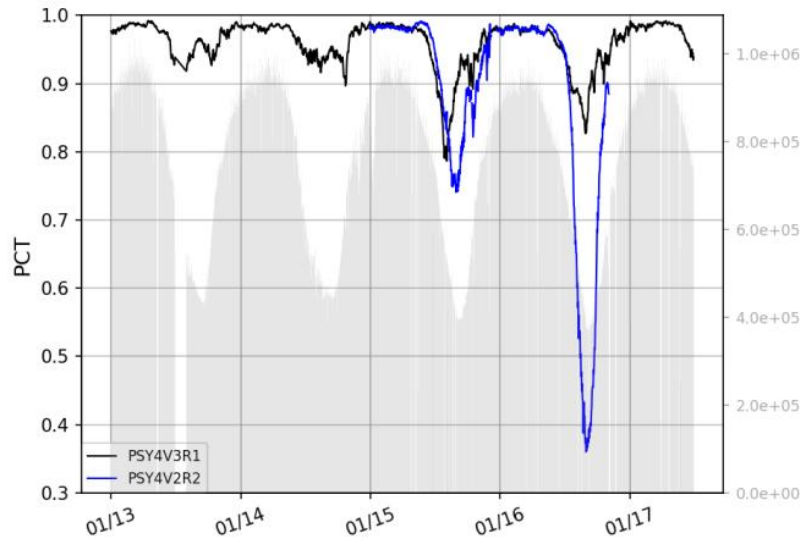


1

2

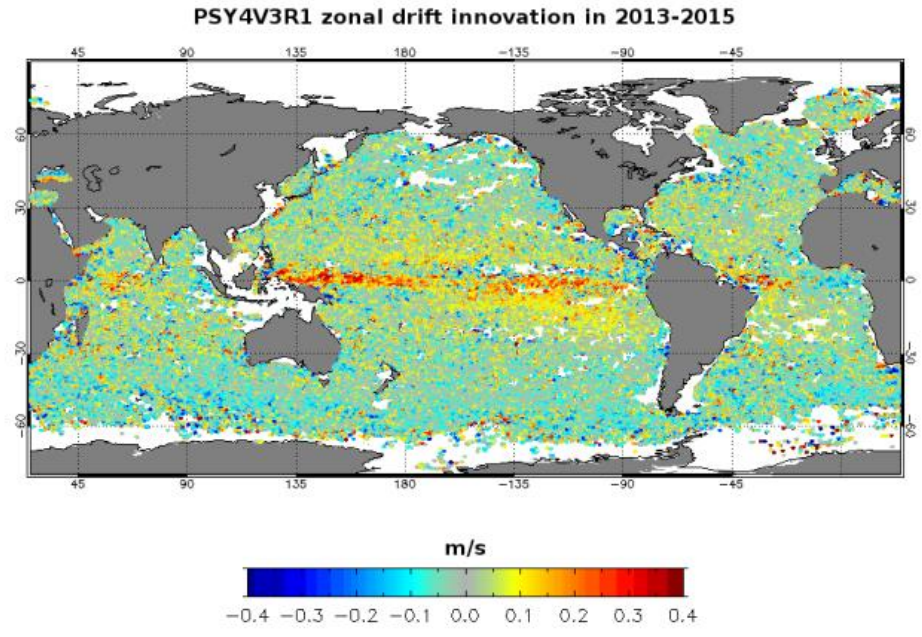
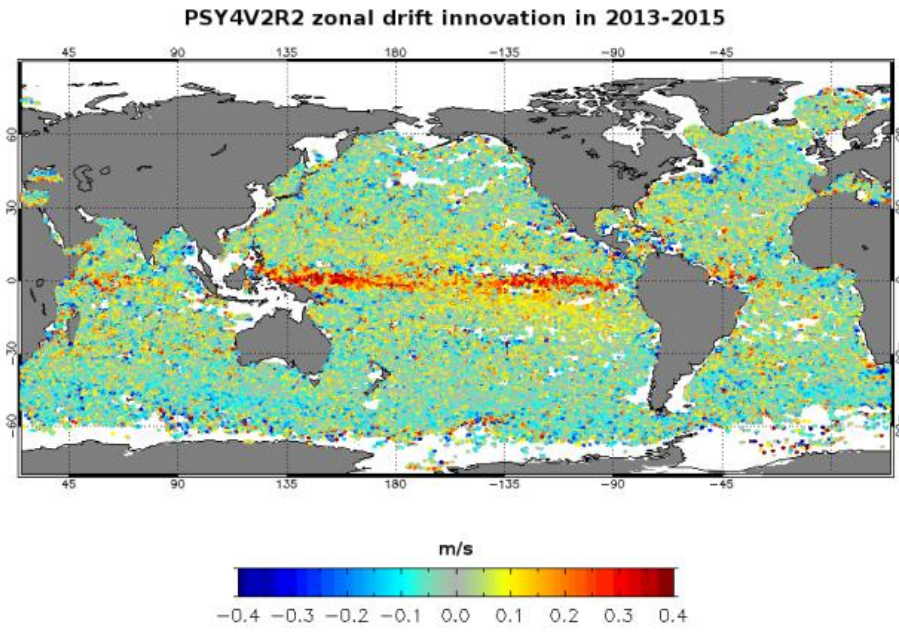
Figure 27: Time series over the 2007-2016 period of the sea ice volume in Arctic for several systems: GREP composed by the four members GLORYS2V4 from Mercator Ocean (France), ORAS5 from ECMWF, FOAM/GloSea from Met Office (UK) and C-GLORS from CMCC (Italy); PSY4V3 from Mercator Ocean (France); PIOMAS product. The spread of GREP product is represented in light red. Unit is km³.

4



1
2
3

Figure 28: Time series of the PCT quantity for PSY4V2 (in blue) and PSY4V3 (in black). The left panel corresponds to Arctic and the right panel to Antarctic. Time series of the number of available observations appear in grey.



1
2
3
4

Figure 29: Mean zonal drift innovation (m s^{-1}) with PSY4V2 (on the left) and PSY4V3 (on the right) over the time period 2013-2015. Observations come from Argo surface floats and a surface drifters corrected dataset (Rio, 2012). Units are m s^{-1} .

Mercator Ocean system reference	Domain	Resolution	Model	Assimilation	Assimilated observations
PSY3V2R1	global	Horizontal: 1/4° Vertical: 50 levels	ORCA025 NEMO 1.09 LIM2, Bulk CLIO 24 h atmospheric forcing	SAM (SEEK)	“RTG” SST SLA T/S vertical profiles
PSY3V3R1	global	Horizontal: 1/4° Vertical: 50 levels	ORCA025 NEMO 3.1 LIM2 EVP, Bulk CORE 3 h atmospheric forcing	SAM (SEEK) IAU 3D-VAR bias correction	“RTG” SST SLA T/S vertical profiles
PSY3V3R3	global	Horizontal: 1/4° Vertical: 50 levels	ORCA025 NEMO 3.1 LIM2 EVP, Bulk CORE 3 h atmospheric forcing New parameterization of vertical mixing Taking into account ocean colour for depth of light extinction Large scale correction to the downward radiative and precipitation fluxes Adding runoff for iceberg melting Adding seasonal cycle for surface mass budget	SAM (SEEK) IAU 3D-VAR bias correction Obs. errors higher near the coast (for SST and SLA) and on shelves (for SLA) MDT error adjusted Increase of Envisat altimeter error QC on T/S profiles New correlation radii	“AVHRR+AMSRE” SST SLA T/S vertical profiles MDT “CNES-CLS09” adjusted Sea Mammals T/S vertical profiles

1 **Table 1:** Specifics of the Mercator Ocean IRG systems. In bold, the major upgrades with respect to the previous version. Available and operational production periods are described in Fig. 1.

Mercator Ocean system reference	Domain	Resolution	Model	Assimilation	Assimilated observations
PSY4V1R3	global	Horizontal: 1/12° Vertical: 50 levels	ORCA12 NEMO 1.09 LIM2, Bulk CLIO 24 h atmospheric forcing	SAM (SEEK) IAU	“RTG” SST SLA T/S vertical profiles
PSY4V2R2	global	Horizontal: 1/12° Vertical: 50 levels	ORCA12 NEMO 3.1 LIM2 EVP, Bulk CORE 3 h atmospheric forcing New parameterization of vertical mixing Taking into account ocean color for depth of light extinction Large scale correction to the downward radiative and precipitation fluxes Adding runoff for iceberg melting Adding seasonal cycle for surface mass budget	SAM (SEEK) IAU 3D-VAR bias correction Obs. errors higher near the coast (for SST and SLA) and on shelves (for SLA) MDT error adjusted Increase of Envisat altimeter error QC on T/S profiles New correlation radii	“AVHRR+AMSRE” SST SLA T/S vertical profiles MDT “CNES-CLS09” adjusted Sea Mammals T/S vertical profiles
PSY4V3R1	global	Horizontal: 1/12° Vertical: 50 levels	ORCA12 NEMO 3.1 LIM2 EVP, Bulk CORE 3 h atmospheric forcing New parameterization of vertical mixing Taking into account ocean colour for depth of light extinction Adding seasonal cycle for surface mass budget 50 % of model surface currents used for surface momentum fluxes Updated runoff from Dai et al., 2009 + runoff fluxes coming from Greenland and Antarctica Addition of a trend (2.2mm yr⁻¹) to the runoff Global steric effect added to the sea level New correction of precipitations using satellite data + no more correction of the downward radiative fluxes Correction of the concentration/dilution water flux term Relaxation toward WOA13v2 at Gibraltar and Bab-el-Mandeb	SAM (SEEK) IAU 3D-VAR bias correction (1 month time window) MDT error adjusted Increase of Envisat altimeter error QC on T/S profiles New correlation radii Addition of a second QC on T/S vertical profiles Adaptive tuning of observation errors for SLA and SST New 3D observation errors files for assimilation of in situ profiles Use of the SSH increment instead of the sum of barotropic and dynamic height increments Global mean increment of the total SSH is set to zero	CMEMS OSTIA SST SLA T/S vertical profiles MDT adjusted based on CNES-CLS13 Sea Mammals T/S vertical profiles CMEMS Sea Ice Concentration WOA13v2 climatology (temperature and salinity) constrain below 2000m (assimilation using a non-Gaussian error at depth)

Table 2: Specifics of the Mercator Ocean HRG systems. In bold, the major upgrades with respect to the previous version. Available and operational production periods are described in Fig. 1.

	AMSR Ice	AMSR Water
Model Ice	Hit ice	False Alarm
Model Water	Miss	Hit water

Table 3: Contingency table entries for sea ice verification of PSY4V3 system as compared to AMSR sea ice concentration observations

1
2
3